Experimental investigation of fatigue behavior of adhesively-bonded glass fiber joints

I Motlhakudi

orcid.org/0000-0001-7404-3319

Dissertation submitted in partial fulfilment of the requirements for the degree *Master of Engineering* in Mechanical Engineering at the North-West University

Supervisor: Prof AS Jonker

Graduation May 2018

Student number: 20469616

DECLARATION

I hereby declare that all work done in this research dissertation is my own unassisted work, except for the parts where specific references are credited. This research work has not been submitted for degree purposes at any other university, nationally or internationally.

Signed: _____

Isaac Motlhakudi

ACKNOWLEDGMENTS

Firstly, I would like to thank our Father in heaven for the strength and persistence that he provided to me throughout the course of this research.

I would also like to acknowledge the following people:

- Julia Motlhakudi for always being at my side.
- Prof A Jonker for his guidance throughout the period of this study.
- All my friends for always encouraging me.
- Special thanks to a group of students that I worked with in the past two years. This work would not have been complete without their inputs.
- To my two late bothers and friends, Isak Ponya Motlhakudi and Darryl Makhurumetsa Phahlamohlaka, “we will never forget”.

ABSTRACT

The fatigue behavior of adhesively-bonded laminates made out of glass fiber reinforced plastics was experimentally investigated and modeled under constant amplitude loading. Double strap lap joints were examined under seven various stress-ratios (R) denoting the ratio of minimum to maximum cyclic stress. The ratios selected represent tension-tension (T-T), tension-compression (T-C), compression-tension (C-T) and compression–compression (C-C) fatigue-loading conditions. The R-ratios selected for these fatigue-loading conditions were R = 0.5 and R = 0.1 for T-T, R = -1 and R = -0.5 for T-C, R = -2 for C-T, and R = 10 and R = 2 for C-C.

The S-N curves under different R-ratios showed both mean and amplitude strength of the joints to be decreasing with an increasing number of applied numbers of cycles. The S-N curves also showed that amplitude strength of the joints was low under tension-tension and compression-compression fatigue loading. Amplitude strength was high under both compression-tension and tension-compression fatigue loading. The mean strength of joints was high under both tension-tension and compression-compression fatigue loading. Mean strength was low under compression-tension and tension-compression loading. The relationship between mean and amplitude stresses was investigated using a constant life diagram (CLD). The diagram demonstrated that joints examined under R = -1 have the highest stress amplitude when plotted against mean stress. For all constant lives, the amplitude stress changed linearly with the mean stress under different loading conditions. Changing of failure type from compression to tension was observed on this diagram as mean stress increases from negative to positive values.

The relationship between mean and amplitude stress at any constant life was then modeled using different mathematical formulae. Linear, second-order polynomial, third-order and fourth-order polynomial expressions were used to model this relationship for the entire range of values of mean stress defined between ultimate compression strength and ultimate tensile strength. The predictive accuracy of each of these models was evaluated by calculating the statistical distance (r^2-value) between experimentally-derived amplitude values and the amplitude values predicted by the model at randomly chosen number of cycles. Four more models commonly used for composite materials were then applied, to compare with the established formulas. Piecewise-linear modeling was established as a preferable method for modeling mean and amplitude stress.

Keywords: Composite materials, glass fiber**,** bonded joints, stress-ratio, constant life diagrams, S-N curves, fatigue loading conditions, static loading, mean stress, amplitude stress, constant life, predictive accuracy, r^2-value

---

LIST OF FIGURES

LIST OF TABLES

LIST OF SYMBOLS

Symbol	Description	Unit
A	Adhesive thickness	mm
F_a	Amplitude load	kN
σ_a	Amplitude stress	MPa
$\sigma_{R=0.1}$	Amplitude stress at R=0.1	MPa
$\sigma_{R=0.5}$	Amplitude stress at R=0.5	MPa
$\sigma_{R=-0.5}$	Amplitude stress at R=-0.5	MPa
$\sigma_{R=-1}$	Amplitude stress at R=-1	MPa
$\sigma_{R=10}$	Amplitude stress at R=10	MPa
$\sigma_{R=2}$	Amplitude stress at R=2	MPa
$\sigma_{R=-2}$	Amplitude stress at R=-2	MPa
σ_a^{γ}	Amplitude stress for critical R-ratio	MPa
$\bar{\bar{s}}$	Average of two repeatability standard deviations	
$\sigma_{a,1CC}$	Compression-compression experimental stress amplitude	MPa
z_{cr}	Critical value of standardized $\bar{\bar{s}}$	
σ_{max}^{γ}	Fatigue stress at Critical R-ratio	MPa
$\sigma_{a,i}$	First known stress amplitude	MPa
R_i	First known stress ratio	
α, β, γ and δ	Fourth-order model parameters	
B	Grip Area	mm^2
u	Harris model parameter	
v	Harris model parameter	
A_1	Harris model parameter	
B_1	Harris model parameter	
A_2	Harris model parameter	
B_2	Harris model parameter	
A_3	Harris model parameter	
B_3	Harris model parameter	
$T2$	Inner laminate thickness	mm
t_2	Inner laminate thickness	mm
φ_{γ}	Kawai model parameter	
σ_B	Kawai model parameter	
k_1, k_2	Linear model parameters	
F_{max}	Maximum cyclic load	kN
σ_{max}	Maximum stress	MPa
F_m	Mean load	kN
σ_m	Mean stress	MPa
σ_m^{γ}	Mean stress for critical R-ratio	MPa

F_{min}	Minimum cyclic load	kN
σ_{min}	Minimum stress	MPa
N	Number of cycles	
N_f	Number of cycles to failure	
p	Number of different time intervals	
$\#$	Number of repeatability standard deviations	
n	Number of test results in an time interval	
$T1$	Outer laminate thickness	mm
t_1	Outer laminate thickness	mm
L	Overlap length	mm
τ	Percentage of the estimated average shear strength of the adhesive	MPa
r'	Piecewise model parameter	
r_i	Piecewise model parameter	
r_{i+1}	Piecewise model parameter	
r_{1TT}	Piecewise model parameter	
f	Piecewise model parameter	
r_{1CC}	Piecewise parameter	
σ_1	Power law parameter	
$k1$	Power law parameter	
Np	Referenced number of cycles	
s_r	Repeatability standard deviation	
s_y	Reproducibility parameter	
d	Reproducibility parameter	
ω	Reproducibility parameter	
ϖ	Reproducibility parameter	
s_R	Reproducibility standard deviation	
αC	Scale parameter of Weibull in compression	
αT	Scale parameter of Weibull in tension	
σ_{i+1}	Second known stress amplitude	MPa
R_{i+1}	Second known stress ratio	
a and b	Second-order model parameters	
δC	Shape parameter in compression	
δT	Shape parameter in tension	
β_C	Shape parameter of Weibull in compression	

β_T	Shape parameter of Weibull in tension	
C	Shear/overlap area	mm^2
D	Skewness parameter	
m_0	Slope of S-N curve at $\sigma_m = 0$	
s	Standard deviation of test results	
$\bar{s}$	Standard deviations between two repeatability standard deviations	
r^2	Statistical distance	
σ_{AP}	Stress amplitude at $\sigma_m = 0$	MPa
R	Stress ratio	
$\sigma_{a,1TT}$	Tension-tension experimental stress amplitude	MPa
α, β and γ	Third-order model parameters	
K	Triangular model parameter	
σ_0	Triangular model parameter	
	Unknown amplitude stress	MPa
σ_{ap}	Unknown stress amplitude	MPa
R'	Unknown stress ratio	
F_{ty}	Yield point of adherent	MPa

ABBREVIATIONS

AMTS	Advanced Manufacturing Technology Strategy
ASTM	American Society for Testing and Materials
C-C	Compression-compression
CI	Confidence interval
CFRP	Carbon fiber reinforced polymer
CL	Constant lines
CLD	Constant life diagram
C-T	Compression-tension
DLJs	Double lap joints
EN	European Standard
Exp.	Experimental
GFRP	Glass fiber reinforced polymer
ISO	International Standards Organization
MTS	Material Testing systems
Repeat. Standard dev.	Repeatability standard deviation
SLJs	Single lap joints
S-N	Stress-cycles
Standard Dev.	Standard deviation.
T-C	Tension-compression
T-T	Tension-tension
UCS	Ultimate compression strength
UTS	Ultimate tensile strength

TABLE OF CONTENTS

CHAPTER 1: INTRODUCTION

1.1. Background

A composite material consists of two or more materials combined together to give more enhanced properties than those of the individual materials on their own. Each material in the composite maintains its separate chemical, physical and mechanical properties. Composite materials provide good strength and stiffness combined with low density, as compared to conventional engineering materials. The two main constituents of composite materials are reinforcement and matrix material. According to Advanced Manufacturing Technology Strategy standard workshop practice, AMTS (2011), common reinforcement materials are glass fiber, carbon fiber and aramid (Kevlar) fiber. An epoxy resinous binder that consists of two components named resin and hardener is normally used as matrix material (AMTS, 2010). The AMTS (2011) standard describes glass fiber reinforced polymer (GFRP) as material commonly used for primary aircraft structures, especially for components like fuselage and wing skins. Carbon fiber reinforced polymer (CFRP) is used primarily for rigid structures because of higher strength and greater rigidity. Aramid fiber reinforced polymer, also known as Kevlar, differs from carbon and glass because of its unique toughness. A composite material containing two or more types of reinforcing fibers is called a hybrid, according to Harris (2003).

Conventional alloy materials such as aluminum and steel are currently being replaced by fiber reinforced polymer materials in most engineering applications, particularly in the aerospace sector (Chowdhury, et al., 2014). Modern processes have encouraged commercial aircraft companies to increase the use of composite materials for primary and secondary structures. This is compelled by the demand for fuel-efficient, lightweight, and high-stiffness structures with good fatigue toughness and corrosion resistance. Chowdhury et al (2014) conclude that the use of composite materials provides these required structural properties and also improves further flexibility in the design and fabrication of various components and joints.

Due to the complexity in design and construction of aircraft structures, the need to join components or parts plays an important role. The three main categories of joints found in composite materials, according to Chowdhury et al (2014), are mechanically fastened joints, adhesively-bonded joints, and a combination of both known as hybrid joints. The use of fasteners as a method of joining composite components creates high-stress concentrations around fastener holes, and hence weakens the components (Duthinh, 2000). Adhesive bonding is sensitive to environmental factors,

and its defects are difficult to detect where the bonds are weak during application (Chowdhury, et al., 2014).

Engineering structures consist of parts or components (such as bonded joints) that are subjected to fatigue loadings. Most failures of large complex structures are the result of mechanisms driven by fatigue. Therefore the structural integrity of minor components that constitute complex structures is of great importance to these structures (Sarfaraz, et al., 2012). Extensive testing and validation is therefore required to fully understand the effectiveness and integrity of composite bonds for large complex structures such as wind turbines and aircraft wings.

1.2. Problem statement

The manufacture of components, such as wind turbine rotor blades and sailplane wings, usually involves the process of joining composite parts or components together through bonding. Wind turbines and sailplanes are safe-life constructions, meaning their full integrity should be guaranteed over the total service life of around 20 years. Wings and rotor blades are expected to endure over 10^7 repeated loads during this period.

A limited amount of reliable fatigue data is currently available for adhesively-bonded composite joints. This means conservative design allowable values are normally used, and this leads to unnecessarily high structural masses for components or parts. Obtaining reliable experimental fatigue data on composite bonds is therefore of great importance and fundamental to manufacturing.

1.3. General aim and objectives

The aim of this study is to experimentally investigate fatigue behavior of adhesively-bonded glass fiber joints under constant amplitude fatigue loading. Objectives in this research will be:

- Reviewing literature from other similar research studies.
- Developing an experimental methodology.
- Compiling an experimental fatigue database.
- Evaluation of the database.
- Interpretation of the results.
- Modeling of the experimental results.

1.4. Chapter outline

Chapter 2 – Literature review.

This chapter discusses the recent work done on the topic by other scholars. The basic principles in adhesive-bonding, failure modes associated with bonding, general fatigue and failure of materials, fatigue loading and fatigue life of materials, mean and amplitude effect, and modeling of mean and amplitude effect are discussed. The review also aims to identify and comment on methods and standards available to assist in the present study.

Chapter 3 - Experimental methodology.

Chapter 3 presents the methodology executed in this study. Materials tested, specimen geometry and fabrication, experimental set-up and testing are described.

Chapter 4 – Experimental results.

The results obtained from the experiments are presented in this chapter. Visual observations are made by describing the failure modes of the bonds. Control parameters recorded in the experiments and parameters calculated using applicable theories are presented, analyzed and validated. Various combinations of constant life diagrams are also investigated.

Chapter 5 – Modeling and discussions.

The chapter presents detail modeling and analysis of mean and amplitude effect on fatigue life. Detailed application of various models and their prediction accuracy are discussed.

Chapter 6 – Conclusions and recommendations.

This last chapter of this study reconsiders the objectives set out at the beginning, and conclusions are drawn from the outcomes of the study. Study contributions and limitations are specified, and recommendations for further studies are discussed.

CHAPTER 2: LITERATURE REVIEW

2.1. Introduction

This chapter aims to identify and comment on up-to-date literature. The definition of adhesive-bonding of composites and failure modes associated with adhesively-bonded joints are discussed in section 2.2 and section 2.3. The basic theories of fatigue and the failure of materials are then discussed in section 2.4. Specific theory based on different types of fatigue loading conditions is then deliberated in section 2.5. Various fatigue life methods which can be used to analyze and interpret the experimental data are explained in section 2.6. The effect of mean and amplitude stress on the fatigue behavior of materials is discussed in section 2.7; observations from other studies are also discussed. Modeling of mean and amplitude stress for any constant life is discussed in section 2.8. Tests methods and standards which can be considered for the present study are explained in section 2.9. The need for fatigue testing of adhesively-bonded double strap lap joints and the way forward is addressed in section 2.10.

2.2. Adhesive-bonding of composites

One of the advantages of composite materials is the use of larger complex components with fewer individual components. Components or parts can be joined together using a variety of joining options. These can be bolted-together joints, bonded joints, or a combination of both. Although each type of joint has its own advantages and disadvantages, adhesively-bonded joints are preferred for permanent connections in civil engineering structures, according to Shahverdi et al (2012). The work done by Duthinh (2000) discusses the advantage of using adhesively-bonded joints where large surfaces and thin members are required for joining. The joints must be designed to withstand environmental conditions found in their service life, and regular inspections must be performed to ensure their integrity. Extensive testing and validation of joints is therefore required to understand how they behave under different loads.

A definition by Hoke (2005) can be used to describe adhesive bonding of composite materials. Composite adhesive bonding may be defined as a process of joining two or more pre-cured composite parts using an adhesive as a bonding material. The only chemical or thermal reaction occurring during this process is the curing of the adhesive system. This joining or assembling of parts together provides flexibility in the design of more complex structures. Figure 1 below shows an example of an adhesively-bonded composite joint.

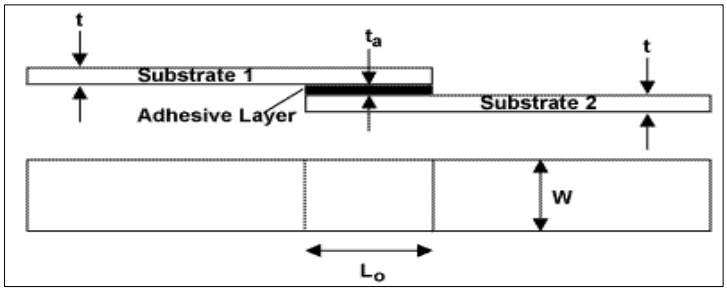

Figure 1: Composite adhesive bonding (Hoke, 2005)

Where:

t is the substrate thickness.

ta is the bond/overlap thickness.

L_o is the bond/ overlap length and.

W is the sample width.

Substrate 1 and 2 are composite laminates which can be made out of fibers of glass, carbon or Kevlar. These laminates are then bonded together to form a joint using an adhesive system. Various types of adhesive systems can be used for an adhesive layer, examples include:

- Bonding epoxy - 2 component
- Polyurethane - 2 component
- Film strips adhesives
- Cyanoacrylates
- Laminating epoxy with additives

The design above (to illustrate composite adhesive bonding) is called a single lap joint. More design configurations of joints are summarized in Table 1 below:

Table 1: Common joint types (Hoke, 2005)

Joint type	Joint design
Single lap	
Tapered single lap	
Single strap lap	
Double lap	
Double tapered strap lap	
Double strap lap	
Tapered scarf	

These joints can be subjected to different loads, which may be static or dynamic in the practical application. It is necessary to know how the joints perform under the action of these loads, how they fail, or what damage is caused by these loads.

2.3. Bond failure modes

Duthinh (2000) describes failures of adhesively bonded joints in three distinct ways, explained as: breaking of fibers in the composite layer; de-bonding in the interface between adhesive and composite layer; and failure of adhesive under peel stresses. Hoke (2005) defines these modes of failure as substrate failure, adhesive failure (interface de-bonding) and cohesive failure (failure of the adhesive). The modes are illustrated and explained in Figures 2, 3 and 4 for a single adhesively lap joint.

2.3.1. Substrate failure

Substrate failure, as shown by Figure 2, is simply defined as fiber-breakage of a composite in any of the laminates. This breaking of fibers usually occurs between the first and the second layer, next to the bond line. Duthinh (2000) explains this failure of joint as occurring outside the bond area at 100% tensile strength of the adherent. The failure is one of the acceptable modes of failure where a joint strength is proportional to laminate thickness (**t**).

Figure 2: Substrate failure (Hoke, 2005)

2.3.2. Adhesive failure

Also known as interface de-bonding, adhesive failure occurs between the adhesive layer and composite laminate. The adhesive comes clean from one surface or both the laminates, as Figure 3 shows. Strength of the joint in this case is proportional to the square root of the laminate thickness, according to Duthinh (2000). Adhesive failure is also considered as one of the acceptable modes of failure for adhesively-bonded joints.

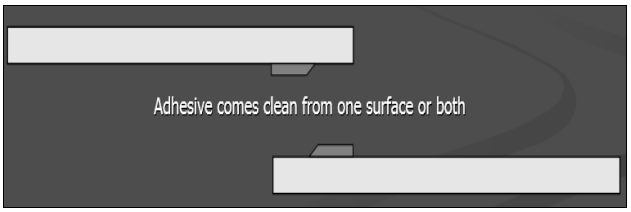

Figure 3: Adhesive failure (Hoke, 2005)

2.3.3. Cohesive failure

Cohesive failure of a joint occurs in the adhesive layer, as illustrated in Figure 4. The fracture or damage happens within the adhesive system. Duthinh (2000) describes this mode as failure associated with adhesive failure under peel stresses. This is the weakest and most times not acceptable failure mode, where peel strength is relative to the quarter power of the laminate thickness.

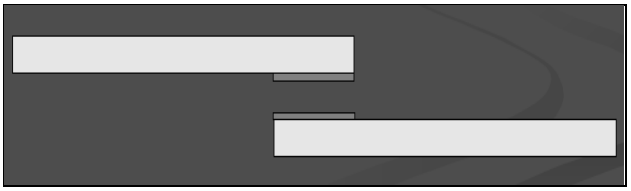

Figure 4: Cohesive failure (Hoke, 2005)

A study by Zhang et al (2008) observed fiber-breakage (thus substrate failure) as the dominant failure mode when testing double strap lap and stepped lap joints of pultruded glass laminates under a single R-ratio, defined in Equation 1 of paragraph 2.5 . Breaking of fibers was also observed when Sarfaraz et al (2011) examined double lap joints of pultruded glass laminates under

three R-ratios. Sarfaraz et al (2012) again observed the same mode of failure when testing the same type of joints under six more R-ratios. Examination of double-cantilever beam joints of glass laminates by Shahverdi et al (2012) also observed fiber breakage as the dominant mode of failure under three different R-ratios.

2.4. Fatigue and failure of materials

In a static component test, machine load is applied gradually until failure. Stress and strain from such a test are plotted to form a stress-strain diagram. The load is applied gradually so that enough time is given for the strain to fully develop. The stresses are applied only once, because the specimen is tested to the point of destruction. Testing of this kind is applicable to static conditions, and closely approximates the actual conditions to which many structural and machine components are subjected (Mischke, et al., 2004). Conditions arise, however, where the stresses produced vary or fluctuate at different levels. Loads applied in these cases are variable, repeated, alternating or fluctuating. Most machine members, components or parts fail under the stress of such loads. The type of failure from these loads is distinct from other failures because the stresses are repeated many times; hence it's called fatigue failure.

Under fatigue loading, the first observed process of degrading in steel and other metallic materials is plastic deformation. This then leads to the formation of numerous cracks. One of these formed cracks normally becomes dominant and grows large enough to result in a sudden final fracture of the material or component. Cerny and Mayer (2011) concurred, saying fatigue loadings in metals usually result in the forming of areas of repeated plastic deformation, initiation of cracks, and expansion of main crack to the point of final failure.

Failure of composite materials is more complex than those of metals. It can occur under cyclic loading due to cracking of the matrix, interfacial de-bonding, delamination or breaking of fibers/fiber-tear (Bendouba, et al., 2014). Fatigue damage process for materials such as glass fibers is mostly repeated and inclusive in the volume. Composite materials normally show little or no plastic deformation, but many small cracks which are formed in the matrix or at the interface between fibers and matrix (Kensche, 1996). A sufficient number of these cracks cluster together into a large group, which then leads to a final failure because of the reduced load bearing cross-sectional area in the material/part or component being loaded.

2.5.Fatigue loading of materials

Fatigue loading can be defined as subjecting components or parts under loads that may be repeated, variable, or fluctuating between different levels. This is in contrast to static loading where the load is applied gradually to allow strain to develop. The amplitude of fatigue loads may be constant or variable, depending on whether the load applied is simple and repetitive (constant amplitude) or completely random and irregular (variable amplitude). Philippidis and Vassilopoulos (2004), for example, tested four-layer (0±45) glass/polyester laminates under variable amplitude fatigue loading to develop fatigue life prediction methodology of GFRP laminates. Factors affecting life prediction of composites under variable amplitude loading were studied by Passipoularidis and Philippidis (2008) by testing four-layer (0±90) glass/epoxy laminates. The work by Sarfaraz et al (2013) also performed variable amplitude fatigue loading to develop a modified fatigue life prediction methodology of bonded GFRP double-lap joints. The joints were composed of pultruded GFRP laminates bonded by an epoxy adhesive system.

However, according to Harris (2003), most of laboratory fatigue tests are performed under the conditions of both constant frequency and constant amplitude between the maximum and minimum stresses. A constant ratio of minimum and maximum stress is usually chosen and applied. This ratio is known as stress ratio and it is calculated for different peak stresses by:

$$R = \frac{\sigma_{min}}{\sigma_{max}} \qquad 1$$

The symbols, σ_{min} and σ_{max}, represent minimum and maximum stress respectively. The R-ratio is used to identify the type of fatigue loading applied; $0 < R < 1$ represents tension-tension , $1 < R < +\infty$ is compression-compression while $-\infty < R < 0$ represents mixed tension-compression loading which can either be tension or compression dominated (Sarfaraz, et al., 2012).

An example is the study done by Shahverdi et al (2012) where the effect of stress ratio on fatigue and fracture behavior of adhesively-bonded GFRP joints was investigated by testing double cantilever beam joints. The ratios selected represented tension-tension, compression-compression and the combined tension-compression fatigue loading. The joints were made out of (0±90) glass/epoxy laminates bonded by epoxy system, and crack length was determined for this particular study. Sarfaraz et al (2011) also investigated fatigue response of bonded pultruded GFRP double-lap joints by performing similar fatigue tests with three different stress ratios. Sarfaraz et al (2012) further studied the effect of mean load on fatigue behavior of double lap joints, by testing

another six different stress ratios, in addition to the three ratios already tested in previous experiments.

2.6.Fatigue life of materials

Component lifetime is of utmost significance for fatigue loadings. The component in this case may be the structure, parts of the structure, or materials making up the parts. Lifetime or fatigue life is measured as the number of cyclic or repeated loads which the structure, part, or material can withstand before failure. Kensche (1996) describes this failure as degradation or damage of material by plastic deformation, or cracking, or both of these processes.

Mischke et al (2004) describes fatigue life methods used in design and analysis as stress-life, strain-life and linear-elastic fracture mechanics. These methods attempt to predict the life in number of cycles to failure (N) for a specific level of loading. Life of $1 \leq N \leq 10^3$ cycles is known as low cycle fatigue and life of $N > 10^3$ as high cycle fatigue. The stress-life method is based on levels of stress only, and is the traditional fatigue analysis method, since it is the easiest to implement. The fatigue behavior is represented by plotting a diagram of stress (or load) against number of cycles to failure (S-N diagram). The strain-life method involves more detailed analysis of plastic deformation at localized regions where the stresses and strains are considered for life estimates. This method is mostly suitable for low-cycle fatigue loading. This method of fracture mechanics assumes a crack is already present and detected. It is then applied to estimate crack growth with respect to stress intensity. The method is mostly practically applicable to large components where computer codes and inspection program can be utilized.

Zhang et al (2008) used stress-life method to experimentally investigate stiffness degradation and fatigue life for double strap lap and stepped-lap GFRP bonded joints under a single stress ratio representing tensile loading. Strain-life method was used when back-face strain and fatigue life were experimentally studied by Solana et al (2010), by testing single-lap aluminum joints. In the study done by Zhang et al (2008), fatigue life under the applied loads was plotted against maximum applied cyclic loads to simulate fatigue behavior. Figure 5 below illustrates that stepped joints showed longer fatigue lives than double lap joints for the same normalized load.

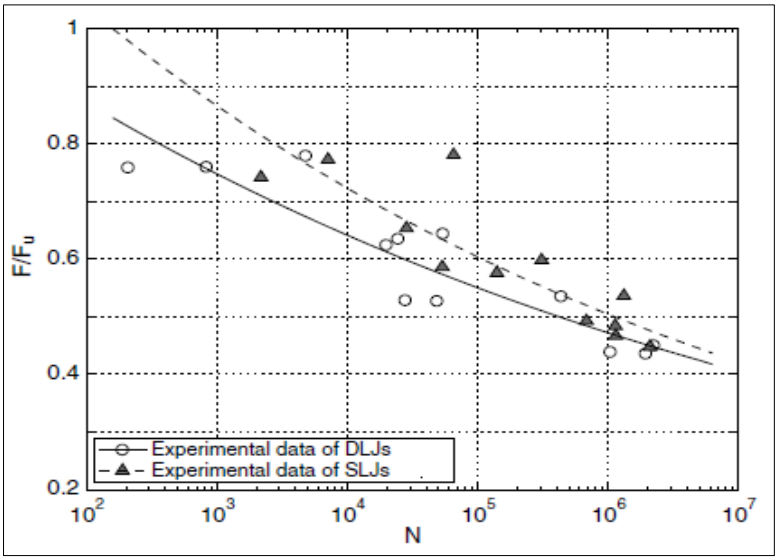

Figure 5: S-N curves for DLJs and SLJs (Zhang, et al., 2008).

Stress-life method was again used in the investigation done by Sarfaraz (2011). The Power law equation was used to simulate the relationship between fatigue life and cyclic loads in the work done by Sarfaraz et al (2011). The S-N curve under R = -1 showed the highest slope between the three tested R-ratios. The same curve showed the highest slope for tension-tension dominant region (mean stress ≥ 0) when Sarfaraz et al (2012) included six more R-ratios in the tests. See Figure 6.

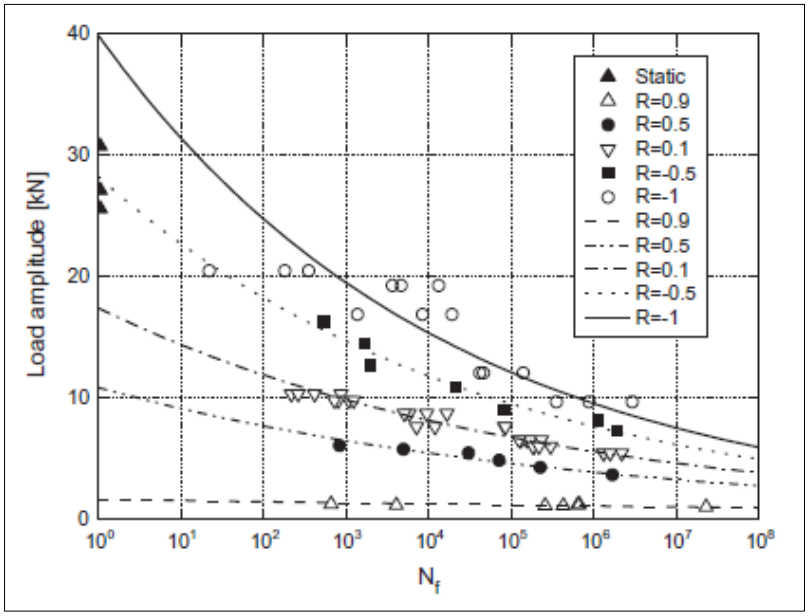

Figure 6: S-N curves during tension-tension (Sarfaraz, et al., 2012).

The fatigue strength of double lap joints decreases under higher R-ratios at tensile and tensile-dominated loading, and decreases under lower R-ratios at compression and compression-dominated loading (Sarfaraz, et al., 2012).

Harris (2003) explains that, in a structure that consists of adhesively bonded joints, maximum load or load amplitude versus number of cycles are used to represent fatigue life - instead of maximum stress or strain amplitude versus number of cycles. This is because of highly non-uniform stress distributions along the bond line. The stress distribution is rather complicated and the state of stress tends to be multi-axial, according to Harris (2003). It is, however, possible to determine average stress values on the overlap as applied load divided by the overlap area. This resulting stress will be significantly lower than the actual values of stresses (consisting of peel and shear) acting on the joint overlap.

2.7. Mean and amplitude stress effect on fatigue life

For any given number of cycles, stress amplitude, mean stress and R-ratio are the required load parameters to construct a constant life diagram (Vassilopoulos, et al., 2010). These parameters obey the relationship given in Equation 4. Any set of these two parameters is therefore enough to describe the fatigue behavior, since the third one can be calculated through this equation. The case where R = 1 refers to static tensile or compressive loading. Fatigue loading data is normally plotted on the mean-amplitude plane where the constant life line describes the behavior of the material in response to the employed fatigue parameters. Linear interpolation between known values of mean and amplitude stress can be used to produce linear (or piecewise linear) or non-linear curves fitting for different parts of the σ_m-σ_a plane. The curves can be fitted for the entire range of values of mean stress between the ultimate compressive strength (UCS) and ultimate tensile strength (UTS). There is, however, no rational method for the selection of the load parameters, according to Vassilopoulos et al (2010).

Boerstra (2006), however, remarks that fatigue data of the material should consist of a number of cycles to failure, and a specific combination of mean and amplitude stress. The data can be presented as a three-dimensional figure composed of S-N curves and constant-life (CL) lines. The S-N lines are parallel to the N-axis, and CL lines are in the $\sigma_m - \sigma_a$ plane. Harris (2003) also explains that, in order to use stress and life information from the S-N curve, a procedure is used to cross plot the data to show the expected life for a given combination of mean and amplitude stress. The cross plot is called the constant life diagram and reflects the combined effect of mean and amplitude stress on the fatigue life of the examined material - as stated by Vassilopoulos et al (2010) . The main components of the diagram include mean stress (σ_m), amplitude stress (σ_a), R-ratios and fatigue life curves.

The stresses can be calculated using the equations below, according to Harris (2003):

$$\sigma_m = \frac{\sigma_{max}+\sigma_{min}}{2} \quad 2$$

$$\sigma_a = \frac{\sigma_{max}-\sigma_{min}}{2} \quad 3$$

Where σ_{max}, σ_{min} are maximum and minimum applied cyclic stresses (loads) respectively. Using the chosen ratio, the relationship between the mean and amplitude stress can be determined by the following equation:

$$\sigma_a = \left(\frac{1-R}{1+R}\right)\sigma_m \quad 4$$

The constant life diagram (CLD) is then plotted on the mean-amplitude (σ_m-σ_a) plane as radial lines emanating from the origin of the coordinate system. Each of these radial lines represents a single S-N curve under the chosen R-ratio (Sarfaraz, et al., 2012). Fatigue life curves are formed by joining together (in a linear or non-linear way) the points that correspond to the same number of cycles on these R-ratios lines. The CLD also offers a predictive tool for the estimation of the fatigue life of the material under loading patterns for which no experimental data exists, according to Vassilopoulos et al (2010).

The CLD established by Sarfaraz et al (2011) showed that the fatigue strength of the examined joints were higher under R = -1; this corresponded to what was obtained from the S-N curves. The diagram was symmetric with respect to the zero mean load axis (R = -1). However, the second study on the same type of joint established a non-symmetric CLD when more R-ratios were tested. The CLD in the second study produced, as its highest points, the data corresponding to the S-N curve under R = -2, as shown on Figure 7 (Sarfaraz, et al., 2012).

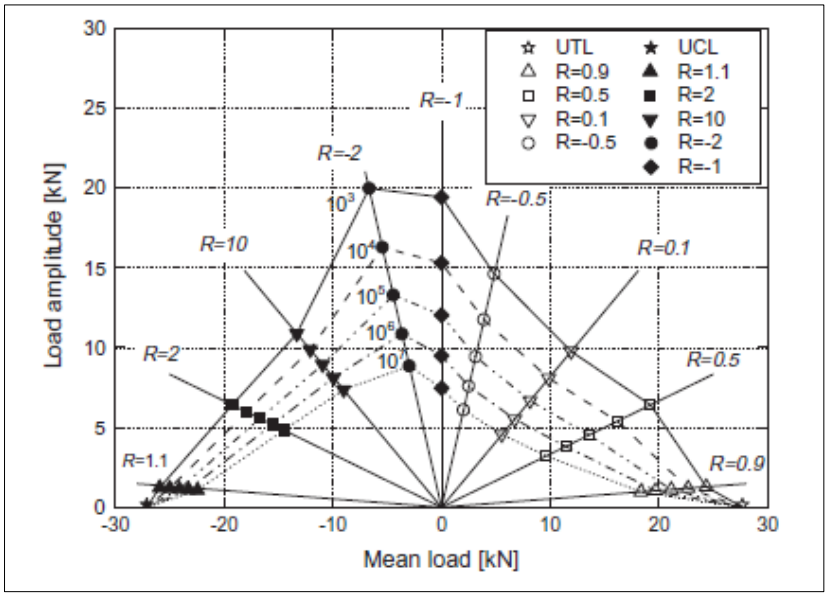

Figure 7: Mean-amplitude stress (Sarfaraz, et al., 2012)

All fatigue life curves converged to both ultimate tensile and compression loads on the zero-amplitude axis for both of these studies.

Models can be developed to mathematically simulate and predict fatigue behavior of these joints under various loading conditions. The next section discusses the specific theories that are associated with modeling fatigue behavior of composites, in terms of mean and amplitude stresses.

2.8. Modeling of mean and amplitude stress

The conventional method that is normally used to plot the relationship between mean and amplitude stress at any constant life is the Goodman relation (Boerstra, 2006). The diagram can also be used to predict fatigue life of the material under fatigue loading conditions for which no experimental data exists. However, more sophisticated methods/models with more parameters may be necessary in order to improve the accuracy of these predictions, according to Boerstra (2006). This section therefore discusses six constant life diagram formulations that are normally used to predict and simulate fatigue behavior of composite materials. The aim of these models is to minimize the amount of experimental data required. The outcome of the application of these models from other studies is also discussed. In all these studies, the predictive accuracy of each model was evaluated by comparing the predicted fatigue data with the derived experimental data. The statistical distance (r^2-value) between the predicted and experimentally derived σ_a-N curve was used as an accuracy tool for each model. A high r^2-value (close to 1) means the prediction accuracy of the model is good, while poor accuracy is indicated by a low r^2-value (close to zero).

2.8.1. Triangular modeling

The model can be used to predict fatigue behavior by using a single existing S-N curve that should be experimentally derived. Other S-N curves are therefore determined from the existing one by simple calculations (Vassilopoulos, et al., 2010). Each constant life on the σ_a-σ_m plane can be determined by:

$$\left(\frac{\sigma_a}{\sigma_0}\right) + \left(\frac{\sigma_m}{\sigma_0}\right) = N^{-\frac{1}{k}} \qquad 5$$

Where k and σ_0 are parameters of the power law equation that describes the S-N curve for the single selected R-ratio. The study by Vassilopoulos et al (2010), for example, used the S-N curve under R = -1 for the construction of this CLD. The model was found to be less accurate when comparing the predicted data to the experimentally derived data. The r^2-value proved a good accuracy for this model in the work done by Sarfaraz et al (2012). The predictive accuracy of the model was very high for S-N curve under R = -0.5. The triangular model is therefore a generalized form of the Goodman diagram, according to Passipoularidis & Philippidis (2008).

2.8.2. Piecewise linear modeling

The model is based on calculating unknown S-N curves through linear interpolation between the known fatigue and static data. The CLD therefore requires a limited number of experimentally derived fatigue data together with the ultimate tensile and compressive stresses (Vassilopoulos, et al., 2010). The following analytical expressions are used for each region of the constant life diagram to interpolate between unknown and known fatigue data:

- If the unknown R-ratio (S-N curve to be predicted) is in the tension-tension region, the interpolation is done between R = 1 data and the known R-ratio data (experimentally derived) to calculate the unknown data by:

$$\sigma_{a'} = \frac{UTS}{\left(\frac{UTS}{\sigma_{a,1TT}}\right) + r' - r_{1TT}} \qquad 6$$

  Where:

  UTS = Ultimate tensile stress of the material

  $\sigma_{a'}$ = Unknown stress amplitude

  $\sigma_{a,1TT}$ = Experimentally derived stress amplitude

  $r' = (1+R')/(1-R')$ where R' is the unknown R-ratio

r_{1TT} = *(1+R)/(1-R)* where R is the known R-ratio

- If R is between any known R-ratios, R_i and R_{i+1}, the interpolation is done through

$$\sigma_a' = \frac{\sigma_{a,i}(r_i - r_{i+1})}{(r_i - r')\left(\frac{\sigma_i}{\sigma_{i+1}}\right) + (r' - r_{i+1})} \qquad 7$$

With:

r_i = *(1+Ri)/(1-Ri),* R_i is the first known R-ratio

$\sigma_{a,i}$ is the first known stress amplitude at R= R_i

- If the R-ratio is in the compression-compression region, the interpolation is done between R = 1 data and the known R-ratio data (experimentally derived) to calculate the unknown data by:

$$\sigma_{a'} = \frac{UCS}{\left(\frac{UCS}{\sigma_{a,1CC}}\right) - r' + r_{1cc}} \qquad 8$$

Where:

UCS = Ultimate compressive stress

$\sigma_{a,1CC}$ = Experimentally derived stress amplitude

r_{1CC}= *(1+R)/(1-R)* where R is the known R-ratio

Five experimentally derived S-N curves (five R-ratios) were used in the work done by Vassilopoulos et al (2010) to predict fatigue data under R-ratios for which no experimental work exists. A high accuracy (r^2-value) was established when the model was applied. The model provided more accurate predictions when Sarfaraz et al (2012) employed three experimentally derived R-ratio data to predict fatigue data for which no experimental data exists. The accuracy of the model was, however, poor under high mean loads.

2.8.3. Harris modeling

Harris (2003 b) proposed the following model:

$$\frac{\sigma_a}{UTS} = f\left(1 - \left(\frac{\sigma_m}{UTS}\right)\right)^u \left(\left(\frac{UCS}{UTS}\right) + \left(\frac{\sigma_m}{UTS}\right)\right)^v \qquad 9$$

Where *UTS* and *UCS* are static tensile and compressive strengths of the material, while mean and amplitude stresses are denoted by σ_m and σ_a respectively. *f, u* and *v* are adjustable parameters which

are also functions of fatigue life. The parameter *f* controls the height of the curve while *u* and *v* determine the shape of the two wings of the bell-shaped curve; *u* relates to the slope of the curve in the tensile region and *v* to the slope of the curve in the compression region. These parameters were found to depend linearly on the logarithm of fatigue life as follows:

$$f = A_1 logN + B_1 \qquad 9a$$

$$u = A_2 logN + B_2 \qquad 9b$$

$$v = A_3 logN + B_3 \qquad 9c$$

The coefficients, *Ai* and *Bi for i =1 to 3,* can be determined by fitting the above equations to the available experimental data. Application of this model requires more computational effort and its precision is based on the accurate prediction of model parameters (Sarfaraz, et al., 2012). Vassilopoulos et al (2010) found the model to be sufficiently accurate in prediction of fatigue data under R = 0.8 and R = -0.5. The use of this equation provided more accurate predictions than those produced by the piecewise linear model, according to the study done by Sarfaraz et al (2012). Some deviations between the derived constant life lines and the experimental data used for prediction could be seen. Harris (2003), for example, discovered mean percentage deviation of 6% between the experimental derived and predicted fatigue stress values at R = 0.1. Passipoularidis & Philippidis (2008) also discovered that the use of the Harris model produces more accurate results than using the Triangular model.

2.8.4. Kawai modeling

Kawai & Koizumi (2007) developed a formula that can be used for the prediction of an asymmetric nonlinear constant life diagram. The application of the equation is based on a single experimentally-derived S-N data set (Critical S-N curve) in addition to static strengths in both tension and compression. The following formula is used:

$$\frac{{\sigma_a}^\gamma - \sigma_a}{{\sigma_a}^\gamma} = \left(\frac{\sigma_m - {\sigma_m}^\gamma}{UTS - {\sigma_m}^\gamma}\right)^{2-\varphi_\gamma} for\ \ UTS \geq \sigma_m \geq {\sigma_m}^\gamma \qquad 10$$

$$\frac{{\sigma_a}^\gamma - \sigma_a}{{\sigma_a}^\gamma} = \left(\frac{\sigma_m - {\sigma_m}^\gamma}{UCS - {\sigma_m}^\gamma}\right)^{2-\varphi_\gamma} for \quad UCS \leq \sigma_m \leq {\sigma_m}^\gamma \qquad 11$$

Where ${\sigma_m}^\gamma$ and ${\sigma_a}^\gamma$ is mean and amplitude stress of the experimentally-derived fatigue data respectively (critical R-ratio). The formulation therefore depends on whether the position of mean

stress is in the tensile or compressive region. φ_γ symbolizes the ratio between fatigue stress of the critical S-curve and the absolute maximum stress value between UTS and UCS.

$$\varphi_\gamma = \frac{{\sigma_{max}}^\gamma}{\sigma_B} \qquad 11a$$

Where:

σ_B is the abolute maximum value between UCS and UTS

${\sigma_{max}}^\gamma$ is fatigue stress from existing experiments (critical R-ratio)

The work done by Kawai & Koizumi (2007) observed a good accuracy between the predicted and experimentally-derived fatigue data for various fatigue loading conditions (tension-tension, compression-compression and tension-compression). Using S-N under R = -1 as critical, Sarfaraz et al (2012) obtained a CLD with convex constant life curves when this model was applied. The study done by Vassilopoulos et al (2010) concurs, by saying the model should be applicable to any S-N curve other than the critical S-N for its accuracy to be assumed reliable. Any S-N curve should therefore be applicable for good prediction accuracy, not only the critical R-ratio. The model also cannot be used to evaluate random variable amplitude fatigue loading with continuously changing mean and amplitude.

2.8.5. The Multi-slope modeling (Boerstra)

A modified Gerber diagram was proposed by Boerstra (2006) as formulation of CLD for randomly chosen fatigue data. The exponent in the Gerber equation is replaced by two variables that represent tension and compression. The formulas are given as:

$$\sigma_{ap} = \sigma_{AP}\left(1 - \left(\frac{\sigma_m}{UTS}\right)^{\delta T}\right) for\ \sigma_m > 0 \qquad 12$$

$$\sigma_{ap} = \sigma_{AP}\left(1 - \left(\frac{\sigma_m}{UCS}\right)^{\delta C}\right) for\ \sigma_m < 0 \qquad 13$$

The parameters, δT and δC, are two shape parameters of the CLD curves in tension and compression respectively. The σ_{ap} in the formulas is stress amplitude for a referenced number (N_p) of cycles while σ_{AP} an apex stress amplitude when $\sigma_m = 0$ (Vassilopoulos, et al., 2010). This model can be applied to any fatigue data with changing mean and amplitude stress values, since the R-ratio (S-N curve data) is not considered as parameter. A further expansion of the above equations

is made by introducing variable slopes of S-N lines with mean stress values. Linear or exponential relation can be used for modeling the slope, as shown below:

$$m = m_0\left(1 - \frac{\sigma_m}{D}\right) \qquad 13a$$

$$m = m_0 e^{\left(-\frac{\sigma_m}{D}\right)} \qquad 13b$$

Where:

m_0 is the measure of the slope of S-N line at $\sigma_m = 0$

D represents the skewness parameter

Five parameters, m_0, D, Np, δT and δC must therefore be solved to construct the CLD. Estimation of these parameters requires an optimization process that gives a short distance between each experimental value of mean stress and its predicted value. Vassilopoulos et al (2010) explain that estimation of parameters requires a multi-objective optimization process. The use of these parameters makes the Boerstra modeling very flexible and gives it the ability to accurately predict fatigue behavior of a large number of different material systems, as explained by Sarfaraz et al (2012).

Boerstra (2006) found the most reliable resemblance between experimental fatigue data and fatigue data predicted by this model. This model was also one of the models with sufficient accuracy in the work done by Vassilopoulos et al (2010). The average accuracy of this model was one of the highest (r^2-value = 0.748) among the examined models, in the study done by Sarfaraz et al (2012).

2.8.6. Kassapoglou modeling

A method to model load against number of cycles was proposed by Kassapoglou (2007). The method is based on assuming the number of cycles to failure as a function of probability of failure for any given cycle. Probability of failure for any given cycle is assumed to be constant and the same as the probability of failure under static loading, regardless of the number of fatigue cycles applied. The assumption that, statistically, distribution of failure under static loading can be used to describe fatigue failure oversimplifies this model, according to Vassilopoulos et al (2010, p. 662). However, the model does not need any fatigue tests or any experimentally derived parameters (Kassapoglou, 2007). This model is given by the following equations for the calculation of maximum and minimum loads as functions of number of cycles:

$$\sigma_{max} = \frac{\beta_T}{N^{\frac{1}{\alpha T}}} \quad for\ 0 \leq R < 1 \qquad 14$$

$$\sigma_{max} = \frac{\beta_C}{N^{\frac{1}{\alpha C}}} \quad for\ R > 1 \qquad 15$$

$$N = \frac{1}{\left(\frac{\sigma_{max}}{\beta_T}\right)^{\alpha T} + \left(\frac{\sigma_{min}}{\beta_C}\right)^{\alpha c}} \quad for\ R < 0 \qquad 16$$

$$N = \frac{1}{\left(\frac{\sigma_{R=-1}}{\beta_T}\right)^{\alpha T} + \left(\frac{\sigma_{R=-1}}{\beta_C}\right)^{\alpha c}} \quad for\ R = -1 \qquad 17$$

The maximum and minimum stress values therefore need to be calculated first before using Equation 3 to determine amplitude stress. Mean stress can be calculated using either Equation 2 or 4. The $\sigma_{R=-1}$ in the equations denotes stress amplitude under R = -1 while parameters α, β in each equation are scale and shape of a two-parameter Weibull distribution that describes the static loading data in tension and compression. Symbol *T* and *C* denote tension and compression respectively. The model proved to be inaccurate for predicting fatigue data of most of the materials examined by Vassilopoulos et al (2010) . Although the model accuracy is a concern, it can be used as a piecewise nonlinear model.

2.9. Testing methods and standards for fatigue loading

The type of damage and accumulation in composite material depends directly on the type of fiber, the matrix, geometry and specimen shape, as well as on the level, type and direction of the applied stress (Harris, 2003). For the purposes of test-data credibility, it is necessary to give full details regarding the material, fabrication, specimen conditioning and test method used.

2.9.1. Material and specimen fabrication

Some of the material characterization standards, according to Harris (2003) include:

- Measurement of fiber volume fraction using:
    i. ISO 1172-glass fiber based systems
    ii. ISO/DIS 14127-carbon fiber based systems
- Assessment of cure by measurement of the glass-transition temperature using:
    i. ISO 6721(11)-dynamic mechanical properties
    ii. ISO 11375-differential scanning calorimeter

Harris (2003) went further by specifying ISO 1268 (2005) as an appropriate standard for manufacturing test plates. The standards discuss different methods in which test plates can be manufactured. These methods include filament winding, pultrusion, and prepreg manufacturing. The plates can then be machined to conform to the required specifications.

The ASTM (1996) standard test method for strength properties of double lap shear adhesive joints (by tension loading) recommends that test plates be wide enough to be cut into five specimens. The cutting operation should be done in such a way that it will not overheat, damage the plates by exposure to coolants, or mechanically damage the bonded joints. The test specimen should conform to one of the following alternatives types of specimen configurations, as show on Figure 8 and Figure 9 below:

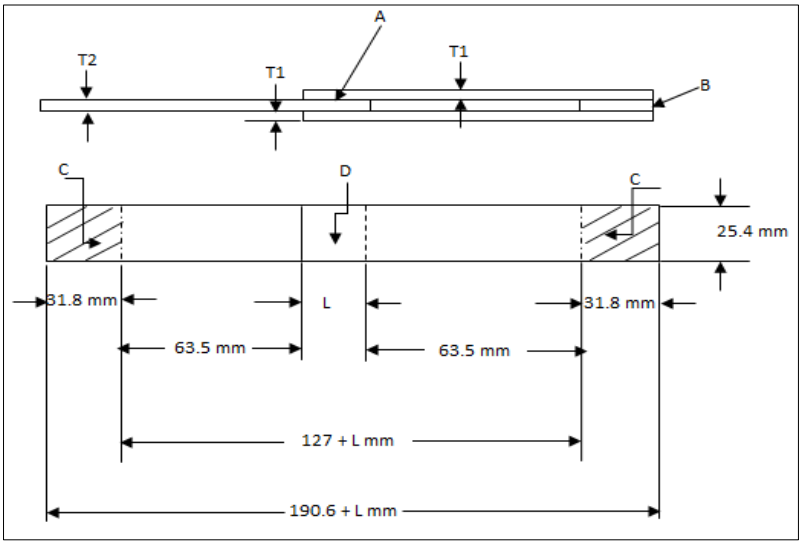

Figure 8: Type A Specimens (ASTM, 1996)

Where:

T1 = 1.6 mm

T2 = 3.2 mm

A = Overlap thickness

B = Spacer

C = Test grip area

D = Shear area

L = Overlap length

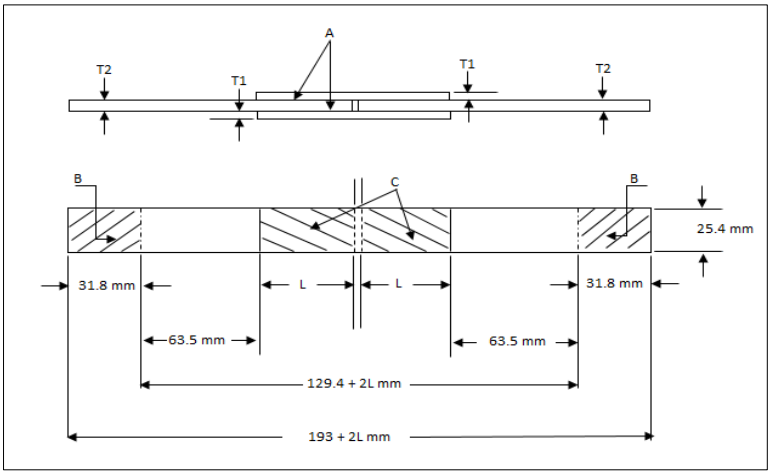

Figure 9: Type B specimens (ASTM, 1996)

Where:

T1 = 1.6 mm

T2 = 3.2 mm

A = Overlap thickness

B = Test grip area

C = Shear area

L = Overlap length

Since the yield point of the adherent material cannot be exceeded in tension testing, the standard notes that the overlap length (L) varies with the thickness and type of adherent material used. The overlap length also depends on the strength of the adhesive being investigated, and may be computed using the following equations:

$$L = \frac{F_{ty} t_1}{\tau} \quad \text{and} \qquad 18$$

$$L = \frac{F_{ty} t_2}{2} \qquad 19$$

Where:

t_1 = T1

t_2 = T2

F_{ty} = yield point of the adherent material in MPa

τ = 150 % of the estimated average shear strength of the adhesive bond in MPa.

The work done by Sarfaraz et al (2011), for example, tested Type A specimens to investigate fatigue behavior of adhesively-bonded GFRP joints under different R-ratios. The study by Zhang et al (2008) comprised Type B specimens in studying stiffness degradation and fatigue life prediction of adhesively-bonded GFRP joints under R = 0.1.

2.9.2. Test methods

Harris (2003) explains that the key requirement of any fatigue test machine is to be able to perform different test modes (e.g. tension, compression, flexure or shear) at a high number of cycles. The machine should also have the ability to avoid excessive deflections and any resonant frequency of the machine or loading train should exceed the applied test frequency. The machine should be selected so that the breaking load of the specimens falls between 15% and 85% of the full load scale capacity of the machine, according to ASTM standard (1996). The standard goes further by citing the capacity of rate of loading from 8.27 MPa to 9.65 MPa, as one of the requirements for the test machine.

Harris (2003) also discusses various factors that affect fatigue testing, and hence should be considered, regarding testing method. These factors include the dependence of fatigue properties on the following:

- Rate of loading and the self-generated heat.
- The effect of buckling of specimens under compression loads.
- The effect of grip failures.
- Loading point stress concentrations and fretting.
- Effect of applied test temperature and stress concentrations.

Various standards exist for coupon fatigue testing (Harris, 2003). One of the standards, EN ISO 13003 (2003) discusses determination of fatigue properties under cyclic conditions. Factors such as the effect of rate dependence, self-generated heat, and failure are explained in this standard.

The ASTM (2002) standard test method for tension-tension fatigue of polymer matrix composite materials discusses two procedures that each defines a different control parameter for the fatigue testing method. The load (stress) is used as a test control parameter in the first procedure where the machine is controlled in such way that the test specimen is subjected to repetitive, constant amplitude cycles. The sample is loaded between minimum and maximum in-plane axial load at a specified frequency. The number of load cycles to failure can be determined for a specific load

(stress) ratio and maximum stress. The test control parameter may be described using either the applied load or calculated stress as a constant amplitude fatigue variable.

The second procedure uses the strain in the loading direction as the test control parameter and the machine is controlled in such a way that the specimen is subjected to repetitive, constant amplitude strain cycles. The sample is therefore loaded between minimum and maximum in-plane axial strain at a specified frequency. In this case, the number of strain cycles at which the sample fails can be determined for a specific strain ratio and maximum strain. The test control parameter can be described using the strain in the loading direction as a constant amplitude fatigue variable.

The work done in both Sarfaraz (2011) and Sarfaraz (2012) uses the first procedure for fatigue testing of sample joints. Other standards which can be considered for fatigue testing include:

- Standard test method for mode I fatigue delamination growth onset of unidirectional fiber reinforced polymer matrix composites (ASTM D 6115)
- Mode II fatigue delamination crack growth
- Bearing Fatigue (new ASTM work item)

2.9.3. Precision of data

The International Standard Organization (ISO, 1994) describes accuracy of measured results as trueness and precision. Trueness is defined as the closeness of agreement between the arithmetic mean of a large number of test results and true or accepted reference value. The ASTM standard (2006) also describes trueness as a general term used to express the closeness of test results to the "true" value or the accepted reference value. The trueness of measured data can therefore only be determined if a true or accepted reference value exists.

Precision, on the other hand, is defined by International Standard Organization (ISO, 1994) as the closeness of agreement between test results obtained from experimental investigation. The need to consider "precision" arises because tests performed on identical materials and identical circumstances do not yield identical results. This is because of the unavoidable random errors inherent in every measurement procedure, meaning variability has to be taken into account in practical interpretation of measurement data. Harris (2003) concurs that there is therefore a requirement to provide the precision of measured or experimental data. Variability of experimental data may be due to difference in material batch, testing by different operators, or testing on different machines at different times. There may also be uncertainties associated with a test method regarding accuracy of load or dimensional measurements. Harris (2003) then explains that the

precision of a test method is determined through experimental validation actions reported as repeatability and reproducibility. Conditions for both repeatability and reproducibility are shown below in Table 2 below:

Table 2: Precision conditions

Repeatability conditions	Reproducibility conditions
Same method	Same method
Identical material	Identical material
Same laboratory	Different laboratory
Same operator	Different operators
Same equipment	Different equipment
Different time intervals	

Repeatability is therefore defined as the closeness of agreement between results obtained using the same method, the same material and under the same conditions (same operator, same equipment, same laboratory and at different intervals of time). Harris (2003) also explains repeatability as the value below which the absolute difference between two single test results obtained under repeatability conditions is expected to lie within a probability of 95%. Repeatability may be expressed quantitatively in terms of the distribution characteristics of the results. According to Taylor & Kuyatt (1994), the measure of repeatability is the standard deviation qualified with the term, "repeatability" and is known as repeatability standard deviation.

The ASTM standard (ASTM, 2006), uses the following equation to calculate repeatability standard deviation:

$$s_r = \sqrt{\sum_1^p s^2/p} \qquad 20$$

Where:

p is the number of different time intervals.

s is standard deviation of test results from the arithmetic average value during each time interval.

s_r is repeatability standard deviation.

Taylor & Kuyatt (1994) describe reproducibilty as the closeness of the agreement between the results obtained with the same method and identical test material, but under different conditions (different operators, different equipments and laboratries, and different time intervals). Reproducibility may also be expressed quantitativily in terms of the distribution charateristics of

the results. The measure of reproducibility is the standard deviation qualified with the term, "reproducibility" and is known as reproducibility standard deviation.

The ASTM standard (ASTM, 2006), uses the following equation to calculate reproducibility standard deviation:

$$s_R = \sqrt{\left(s_y\right)^2 + \frac{(s_r)^2(n-1)}{n}} \qquad 21$$

Where:

s_r is repeatability standard deviation calculated in Equation 20.

n is the number of test results obtained per time interval and

$$s_y = \sqrt{\sum_1^p d^2/(p-1)} \qquad 21a$$

with $d = \omega - \varpi$, where ω is arithmetic average of test results for each time interval and

$$\varpi = \sum_1^p \frac{\omega}{p} \qquad 21b$$

A repeatability exercise is therefore carried out within an experimental study and reproducibility is carried out by comparing with other experimental studies. The standard also explains that repeatability and reproducibility standard deviation provide an inverse measure of precision; high measure of repeatability and reproducibility standard deviation implies low (or poor) precision of test results. Repeatability and reproducibilty are therefore the significant requirements for precison of experimental data. The trueness of test results (as described above) can only be proved if true or accepted reference values of repeatability and reproducibilty exist.

2.10. Conclusion

A need exists for improving the consistency and value of a fatigue database of bonded joints. Harris (2003) mentions that the fatigue behavior of composite laminates is affected by various factors, such as fiber type (fabric orientation), the matrix and environment, hybrid composites, short fiber composites, interleaving, and loading conditions. The fatigue properties of adhesively-bonded laminates joints may then be affected by factors such as fabric orientation of fibers in the composite laminates layer, forming process of the laminates, adhesive system used for bonding, loading conditions, and others. Since manufacturing and testing methods of composites (and

therefore of composites bonds) is not conventionally defined, a research opportunity arises because more studies (and hence more fatigue testing) are needed to derive an extensive experimental database.

An experimental investigation into fatigue testing of adhesively-bonded double strap lap joints of GFRP can therefore be established to study the behavior of these joints. The present study will therefore employ Type B specimen as specified by ATSM (1996) for the configuration of joint samples. The joint configuration for the samples are normally used by Jonker Sailplanes and therefore of specific interest to this study. The first procedure provided by ATSM (2002) will be followed for constant amplitude loading of these joints. Testing will be done at various chosen fatigue loading conditions so that enough regions/sections of the constant life diagram are covered. Reproducibility analysis will be carried out if comparable data from other investigations exists; otherwise curve-fitting will be established to compare the shape of the resulting experimental curves to the curves established from other investigations. The precision of measured fatigue data will be validated through repeatability analysis. Failure modes for the type of joints examined will also be investigated. Stress-life method will be used to describe fatigue life in number of cycles to failure for various loading conditions. The effect of mean and amplitude stress on fatigue life will be explored through a constant life diagram. Modeling of mean and amplitude will be established by employing four conventional mathematical formulas, together with the first four model equations discussed above. The accuracy of these models will be evaluated by comparing the experimental data with the data given by each model.

CHAPTER 3: EXPERIMENTAL METHODOLOGY

3.1. Introduction

The present work aims to study fatigue behavior of double strap lap joints of GFRP under constant amplitude loading. This chapter introduces the experimental methodology executed for this study. The experimental methodology was designed in such a way that the experimental data covers at least the entire lifetime range between ten and one million cycles. Six load levels with at least three specimens under each load level were investigated per stress-ratio. The lifetime range and load levels were selected in order to cover as many scenarios of loads, and expected lifetimes of a component, as possible. Seven stress-ratios were selected so that as many regions as possible in the constant life diagram are covered. All experimental tests (static and fatigue) were carried out on an MTS landmark servo-hydraulic testing station under laboratory conditions (26 ± 5 ^{o}C and 50 ±10% relative humidity) and load control. Static tests were carried out so that the ultimate loads could be determined; percentages of these ultimate loads ranging from 40-90% were used as load levels in fatigue loading. Using the ASTM (2002) discussed in section 2.9 as guideline, fatigue tests were performed also under load control at a specified constant sinusoidal waveform and frequency. The tests under three R-ratios; R = 0.1, R = -1 and R = 10 were carried out at 4 Hz. Samples under R = 0.5, R = -0.5, R = -2 and R = 2 were tested at frequency of 15 Hz.

Section 3.2 discusses in detail the material selected for joint samples. The geometry and fabrication of the specimen is discussed in Section 3.3. Section 3.4 discusses experimental setup and testing procedure. Section 3.5 then concludes the chapter.

3.2. Material

Adhesively bonded double strap lap joints composed of GFRP laminates were tested. The material and joint configuration for the samples are normally used by Jonker Sailplanes and therefore of specific interest to this study. Both the inner and outer laminates of the joint consisted of E-glass fiber of twill woven 92125 fabric. The binder or matrix used was a laminating epoxy that consists of L285 resin system and L287 slow hardener. The adhesive used for bonding consisted of a mixture of this laminating epoxy together with cotton flocks and cab-o-sil additives. The use of these additives improves the viscosity and gap-filling capabilities of the epoxy. The mixing of resin and hardener for laminating epoxy was done according to workshop standards followed by AMTS standard workshop practice (2010). Mixing sheets were provided for mixing laminating epoxy as well as epoxy adhesive. In general, the workshop standard practices provided by AMTS were followed in building the samples (See Appendix E).

3.3. Specimen geometry and fabrication

The general design of the sample was carried out following the Type B specimen form and dimensions provided by ASTM (1996). Initial static testing of samples also provided guidelines for final specimen design. Determination of the overlap length was based on Equation 18 and 19, as recommended by the standard. 200% of the estimated average shear strength of the adhesive bond was used, instead of 150% as recommended by the standard. The yield point of the adherent material and the estimated shear strength of the adhesive were taken from the technical data sheet provided by Hexion specialty chemicals (Hexion, 2006) as 500 MPa and 42 MPa respectively. Table 3 below summarizes design parameters used to calculate the overlap length of the examined joint using Equation 18:

Table 3: Design parameters

Parameter	Value	Unit
Adhesive shear strength	42	MPa
Adherent yield point	500	MPa
t_1	1.5	mm

A double strap lap joint configuration of 192 mm length and width of 25 mm was used, as shown below on Figure 10. Adhesive thickness of 2 mm was chosen for fatigue loading tests after initial investigation of the effect of adhesive thickness on static strength of the examined joint (see Figure 12 in section 4.1).

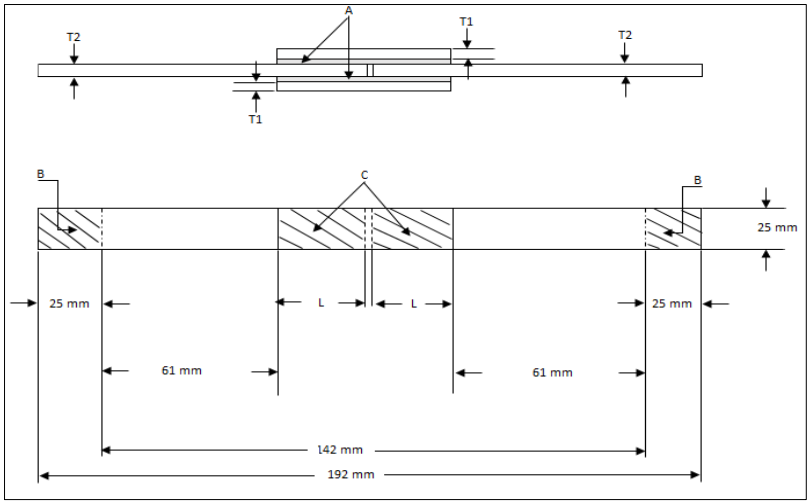

Figure 10: Double lap strap joint

Where:

T1 = 1.5 mm

T2 = 3 mm

A = 2 mm

B = 25 x 25 mm^2

C = 2 x 25 x 9 mm^2

L = 9 mm

The glass laminates of the joint were produced through a hand wet lay-up process. Wet lay-up process is a method of making a reinforced part by applying an epoxy system (mixture of resin and hardener) to a fiber or fabric of glass, carbon or Kevlar, and so on. Twelve layers of glass fabric were used for the inner GFRP laminate, while six were used for the outer GFRP laminate. The lay-up schedule (orientation) of the fabrics in the single glass fiber laminate was $0/90^0$. All bonding surfaces were abraded with a sand paper and degreased with acetone before manufacturing.

3.4. Experimental set-up and testing

All experimental tests were performed on an MTS landmark servo-hydraulic testing station available at North-West University laboratory, as shown by the first picture in Figure 11. The machine uses the modern technology of servo-hydraulics and consists of advanced control systems and MTS software. The load frame fitted in the machine can induce about 100 kN of load.

Figure 11 below illustrates a typical sample during the test and after failure. Failure is considered as degradation or damage in the gauge section of the specimen during the application of the load.

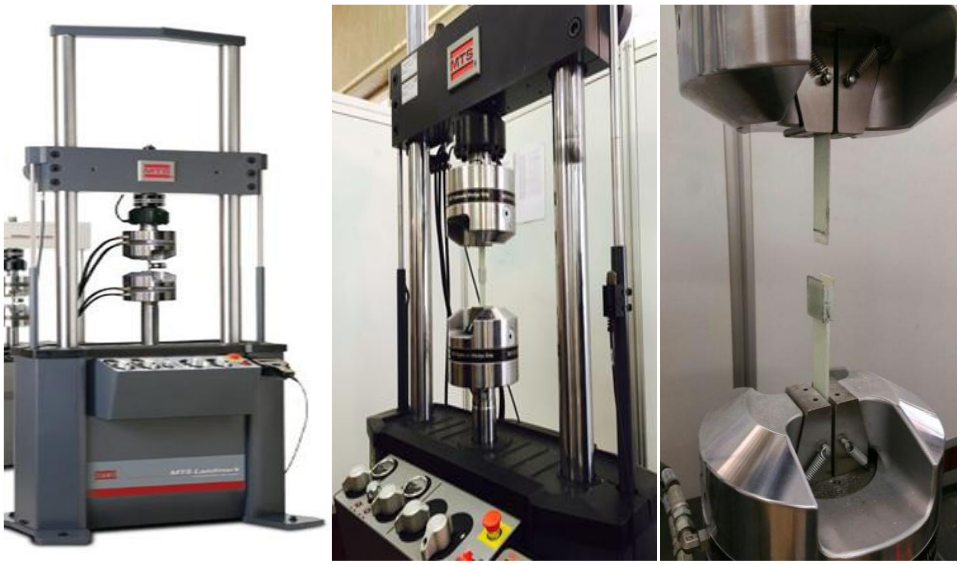

Figure 11: Experimental testing

The acceptable failure mode for the adhesive in these tests was when the break occurs following substrate or adhesive failure, as explained in section 2.3. Detailed instructions regarding experimental set-up and loading are given in Appendix F.

3.4.1. Static testing

Machine templates for both static tension and compression tests are available on the machine computer. Five samples were tested to assess the effectiveness of the adhesive system. Four samples were then tested under static tensile load and another four were tested in static compressive load, in order to assess the joints reliability in terms of strength (see Appendix F for details of set-up and testing). The following steps were followed during these tests:

- The thickness and width were measured at three gauge sections (bond area in Figure 10) using a Vernier so that average cross sectional area of the specimen could be calculated.
- The speed of testing was set to constant strain rate of around 2 mm/min.

- The test was then started once all input parameters are inserted, specimen is placed in the grips, proper alignment is achieved and grips are tightened. The acceptable break/failure is when the specimen fails at the gauge section.
- The load [kN] versus displacement [mm] was recorded during the test.
- The average peak loads of four samples tested in tension and four samples tested in compression were then taken as ultimate tensile and compression loads. Variation of strengths between the two testing modes was 0.35 kN (less than 1 kN), thus the reliability of specimen was good for the two loading modes. This small variation therefore validates chosen specimen configuration for testing. Ultimate load in tension was the highest and therefore taken as ultimate load for fatigue loading. Failure modes in static testing were also observed.

3.4.2. Fatigue testing

As per a key requirement for any fatigue test machine, stated by Harris (2003), the machine is capable of performing different tests modes (e.g. tension, compression, flexure or shear) at a high number of cycles and frequencies. Two frequencies of 4 Hz and 15 Hz were selected for the tests in order to make sure that the machine did not lag behind and produce undesired peak loads. A frequency of 15 Hz was selected after initial monitoring of temperature on four samples was carried out (see Appendix F). These tests were performed to make sure that the test specimen did not experience a 10 ^{0}C increase in temperature and therefore does not generate/accumulate heat during the actual fatigue testing. The temperature difference of 0.2 ^{0}C was obtained from these tests, meaning fatigue tests can be performed safely at this frequency and other lower frequencies, without generating heat and therefore degrading the material properties of the sample. Excessive deflections of the machine were therefore avoided since these applied frequencies were lower than resonant frequency of the machine.

As specified by ASTM (2002), all fatigue tests were conducted using load as a control parameter. Program templates for fatigue testing under different loading conditions were programmed by using Multipurpose Elite software program. Appendix F discusses the layout of this software and fatigue testing in detail. The following section summarizes the steps followed in fatigue testing of each sample:

- The thickness and width were once again measured at three gauge section (bond area in Figure 10) using a Vernier so that average cross sectional area of the specimen could be calculated.

- The ultimate load calculated after conducting static tests was used as an input parameter for testing.
- Percentage load levels of ultimate load from 40% to 90%, with at least three specimens per level, were inserted also as input parameters.
- The frequencies selected were 4 Hz for samples at R = 0.1, R = -1 and R = 10 and 15 Hz for samples R = 0.5, R = -0.5, R = -2 and R = 2.
- The fatigue test was then started once all input parameters are inserted, the specimen is placed in the grips, proper alignment is achieved and grips are tightened. The break/failure is considered acceptable when it occurs on the gauge section.
- The load applied [kN] to the sample, and the number of cycles to failure, were recorded for each sample. An eye inspection of the failure modes observed in the joints was also carried out.

3.5.Conclusion

The credibility of the test data obtained by executing the above method can therefore be guaranteed by the given details regarding the material, specimen geometry and fabrication, and the experimental set-up and testing. The use of different standards and methods discussed in section 2.9 for fabrication and testing of the joint samples endorses the experimental methodology executed in the current study. This is because of the application of these methods in different studies as revealed in Chapter 2. The next chapter discusses the experimental data obtained in executing this method. The interpretation and analysis of the obtained data is also discussed in the next chapter.

CHAPTER 4: RESULTS AND ANALYSIS

4.1. Introduction

This chapter presents the analysis and interpretation of the experimental results. The experimental investigation was done in two steps. The first step was to perform static tests to determine the ultimate strength of the bond; the results are discussed in section 4.2. The second step was the fatigue loading where the applied fatigue load was based on a percentage of the ultimate strength; the results are discussed and analyzed in section 4.3. The relationship between mean, amplitude, stress ratio and number of cycles is discussed in section 4.4. Chapter conclusions are discussed in section 4.5.

4.2. Static testing

This section discusses the observed outcomes established from static testing. The testing was carried out in both tensile and compression mode as outlined in subsection 3.4.1. The effect of adhesive thickness on strength of the joint, and the reliability of the joint strength in tension and compression loading are discussed. The observed failure modes as discussed in section 2.3 are also discussed.

4.2.1. Static testing results

The effect of adhesive thickness on the joint strength was investigated by varying the adhesive thickness from 1 to 5 mm, with an increment of 1 mm in each case. Five samples were then tested under axial tensile loading for each case, in order to establish a relationship between shear strength and bond thickness. The strength-thickness curve in Figure 12 illustrates this relationship. Table 20 in Appendix A gives a summary of the results.

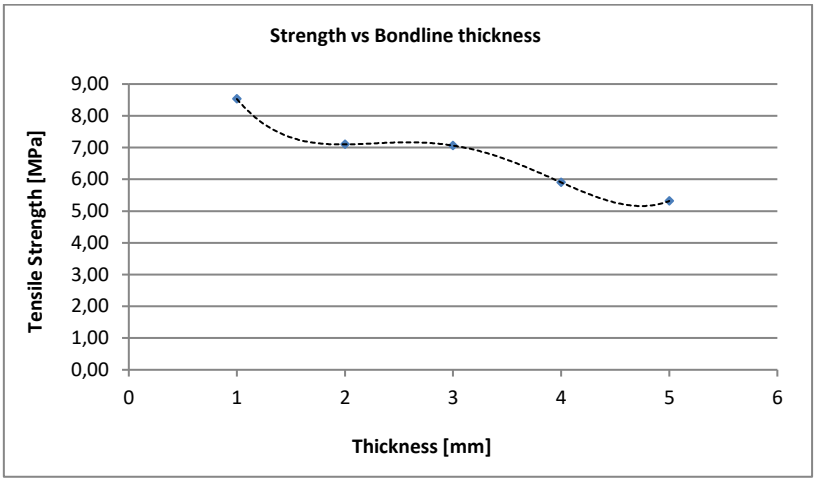

Figure 12: Effect of adhesive thickness

The stress in the above curve is the average ultimate stress (peak load divided by the overlap area of the joint) of five samples tested from each chosen adhesive thickness. The graph shows that the static strength decreases with an increasing thickness of the adhesive. The best fit for the data was a polynomial curve of fourth-order.

As in the studies done by Sarfaraz et al (2011) and Sarfaraz et al (2012), static testing was also performed in tension and compression mode, in order to assess strength reliability of the joint in these two modes. As outlined in subsection 3.4.1, four samples were loaded in tension and another four were loaded in compression. The average stress in the overlap area of the joint was then calculated for each loading mode, by dividing the average peak load of four samples with the overlap or shear area shown in Figure 10. This average stress consists of peel and shear stresses that occur at both ends of the overlap area as explained by Harris (2003). The stress is calculated per overlap area shown in Figure 10. As Table 21 and Table 22 in Appendix A show, this stress was calculated as 7.91 MPa in tensile loading and 7.13 MPa for compression mode. Thus the average stress in the overlap area was very similar for the two loading cases, with variation between the two cases being less than 1 MPa. Ultimate stress value of 7.91 MPa will therefore be considered as both ultimate tensile strength (UTS) and ultimate compression strength (UCS) throughout this paper.

4.2.2. Failure modes in static testing

A visual inspection of the samples after breaking revealed fiber breakage failure as a general mode of failure for most of the static tests; this is illustrated in Figure 13 below.

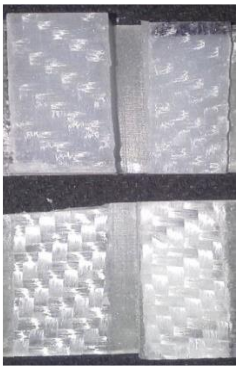

Figure 13: Fiber-breakage in static loading

The failure therefore occurred between the first and the second layer in the joint overlap area for most of the samples. Some of the samples, however, showed cohesive failure and hence the results from such tests were ignored. The failure in these samples occurred within the adhesive system.

This mode of failure is considered incorrect because it means the mixing of the adhesive was not correct or that the adhesive was not thoroughly mixed for these samples. Since nothing conclusive can be made about joint strength from such tests, the results therefore cannot be taken into consideration.

4.3. Fatigue testing

This section discusses the observed outcomes established from fatigue testing. The data obtained from the experiments (load-cycles) is presented and validated through curve-fitting and repeatability exercises. General failure modes observed in most of the joint samples during fatigue testing is also discussed. Data presentation of the final calculated data (stress-cycles data) is discussed. The stress-cycles data is also validated through curve-fitting analysis using amplitude stress values at randomly chosen number of cycles to failure.

4.3.1. Fatigue testing results and validation (Load-cycles data).

Six load levels with at least three specimens in each load level were investigated per R-ratios. The specimens were named accordingly, e.g. T019001 represents the first specimen loaded at a percentage level of 90% of ultimate load (average peak load in Table 19) under R = 0.1. The symbols T, TC, CT, and C therefore represent tension, tension-compression, compression-tension and compression respectively. The measured fatigue data from the experiments is presented in Table 23 of Appendix A, using R-ratios, specimen IDs, percentage load levels, applied load, number of cycles to failure, mean and amplitude load values. The data in Table 23 and the tests method executed in this study is validated below through curve-fitting analysis and also through repeatability exercise discussed in sub-section 2.9.3. The mean and amplitude load values are determined through the following steps:

- First, applied load is taken as maximum cyclic load for all number of cycles under each R-ratio.
- Minimum cyclic load is then calculated for R = 0.5, R = 0.1, R = -0.5 and R = -1 using $R = F_{min}/F_{max}$, with F_{min} and F_{max} as minimum and maximum cyclic loads respectively.
- Minimum cyclic load is also calculated for R = -2, R = 2 and R = 10 using $R = F_{max}/F_{min}$
- Mean load is then calculated for all number of cycles using $F_m = (F_{max} + F_{min})/2$, with F_m as mean load.

- Amplitude load is then calculated for all number of cycles using $F_a = (F_{max} - F_{min})/2$, with F_a as amplitude load.

4.3.1.1. Curve-fitting analysis.

At present, the reproducibility analysis as discussed in sub-section 2.9.3 cannot be carried out because there is no direct data from the literature that can be compared. For instance, there is no direct data from the literature where the adhesive mixture used consisted of laminating epoxy, cotton flocks and cab-o-sil additives, which was the case in the present study. There is also a significant difference in the joint overlap areas of samples tested in the present study and for most samples tested from the literature. However, the shape of the curves established in the present study can be compared to the curves established when some of the parameters or coefficients obtained from the literature are applied to the current experimental data. Hence in this case of validation, curve fitting through established data is analyzed.

As mentioned in section 2.7, any set of two parameters between R-ratio, mean stress (load) and amplitude stress (load) is enough to describe the fatigue behavior for any constant life, since the third parameter can be calculated using Equation 4. In the first case of validation process, the evaluation of the experimental data is analyzed through curve fitting. The present work utilizes the simple power law equation to simulate the relationship between amplitude loads and number of cycles to failure for each R-ratio tested.

$$\sigma_a = \sigma_1 (N)^{k1} \qquad 22$$

Where σ_a represents load amplitude and N is the number of cycles to failure. The coefficients, σ_1 and $k1$, are model parameters which can be determined by fitting the above equation to the amplitude load data calculated for each R-ratio in Table 23. The following process can be used to fit this equation and calculate its parameters for each R-ratio:

- Firstly, logarithmic values of amplitude load values and number of cycles to failure for each sample are calculated.
- Then *k1* is calculated using the slope function in an Excel spreadsheet, using the logarithmic values of amplitude load as known y's and logarithmic values of cycles as known x's.
- The intercept function is then used to calculate the intercept of the logarithmic data calculated in the first step, using again the logarithmic values of amplitude load as known y's and logarithmic values of cycles as known x's.

- Parameter σ_1 is then determined by raising the base number, 10, to the power of the intercept number calculated in the third step. The parameter, σ_1, is therefore a logarithm to the base number 10. This logarithms are commonly used in science and engineering.

Table 4 below shows values of the two parameters, σ_1 and *k1*, for all R-ratios tested.

Table 4: Power law parameters

Parameter	-2	-1	-0.5	0.1	0.5	2	10
k1	-0.078	-0.081	-0.073	-0.050	-0.042	-0.039	-0.060
σ_1	3.595	4.760	3.374	1.701	0.929	0.966	1.832

The power model and parameters established from the experiments done by Sarfaraz et al in 2011 and 2012 were also employed in the present study to calculate amplitude values. The parameters from Sarfaraz experiments are shown in Table 24 of Appendix A. Due to difference in configuration and size of specimen between the present study and Sarfaraz et al studies, amplitude values determined from application of Sarfaraz parameters were multiplied by the fraction of overlap area from current study and the overlap area from Sarfaraz et al studies., This was done to take the size factor into consideration and also create comparable outcomes.

In Figure 14 below, experimental values of amplitudes calculated above, values of amplitude established from fitting current model and Sarfaraz model are plotted against number of cycles to failure for each R-ratio.

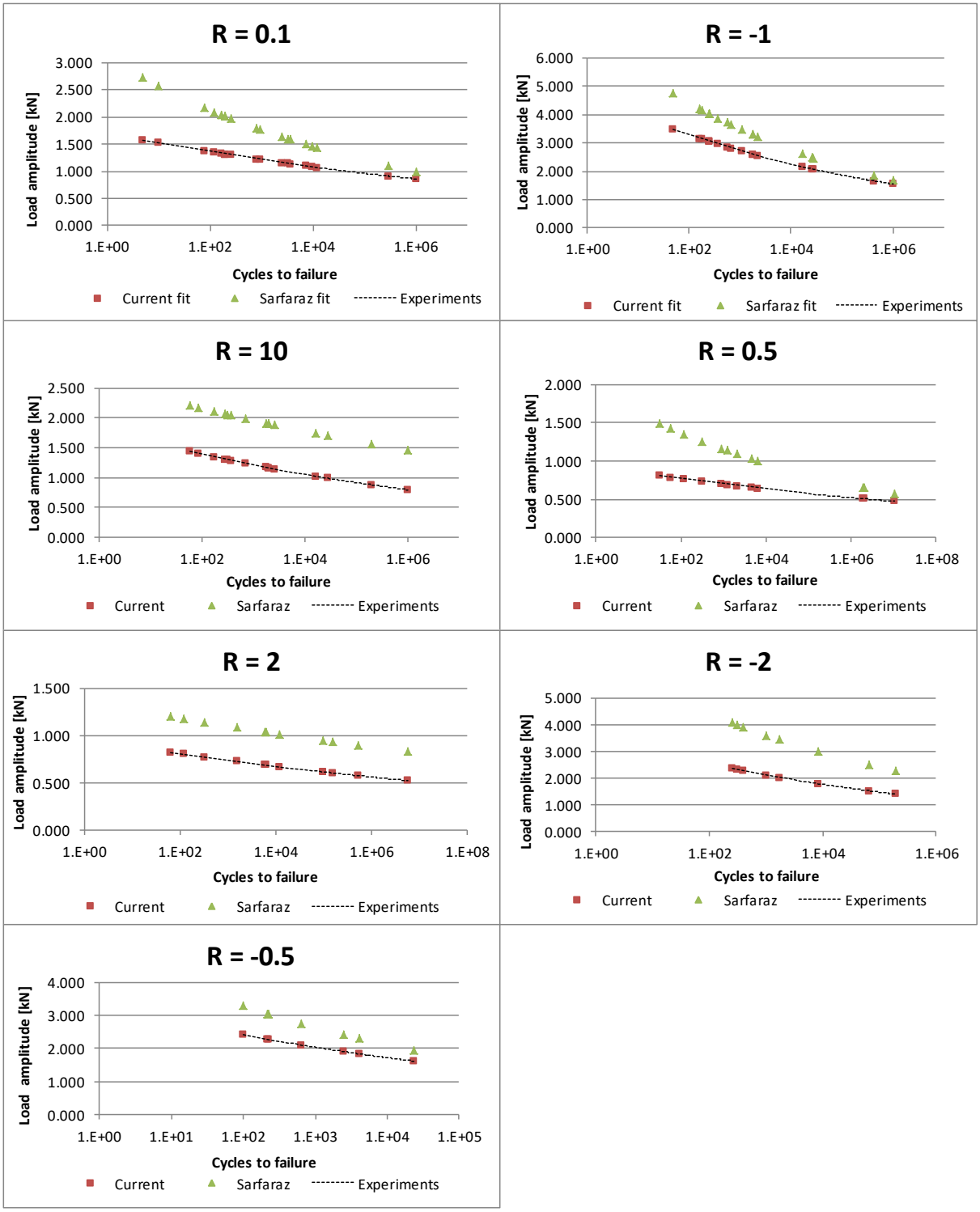

Figure 14: Load vs. cycles

As Figure 14 illustrates, the model and parameters of Equation 22 are a true representation of the relationship between amplitude load values and number of cycles to failure for each R-ratio tested. The figure also shows that, for each R-ratio, there is a closeness of values between model predicted values and experimental values. In Table 25 of Appendix A, %Error [1] indicates the error percentage between experimental value and value predicted by the equation, the error is then calculated per R-ratio tested as shown by %Error per R-ratio [1] in the table. The distance between experimental values and model values is also assessed, as shown by r^2-value [1] per R-ratio in the table. Table 5 below shows a summary of percentage errors and r^2-values per ratio:

Table 5: %Error and r^2-values per ratio (current experiments)

R-ratio	%Error per ratio [1]	r^2-value [1]
0.1	4.57	0.875
-1	4.07	0.947
10	3.27	0.941
0.5	3.96	0.939
2	3.83	0.898
-2	4.56	0.929
-0.5	2.61	0.923

An effort was made to keep the percentage error between model and experiments as low as possible. As illustrated in the above table, the percentage error between model and experiments is less than 5% under each R-ratio. To keep this value at less than 5%, all individual experimental tests results that showed over 10% error between experimental and model value were ignored; an example is sample CT-23001, which indicated 22.58% error. The reason for high error percentage for this sample is probably due to factors such as imperfections in the test sample, inaccuracy in the testing procedure or wrong reading of measured machine parameter. Table 5 also shows that the highest percentage error obtained is for joints tested under R = 0.1 and the lowest for joints tested at R = -0.5. The table above also illustrates that the highest r^2-value obtained is for joints tested under R = -1 and the lowest for joints tested at R = 0.1. The low percentage errors and high r^2-values confirm Equation 22 and its parameters as good modeling of amplitude values.

Amplitude load values resulting from application of the model and parameters established from Sarfaraz et al (2011) and Sarfaraz (2012) are also shown in Figure 14. These values were multiplied by the fraction of joint overlap area in the present study and the joint overlap area from these studies. The joint overlap area from these studies was A = 50 x 50 mm^2, meaning the loads applied

in these studies were higher than the loads applied in the current study. As Figure 14 shows, amplitude load values resulting from application of Sarfaraz et al parameters will always be higher than experimental values established from the current study. However, the gradient of the two curves is almost similar for joints tested under R = -0.5, R = -2, R = 2 and R = 10. The gradient differs for R = 0.1, R = -0.5 and R = -1.

In Table 25 of Appendix A, %Error [2] indicates the error percentage between the current experimental value of amplitude load and the value predicted using Sarfaraz model parameters; the error is then calculated per R-ratio tested as shown by %Error per R-ratio [2] in the table. The distance between experimental values and model values is also assessed, as shown by r^2-value [2] per R-ratio in the table. Table 6 below shows a summary of percentage errors and r^2-values per ratio:

Table 6: %Error and r^2-values per R-ratio (compared to Sarfaraz experiments)

R-ratio	%Error per R-ratio [2]	r^2-value [2]
0.1	30.72	0.851
-1	20.89	0.943
10	38.95	0.934
0.5	35.90	0.945
2	33.83	0.898
-2	40.68	0.929
-0.5	22.64	0.922

As discussed by Harris (2003), there is normally an uncertainty associated with test methods regarding tolerance values such as the accuracy of load or dimensional measurements. The uncertainty is also influenced by other sources such as testing by different operators, testing on different machines and testing at different times. Although the same method and identical fiber materials were examined between the present and Sarfaraz et al studies, it is due to some of these reasons that percentages errors in Table 5 and Table 6 differ. The mixture of adhesive systems used in Sarfaraz et al studies is different from the mixture used in the present study. There is also a significant difference in overlap areas of the joint samples between the present study and Sarfaraz et al studies. The inner and outer laminates in the Sarfaraz et al studies were also produced through a pultrusion process, instead of wet lay-up process as in the current study.

Table 6 also shows that the highest percentage error observed is for joints tested under R = -2 and the lowest for joints tested under R = -1. The table above also shows that the highest r^2-value

obtained was for joints tested under R = 0.5 and the lowest for joints tested at R = 0.1. As can be seen, the r^2-values in Table 6 are similar and consistent to values in Table 5.

4.3.1.2. Repeatability analysis.

In the second case of validation, the experimental data in Table 23 is analyzed using number of cycles to failure, since it is the value measured from experiments. The number of cycles to failure are therefore taken and analyzed as measured data obtained using the same method, same material and under the same conditions (the same operator, same equipment and same laboratory but at different applied loads and R-ratios).

The assessment is first performed by analyzing the change in number of cycles to failure when applied loads are changed (applied loads taken as percentages of ultimate load from 60% to 90%), for each R-ratio examined. Table 7 below shows the complete assessment. The table shows, for instance at R= 0.1, that five samples were tested at an applied load of 3.204 kN (therefore at 90% of the ultimate load, the ultimate load is taken from static tests as 3.56 kN). The loads applied are therefore the same under all R-ratios tested. As shown also on the table, for each R-ratio examined, the analysis is carried out by also determining the arithmetic average number of cycles under each load percentage applied. The deviation of number of cycles from arithmetic average values is also assessed by calculating standard deviation.

Repeatability is first evaluated by assessing the closeness of cycles to failure under each R-ratio when applied load is varied from 60% to 90% of ultimate load. Standard deviation values calculated (shown in column 9 of Table 7) and the number of times of varying applied load were therefore used together with Equation 20 to calculate repeatability standard deviation (column 10 on Table 7), under each R-ratio examined. Arithmetic averages, standard deviations and repeatability standard deviation value for each R-ratio are shown below in Table 7.

Table 7: Repeatability analysis of cycles between applied loads per R-ratio

Applied measure		Measured number of cycles to failure for different test samples					Measure evaluated		
R ratio	Applied load [kN]	1	2	3	4	5	Average	Standard Dev.	Repeat. Standard Dev.
0.1	3.20	5.00E+00	1.00E+01	8.00E+01	1.23E+02	1.66E+02	7.68E+01	6.28E+01	7.14E+04
	2.85	1.92E+02	1.99E+02	2.58E+02	8.10E+02	9.41E+02	4.80E+02	3.26E+02	
	2.49	2.54E+03	3.33E+03	7.26E+03	9.71E+03	3.58E+03	5.28E+03	2.75E+03	
	2.14	1.20E+04	2.98E+05				1.55E+05	1.43E+05	

-1	3.20	1.84E+02	4.90E+01	1.61E+02	2.47E+02	2.51E+02	1.78E+02	7.36E+01	2.54E+03
	2.85	2.50E+02	3.69E+02	5.56E+02	6.84E+02	1.06E+03	5.84E+02	2.82E+02	
	2.49	2.23E+03	1.78E+03	1.78E+03			1.93E+03	2.12E+02	
	2.14	1.65E+04	2.60E+04	2.82E+04			2.36E+04	5.07E+03	
10	3.20	8.60E+01	1.71E+02	5.90E+01			1.05E+02	4.77E+01	4.16E+04
	2.85	3.16E+02	3.63E+02	2.81E+02	6.91E+02		4.13E+02	1.63E+02	
	2.49	1.71E+03	2.63E+03	1.92E+03	1.98E+03		2.06E+03	3.41E+02	
	2.14	1.58E+04	2.81E+04	1.98E+05			8.08E+04	8.33E+04	
0.5	3.20	3.20E+01	5.70E+01	1.18E+02			6.90E+01	3.61E+01	2.56E+04
	2.85	3.20E+02	8.72E+02	1.23E+03			8.07E+02	3.74E+02	
	2.49	2.04E+03	4.66E+03	6.31E+03			4.33E+03	1.76E+03	
	2.14	1.88E+06	1.98E+06				1.93E+06	5.12E+04	
2	3.20	3.15E+02	6.25E+01	1.23E+02			1.67E+02	1.08E+02	1.34E+06
	2.85	1.53E+03	5.81E+03	1.21E+04			6.48E+03	4.34E+03	
	2.49	6.37E+03	9.81E+04	1.58E+05			8.73E+04	6.22E+04	
	2.14	5.22E+05	5.89E+06				3.21E+06	2.68E+06	
-2	3.20	2.54E+02	3.04E+02				2.79E+02	2.50E+01	1.64E+03
	2.85	3.89E+02	1.00E+03				6.94E+02	3.06E+02	
	2.49	8.27E+03	1.74E+03				5.01E+03	3.27E+03	
	2.14	6.71E+04					6.71E+04	0.00E+00	
-0.5	3.20	2.24E+02	9.80E+01				1.61E+02	6.30E+01	4.11E+02
	2.85	2.17E+02	6.39E+02				4.28E+02	2.11E+02	
	2.49	2.49E+03	4.07E+03				3.28E+03	7.91E+02	
	2.14	2.38E+04					2.38E+04	0.00E+00	

Although there were some tests conducted at other percentages of the ultimate load (percentages such as 40% and 50% shown in Table 23), percentages of ultimate load from 60% to 90% occur in most R-ratios examined. These percentages of ultimate load were therefore used for consistency of the analysis. As sub-section 2.9.3 discusses, repeatability standard deviation provides inverse measure of precision; high measure of repeatability standard deviation implies low (or poor) precision of test results. As seen from Table 7, high precision of test results was therefore observed for joints tested at R = -0.5, with repeatability standard deviation of 4.11×10^2 cycles between cycles to failure during load variation from 60% to 90% of ultimate load. The table also shows that the lowest precision was observed for joints tested under R = 2, with repeatability standard deviation of 1.34×10^6 cycles between cycles to failure. In conclusion, it can be seen from the table that repeatability standard deviation between measured cycles to failure during load variation under most R-ratios is above 1×10^3 cycles.

The closeness of cycles to failure when load percentages applied are varied between all R-ratios combined is evaluated in Table 8 below. The median value of cycles between all R-ratios examined

is shown per percentage of load applied. Standard deviation of cycles for each R-ratio from the median value is also shown. The combined repeatability standard deviation is calculated through Equation 20 by using the calculated standard deviation and the number of times applied load is varied. Median value of cycles per percentage load, standard deviation from the median and the combined repeatability standard deviation of cycles are shown in the table below:

Table 8: Combined repeatability analysis of cycles when applied loads are varied

Percent load [%]	0.1	-1	10	0.5	2	-2	-0.5	Median	Standard Dev.
90	7.68E+01	1.78E+02	1.05E+02	6.90E+01	1.67E+02	2.79E+02	1.61E+02	1.61E+02	6.72E+01
80	4.80E+02	5.84E+02	4.13E+02	8.07E+02	6.48E+03	6.94E+02	4.28E+02	5.84E+02	2.07E+03
70	5.28E+03	1.93E+03	2.06E+03	4.33E+03	8.73E+04	5.01E+03	3.28E+03	4.33E+03	2.93E+04
60	1.55E+05	2.36E+04	8.08E+04	1.93E+06	3.21E+06	6.71E+04	2.38E+04	8.08E+04	1.18E+06
								Repeat. Standard Dev.	5.90E+05

The following statements can be made from Table 8 per percentage load applied:

- At 90% of ultimate load (applied load of 3.20 kN), number of cycles to failure is centered around number of cycles established for joints tested at R = -0.5, number of cycles for all R-ratios deviate from this middle value by 6.72×10^1 cycles.
- At 80% of ultimate load (applied load of 2.85 kN), number of cycles to failure is centered around number of cycles established for joints tested at R = -1, number of cycles for all R-ratios deviate from this middle value by 2.07×10^3 cycles.
- At 70% of ultimate load (applied load of 2.49 kN), number of cycles to failure is centered around number of cycles established for joints tested at R = 0.5, number of cycles for all R-ratios deviate from this middle value by 2.93×10^4 cycles.
- At 60% of ultimate load (applied load of 2.14 kN), number of cycles to failure is centered around number of cycles established for joints tested at R = 10, number of cycles for all R-ratios deviate from this middle value by 1.18×10^6 cycles.
- The combined repeatability standard deviation between the number of cycles between all load percentages of ultimate load applied is 5.90×10^5 cycles.

The closeness of cycles to failure when R-ratios are changed between all load percentages combined is evaluated in Table 9 below. The median value of cycles between all percentages of load applied is shown per R-ratio examined. Standard deviation of cycles for each load percentage

from the median value is also shown. The combined repeatability standard deviation is calculated through Equation 20 by using the calculated standard deviation and the number of times R-ratio was varied. Median value of cycles per R-ratio, standard deviation from the median and the combined repeatability standard deviation of cycles are shown in the table below:

Table 9: Combined repeatability analysis of cycles when R-ratios are varied

R-ratio/ Load percent	90%	80%	70%	60%	Median	Standard Dev.
0.1	7.7E+01	4.8E+02	5.3E+03	1.5E+05	2.9E+03	6.62E+04
-1	1.8E+02	5.8E+02	1.9E+03	2.4E+04	1.3E+03	9.83E+03
10	1.1E+02	4.1E+02	2.1E+03	8.1E+04	1.2E+03	3.46E+04
0.5	6.9E+01	8.1E+02	4.3E+03	1.9E+06	2.6E+03	8.36E+05
2	1.7E+02	6.5E+03	8.7E+04	3.2E+06	4.7E+04	1.38E+06
-2	2.8E+02	6.9E+02	5.0E+03	6.7E+04	2.9E+03	2.83E+04
-0.5	1.6E+02	4.3E+02	3.3E+03	2.4E+04	1.9E+03	9.83E+03
					Repeat. Standard Dev.	6.09E+05

The following statements can be made from Table 9 per R-ratio:

- At R = 0.1, number of cycles to failure is centered around number of cycles established for joints tested at 70% of the ultimate load, number of cycles for all percentages of load applied deviate from this middle value by 6.62×10^4 cycles.
- At R = -1, number of cycles to failure is again centered around number of cycles established for joints tested at 70% of the ultimate load, number of cycles for all percentages of load applied deviate from this middle value by 9.83×10^3 cycles.
- At R = 10, number of cycles to failure is also centered around number of cycles established for joints tested at 70% of the ultimate load, number of cycles for all percentages of load applied deviate from this middle value by 3.46×10^4 cycles.
- At R = 0.5, number of cycles to failure is also centered around number of cycles established for joints tested at 70% of the ultimate load, number of cycles for all percentages of load applied deviate from this middle value by 8.36×10^5 cycles.
- At R = 2, number of cycles to failure is also centered around number of cycles established for joints tested at 70% of the ultimate load, number of cycles for all percentages of load applied deviate from this middle value by 1.38×10^6 cycles.

- At R = -2, number of cycles to failure is also centered around number of cycles established for joints tested at 70% of the ultimate load, number of cycles for all percentages of load applied deviate from this middle value by 2.83 x 10^4 cycles.
- At R = -0.5, number of cycles to failure is also centered around number of cycles established for joints tested at 70% of the ultimate load, number of cycles for all percentages of load applied deviate from this middle value by 9.83 x 10^3 cycles.
- The combined repeatability standard deviation between number of cycles between all R-ratios examined is 6.09 x 10^5 cycles.

The two measures of the combined repeatability standard deviation for cycles to failure are close to each other, as both Table 8 and Table 9 show. According to ASTM standard (2006), the larger value between repeatabilty and reproducibility standard deviation can be used to decribe precision of the measured data. Using the same reasoning, the larger value between repeatability standard deviation calculated in Table 8 and Table 9 can be used to describe precison of measured cycles (meaning the closeness of agreement between cycles to failure for all testing condtions examined in the current study). Since at the moment there is no true or accepted reference value that can be used for comparison, the trueness or bias of repeatability standard deviation cannot be determined.

An interval of plausible values of repeatability standard deviation can also be reported for futher analysis of the precison. This interval can be reported at a confidence level of 90%, 95% or 99%. The interval can then be evaluated at the chosen confidence level using the following equation:

$$CI = \bar{x} \pm z_{cr}\left(\frac{s}{\sqrt{n}}\right) \qquad 23$$

Where:

$\bar{x}$ is the average value of two repeatability standard deviations calculated in Table 8 and 9.

z_{cr} is the critical value of the standardised $\bar{x}$, and captures the central area under the chosen confidence level.

s is the standard deviation of the two repeatability standard deviations from the average value.

n = 2 is number of repeatability standard deviations evaluated.

In this study, the interval of plausible values of repeatability standard deviation between measured cycles is analyzed at a confidence level of 95%. According to Devorce and Farnum (2005), this

confidence level is normally used by many investigators because it gives a resasonable compromise between reliability and precision. The critical value that captures the central area under 95% confidence level can be determined through the following equation:

$$\bar{x} \pm z_{cr}\left(\frac{s}{\sqrt{n}}\right) = 0.95 \qquad 24$$

Substituting the value of z_{cr} in Equation 23, the lower limit of the confidence interval can therefore be calculated as 5.94 x 10^5 cycles while the upper limit was calculated as 6.06 x 10^5 cycles. The interval defined between these limits (5.94 x 10^5: 6.06 x 10^5) is reasonably narrower than the interval defined by the repeatability standard deviation calculated in Table 8 and Table 9 (5.90 x 10^5: 6.09 x 10^5); this indicates that the value of repeatibility standard deviation can precisely be defined between 5.94 x 10^5 and 6.06 x 10^5 cycles. In conclusion, it can therefore be stated that the probability of number of measured cycles being close to each other in the current study is 95%. Using the definition of repeatability value as explained by Harris (2003), it can also be concluded that for 95% probability, the value below which the absolute difference in number of cycles measured between two different tests performed under repeatability conditions lies in the interval given by [5.94 x 10^5: 6.06 x 10^5]. As mentioned in the beginning of this sub-section, these testing repeatability conditions are: same operator, same equipment and same laboratory but at different applied loads and R-ratios.

4.3.2. Failure modes in fatigue testing

The general mode of failure for most of the samples tested was again fiber-breakage, as Figure 15 illustrates. This breaking of fibers occurred in one of the inner laminates, between the first and second layer next to the bond line, and propagated until failure.

Figure 15: Fiber-breakage in fatigue loading

Samples tested at R = 0.1, R = 0.5, R = 10 and R = 2 reached over a million cycles without failure at 50% of UTS and UCS for each loading condition. Under reverse loading (R = -1) the samples reached over a million cycles at 40% of UCS. Specimens tested under tension –compression and compression-tension fatigue loading reached over one million cycles without failure at 35% of UTS and 30% of UCS. Under tension-compression, specimens tested at 40% of UTS also reached over million cycles without failure. Samples that failed following cohesive failure were not considered. See Figure 16 below.

Figure 16: Cohesive failure

The failure in the sample, illustrated by Figure 16, occurred within the adhesive system. This mode of failure is considered incorrect because it means the mixing of the adhesive was not correct or that the adhesive was not thoroughly mixed for the particular joint sample. Since nothing conclusive can be made about joint strength from such tests, the results of those samples were not taken into consideration.

4.3.3. Fatigue data presentation and validation (Stress-cycles data)

The final results presentation is given in terms of the calculated mean and stress values determined through the following steps:

- The cyclic stress is first calculated by dividing applied load by the overlap area of the joint. The stress value is per overlap area, as shown in Figure 10.
- This cyclic stress is taken as maximum stress for all R-ratios
- Minimum stress is then calculated for R = 0.5, R = 0.1, R = -0.5 and R = -1 using $R = \sigma_{min}/\sigma_{max}$
- Minimum stress is also calculated for R = -2, R = 2 and R = 10 using $R = \sigma_{max}/\sigma_{min}$
- Mean stress for all R-ratios is then calculated using Equation 2, and
- Amplitude stress for all R-ratios is calculated using Equation 3.

Calculated values of mean and amplitude stress are shown for all R-ratios in Table 26 of Appendix A. These mean and amplitude stress values are the same as values that can be calculated by dividing the mean and amplitude load values in Table 23 by the overlap area of the joint sample. The values were then plotted against number of cycles for each of these R-ratios. Figure 17 illustrates the plots established for all R-ratios examined.

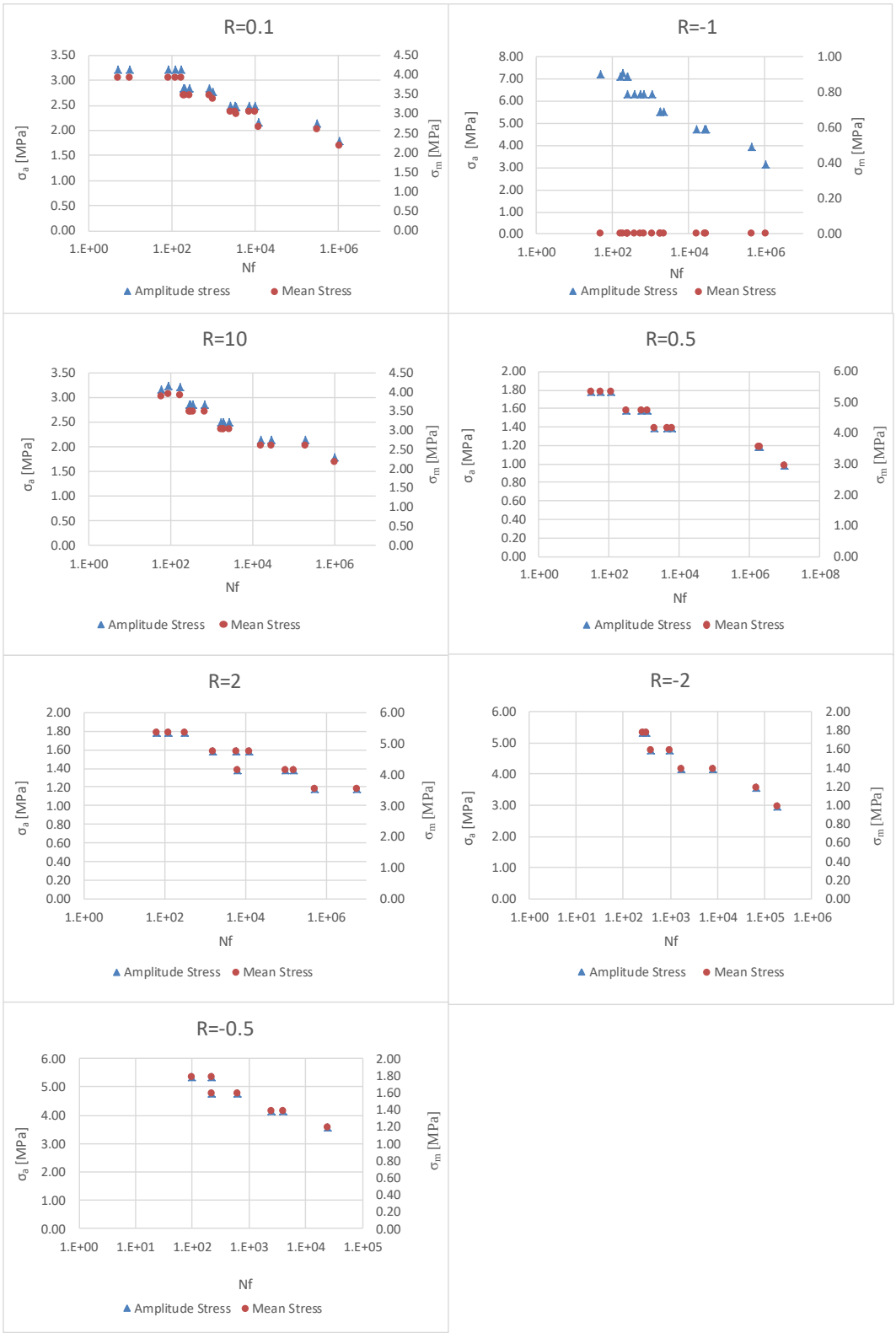

Figure 17: Stress vs. cycles

The amplitude and mean stress values are given by σ_a and σ_m. Number of cycles to failure is symbolized by N_f. The diagram above shows that, as expected, both mean and amplitude stress decrease as the number of applied load cycles increases for all stress ratios tested. This behavior can be observed for all R-ratios tested. In the case of R = 0.1, R = 0.5, R = 2 and R = 10, as Figure 17 shows, mean stress values are higher than amplitude stress values for all number of cycles to failure. The mean stress as expected is zero for all cycles under R = -1. Amplitude stress values are higher than mean stress values for R = -0.5, R = -2.

4.3.3.1. Stress-life comparison

In Figure 18 and 19, the fatigue life of the examined joints is plotted against amplitude and mean stress values for all R-ratios in tension and the tension dominant region. Power law trend lines are fitted for each R-ratio. In drawing conclusions from the total number of cycles applied, Figure 18 shows that the examined joints have highest amplitudes when R = -1 and R = -0.5, and lowest amplitudes when R = 0.5 and R = 0.1, are used. Figure 19 shows that the examined joints have highest mean stress values when R = 0.5 and R = 0.1 and lowest mean values when R = -0.5 and R = -1.

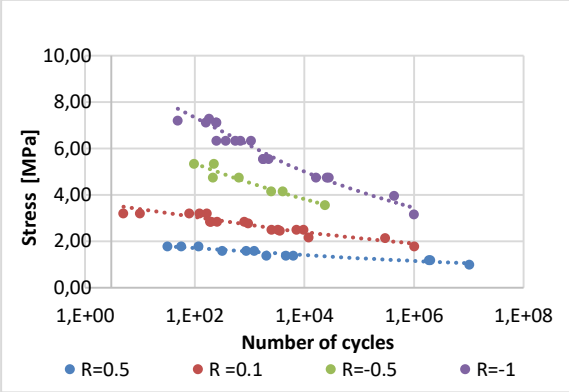

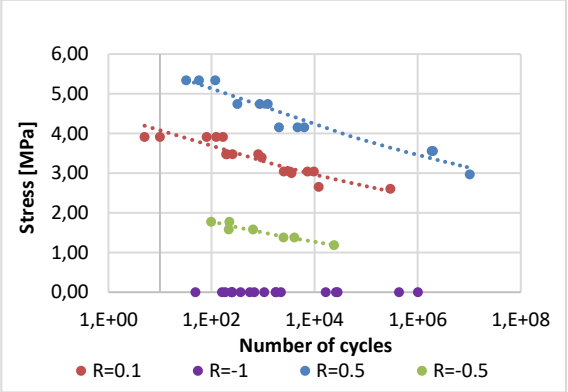

Figure 18: Tension dominant amplitude **Figure 19: Tension dominant mean**

The fatigue life of the examined joints for compression and compression dominant region is also plotted against amplitude and mean stress in Figures 20 and 21. Power law trend lines are fitted for each R-ratio once again. The curve in Figure 20 shows that the joints tested under R = -1 and R = -2 exhibit high amplitudes, while joints tested under R = 2 and R =10 have the lowest amplitude values. The joints tested under R = 2 and R = 10 exhibit higher mean stress values than joints tested under both R = -1 and R = -2, as Figure 21 shows.

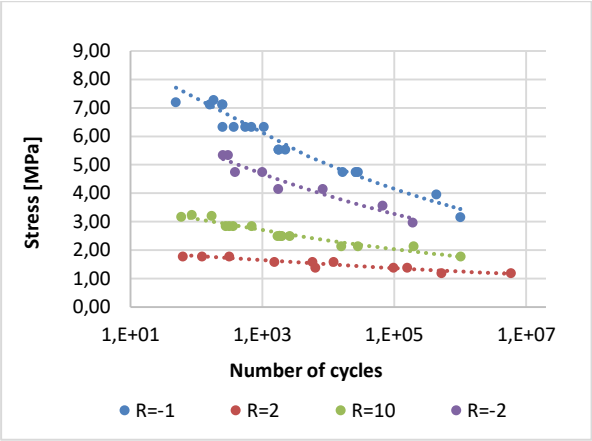

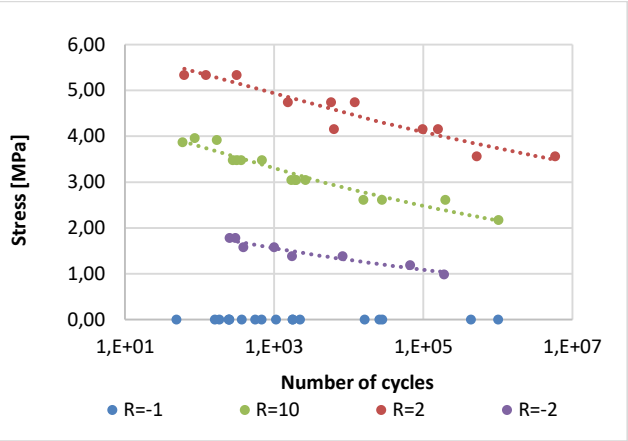

Figure 20: Compression dominant amplitude **Figure 21: Compression dominant mean**

The S-N curves in Figure 18 show that amplitude stress values at higher R-ratios are lower than amplitude stress values at lower R-ratios in the tension and tension dominated region. The amplitude is also low under higher R-ratios for compression and compression region, as illustrated in Figure 20. Mean stress of higher R-ratios is higher than mean stress of lower R-ratio for both cases as shown by Figure 19 and 21. The implications made from these observations is that for tension dominant fatigue loading, the change from high R-ratios to lower R-ratios (from R = 0.5 to R = -1) increases amplitude stress while decreasing mean stress values. In a case of dominant compression fatigue loading, the change from high R-ratios to lower R-ratios (from R = 10 to R = 2 and from R = -1 to -2) decreases the amplitude and increases mean stress.

4.3.3.2. Curve-fitting analysis through stress-cycles

Mean and amplitude stress data calculated in sub-section 4.3.3 can be validated through similar curve-fitting exercises performed in sub-section 4.3.1.2. The model in Equation 22 and parameters in Table 4 can be employed at randomly chosen number of cycles from experiments to compare with amplitude stress values calculated in sub-section 4.3.3. The model and parameters from Sarfaraz et al experiments can also be employed at the same chosen cycles for comparison. For the two cases, the amplitude load values resulting from model application at these random chosen cycles are first divided by overlap joint area of Figure 10 to calculate stress values. The resulting amplitude stress is then compared to the stress values calculated in the beginning of sub-section 4.3.3. Figure 22 shows these stress values plotted against the chosen random number of cycles. Full analysis is given in Table 27 of Appendix A. Although not shown, mean stress values at these random cycles can be calculated using Equation 4, as discussed in section 2.7.

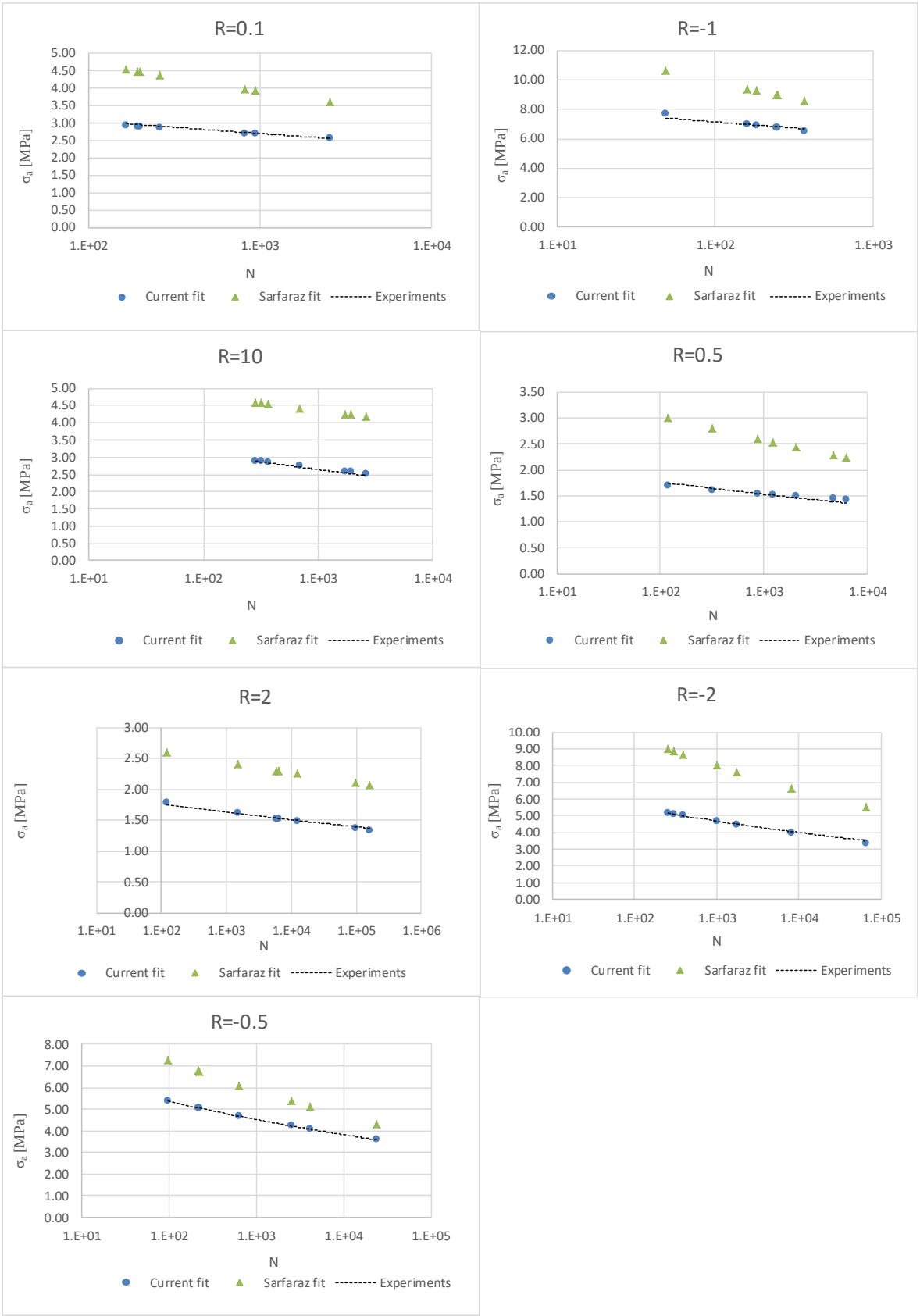

Figure 22: Stress-cycles validation

As Figure 22 illustrates, the model and parameters of Equation 22 can be used to model the relationship between amplitude stress values and number of cycles to failure for each R-ratio tested. The figure also shows that, for each R-ratio, there is a closeness of stress values between model predicted values and experimental values.

In Table 27 of Appendix A, %Error [1] indicates the error percentage between experimental value and value predicted by the equation; the error is then calculated per R-ratio tested as shown by %Error per R-ratio [1] in the table. The distance between experimental values and model values is once assessed, as shown by r^2-value [1] per R-ratio in the table. For the chosen random number of cycles, the table shows that the highest percentage error observed is for joints tested under R = -1 and the lowest under R = 10. The table also shows that the highest r^2-value obtained is for joints tested at R = -0.5 and the lowest for joints tested at R = -1.

Amplitude stress values resulting from application of model and parameters established from Sarfaraz et al (2011) and Sarfaraz et al (2012) are also shown in Figure 22. The figure shows that amplitude stress values resulting from application of parameters from these studies will be higher than experimental values for the same chosen number of random cycles. This is for the same reasons mentioned in sub-section 4.3.1.1. The gradient of the two curves is similar for joints tested under R = 2 and R = 10. The gradient is almost similar for R = 0.1, R = -0.5, R = -1, R = 0.5 and R = -2.

In Table 27 of Appendix A, %Error [2] indicates the error percentage between experimental value and value predicted by the Sarfaraz model parameters; the error is then calculated per R-ratio tested as shown by %Error per R-ratio [2] in the table. The distance between experimental values and model values is also assessed, as shown by r^2-value [2] per R-ratio in the table. The table shows that the highest percentage error observed is for joints tested under R = -2 and the lowest for joints tested under R = -0.5. The table also show that the highest r^2-value obtained was for joints tested under R = -0.5 and the lowest for joints tested at R = -1. As can be seen, the r^2-values in the table are similar and consistent to values obtained when Equation 22 is applied.

4.4.Constant life diagrams

The standard way of representing the relationship between R-ratio, and mean and amplitude stress is by using a constant life diagram. A constant life diagram can be set up by first calculating amplitude and mean stress values. Equation 22 and Equation 4 can therefore be used to determine amplitude and mean stress values. In order to gain more insight into how these stress parameters influence each other, and also to accommodate a wide range of the loading possibilities, number of cycles ranging from 10^1 to 10^7 will be used in the current paper. Three different constant life diagram combinations between applied stress ratios, mean, and amplitude stress values is discussed below.

4.4.1. Failure locus

A diagram representing the fatigue failure locus can be prepared by plotting a surface diagram as shown in Figure 23.

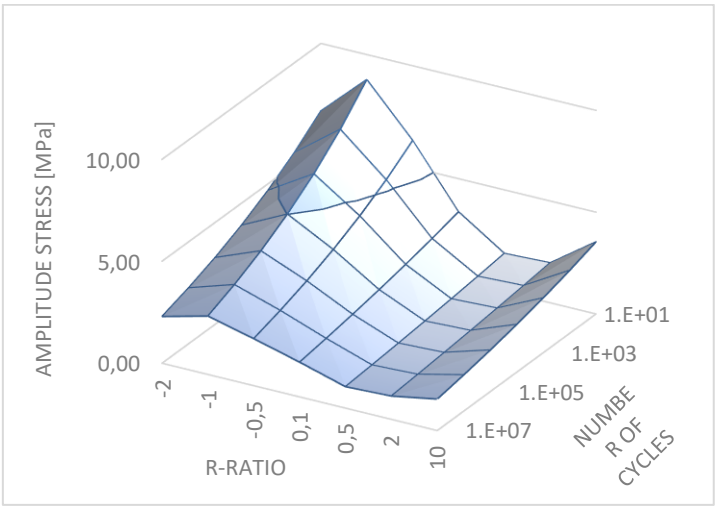

Figure 23: Failure locus of joints

The surface represents the failure locus of the tested joints, according to Vassilopoulos et al (2010). Amplitude stress values were calculated at selected number of cycles using Equation 22. Any combination of the R-ratio and amplitude stress above the surface will cause failure for the examined joints. The highest point is therefore attained for joints tested at R = -1 and the lowest for joints tested at both R = 0.5 and R = 2, the same observations made from S-N curves in Figure 18 and 19. Projecting this surface on the R-σ_a plane may be considered as a constant life diagram.

4.4.2. Stress ratio-amplitude

The second combination also looks at the relationship between the applied stress-ratio and amplitude stress, using the R-σ_a plane diagram as shown in Figure 24.

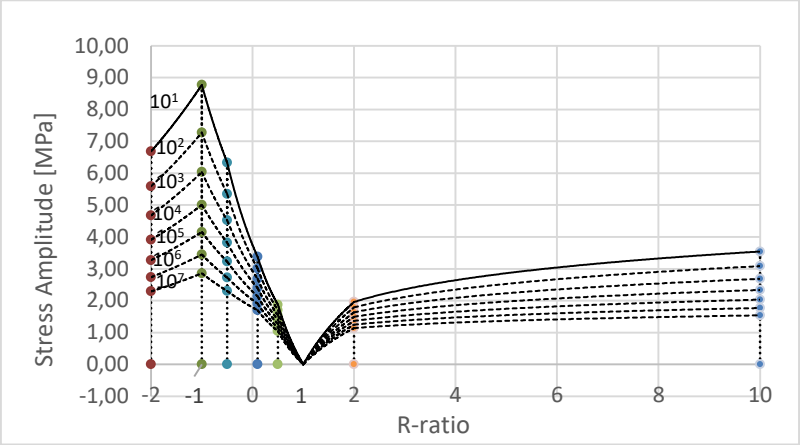

Figure 24: Stress ratio-amplitude constant life

Equation 22 was again applied at the chosen cycles to calculate amplitude values. The diagram above shows that, for any constant life, the amplitude stress is higher under the mixture of compression and tension fatigue loading at R = -1 and lower under tension-tension at R = 0.5 and compression-compression fatigue loading at R = 2. The zero amplitude is at static loading at R = 1. The diagram also shows that, for all number of cycles, the amplitude of the examined joints increases when fatigue load changes from compression-tension at R = -2 to R = -1. The amplitude then decreases for all constant lives when the R-ratio is changed from -1 to tension-compression at -0.5. The change from tension-compression loading (at R = -0.5) to static loading (at R = 1) deceases the amplitude to zero for all constant lives. The amplitude then increases when the load is changed from static loading at R = 1, to compression-compression fatigue loading at both R = 2 and R = 10.

4.4.3. Mean-amplitude

As mentioned in section 2.7, the constant life diagram is normally plotted on the mean-amplitude (σ_m-σ_a) plane as radial lines emanating from the origin of the coordinate system. The last combination of load parameters focuses on the relationship between mean and amplitude stress values. Consider Figure 25 below:

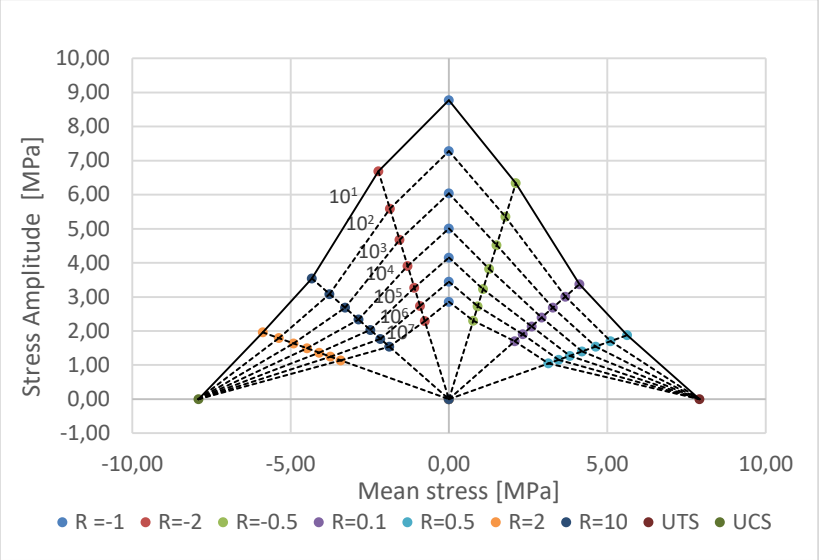

Figure 25: Mean-amplitude constant life

Table 28 in Appendix C shows values for both mean and amplitude stress. Amplitude stress was determined using Equation 22 and the mean stress by using Equation 4. The UCS and UTS in the diagram represent ultimate tensile strength and ultimate compression strength, as determined from static testing and explained in subsection 4.2.1 The highest point on the diagram is under compression-tension loading at R = -1; this corresponds to the observation made from the S-N curves in Figure 18, Figure 20 and Figure 24. The diagram above also shows symmetry around R = -1 axis. The following observations are made from the diagram, about the relationship between mean stress, amplitude stress and applied number of cycles:

The mean stress increases with an increasing amplitude when the applied load is changed from static compression loading (R = 1) to compression-compression loading (R = 10) for any constant life. Transition from compression-compression loading at R = 10 to compression-tension loading at R= -2 increases the mean, while decreasing the amplitude for all constant lives. An increase in mean stress with an increasing amplitude stress is observed for all cycles when the load is changed from R = -2 to R = -1. The change of R-ratio from -1 to -0.5 in a tension-compression loading increases the mean stress, while amplitude stress is decreased for all constant lives. The transition from tension-compression loading at R = -0.5 to static tensile loading at R = 1 shows mean stress to be increasing with a decreasing amplitude stress, for all number of cycles applied.

4.5. Conclusion

Results from static testing were used to assess the effect of adhesive thickness and also to establish the ultimate strength of joints. The general mode or criterion of failure for most of the double strap joints tested was fiber breakage failure for both static and fatigue loading. However, some specimens demonstrated cohesive failure and hence their results were not considered, as explained by sections 2.3 and 3.4. Mean and standard deviations were used to evaluate the center and variability of the experimental fatigue data. Also for evaluation, the two measures were compared to values that were calculated from other studies. Stress-life method was employed to express how mean and amplitude relate to fatigue life using S-N curves plotted for tension-tension and compression-compression regions. A power law model was fitted to simulate amplitude stress values. The model was evaluated by calculating the percentage errors between model and experimental values, at random number of cycles. The distance between model and experimental amplitude values from current experiments was also assessed. The parameters from the current experiments were also compared to parameters from other studies. The distance between model and experimental amplitude values from other experiments was also evaluated. Three combinations of constant life diagrams were established between R-ratio, and mean and amplitude stress values.

The S-N curves and constant life diagrams show that, for any constant life, the highest point is observed for joints tested under R = -1. The joints tested under both R = 0.5 and R = 2 have the lowest points for all constant lives. The bond fatigue strength and life can therefore be summarized as follows: An average applied stress of 2.86 MPa at R = -1, 2.29 MPa at R = -2, 2.30 MPa at R = -0.5, 1.70 MPa at R = 0.1, 1.05 MPa at R = 0.5, 1.14 MPa at R = 2 and 1.54 MPa at R =10 will produce fatigue life of 1×10^7 cycles.

The next chapter discusses different models that can be used to simulate the relationship between mean and amplitude stress values, for all number of cycles, as shown in Figure 25. The models attempt to predict mean and amplitude values at specific R-ratios by using mean and amplitude values from other R-ratios. The models are then evaluated by comparing the amplitude values predicted by each model to the experimental values, at randomly selected number of cycles.

CHAPTER 5: MODELING OF MEAN AND AMPLITUDE STRESS

5.1. Introduction

The constant life curves on the mean-amplitude plane discussed above exhibit different behaviors for various combinations of mean and amplitude stress values. This means different mathematical expressions can be used to model the relationship between these two parameters for various regions of the CLD. As discussed in section 2.6, these regions represent various conditions under fatigue loading (e.g. compression-tension). The fatigue behavior of the bond can then be modeled in terms of mean and amplitude stress, as applied load changes between various loading conditions. The symmetry of the CLD around R = -1 might also be improved by modeling of mean and amplitude. The models can also be used to predict mean and amplitude stresses for the loading conditions at which no experimental data exists. In this chapter, different types of models for mean-amplitude constant life diagram are fitted. The models are fitted for the entire region of mean stress values between UCS and UTS. The existing models normally used for composite laminates, discussed in section 2.8, are also applied to compare these models.

Equation 4 was employed simultaneously with each model equation to calculate mean stress values. In Appendix D, each model was then evaluated by measuring statistical distance between amplitude values chosen at random cycles from the experiments and the amplitude stress values predicted by the model. The evaluation, summarized in Table 10, was performed for each R-ratio for all chosen cycles.

Table 10: Comparison of r^2-values for models

R-ratio	Linear	Second-order	Third-order	Fourth-order
-2	**0.864**	0.787	0.631	0.701
-0.5	0.812	**0.851**	0.642	0.748
0.1	0.011	0.090	**0.356**	0.099
0.5	0.464	0.133	**0.865**	0.785
2	**0.666**	0.028	0.218	0.288
10	**1.000**	**1.000**	**1.000**	**1.000**

Table 10 compares the statistical distance (r^2-value) between amplitude values predicted by each model and the experimental values of amplitude at randomly selected number of cycles. This is done to assess the closeness of the two data sets for each R-ratio examined. The following sections use r^2-values in Table 10 to evaluate each of the models. High r^2-values under each R-ratio are

shown in bold. Derivation of all model coefficients is explained in Appendix B. All amplitude and mean stress values calculated under each of these models are given in Appendix C.

Section 5.2 utilizes linear formulation to predict values of amplitude stress in terms of using values at R = -1. Second-order, third-order and fourth-order polynomial equations are used in section 5.3, 5.4 and 5.5 respectively, the equations are also used in terms of values of amplitude stress values at R = -1. The first four models discussed in section 2.8 are then applied in section 5.6. All models are then compared to each other in section 5.7; four models with high r^2-value values between experimental and predicted amplitude values at randomly chosen cycles are evaluated. Chapter conclusions are then made in section 5.8.

5.2. Linear modeling

The model is based on a single S-N curve. The model in this case uses the fatigue data under R = -1 as basis. Any constant life line in Figure 26 can be calculated by:

$$\sigma_a = k_1\sigma_m + \sigma_{R=-1} \; for \; UCS \leq \sigma_m \leq 0 \qquad 25a$$

$$\sigma_a = k_2\sigma_m + \sigma_{R=-1} \; for \; 0 \leq \sigma_m \leq UTS \qquad 25b$$

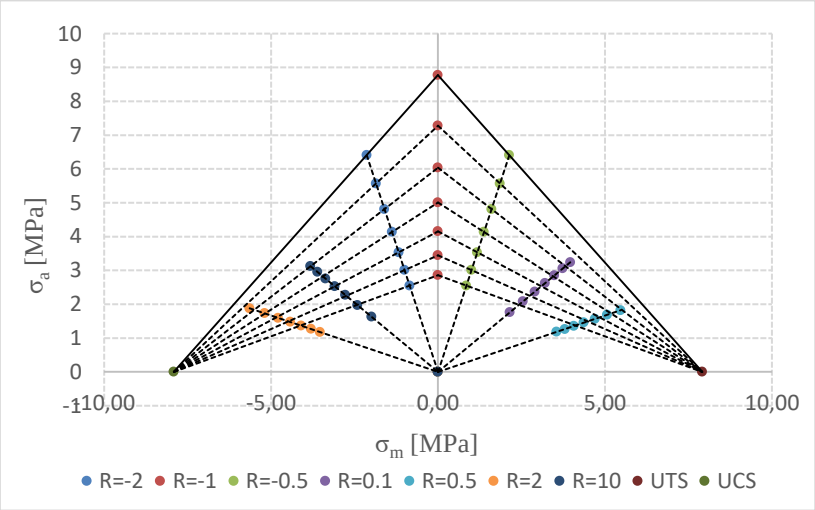

Figure 26: Linear

Mean and amplitude stress values under other R-ratios were calculated simultaneously using Equation 4, Equation 25a and Equation 25b. The two parameters, k_1 and k_2, are model coefficients that can be calculated through the solution of these two equations applied at the points of UCS and UTS as explained in Appendix B; the coefficients are calculated for any constant life as shown in Table 11 . The last parameter, $\sigma_{R=-1}$, represents amplitude stress of fatigue data under R = -1.

Table 11: Linear model coefficients

Cycles	k_1	k_2	$\sigma_{R=-1}$
0	0	0	0
1.E+01	1.109	-1.109	8.773
1.E+02	0.920	-0.920	7.277
1.E+03	0.763	-0.763	6.036
1.E+04	0.633	-0.633	5.007
1.E+05	0.525	-0.525	4.153
1.E+06	0.435	-0.435	3.445
1.E+07	0.361	-0.361	2.858

As both Figure 26 and Table 10 show, the model is highly accurate when simulating fatigue data under R = -0.5, R = -2. Constant life curves connect to all data points under these R-ratios. The table shows the model to have enough accuracy for R = 2 and R = 10; however, constant life lines do not connect to all data points for these R-ratios, as shown in Figure 26. The model is less accurate under both R = 0.1 and R = 0.5, as observed from the table and diagram. As can be seen, the CLD constructed from this model is symmetric about zero mean stress axis. The mean increases from UCS to zero, with an increasing value of amplitude stress for compression and compression dominated region. The mean then increases from zero to UTS with a decreasing amplitude for tension and tension dominated side.

5.3. Second-order modeling

This model is also based on the experimental data of the examined joints under R = -1. Mean and amplitude stress values under other R-ratios were calculated simultaneously using Equation 4 and Equation 26.

Each constant life line in Figure 27 can be calculated by:

$$\sigma_a = a\sigma_m^2 + b\sigma_m + \sigma_{R=-1} \qquad 26$$

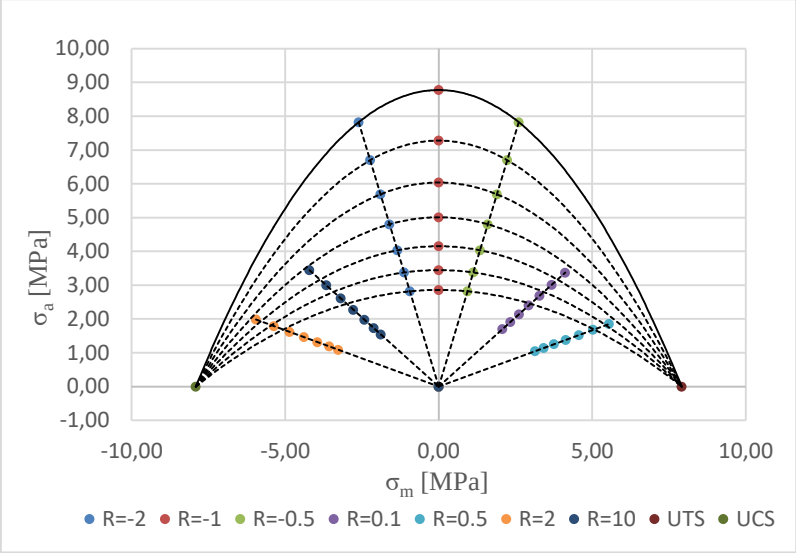

Figure 27: Second-order

The model coefficients (*a*, *b*) can be calculated through the solution of two simultaneous equations applied at the points of UTS and UCS, the coefficients are calculated for constant lives between 1 x 10^1 and 1 x 10^7 cycles as shown in Table 12.

Table 12: Second-order model coefficients

Cycles	*a*	*b*	$\sigma_{R=-1}$
0	0	0	0
1.E+01	-0.140	0.000	8.773
1.E+02	-0.116	0.000	7.277
1.E+03	-0.096	0.000	6.036
1.E+04	-0.080	0.000	5.007
1.E+05	-0.066	0.000	4.153
1.E+06	-0.055	0.000	3.445
1.E+07	-0.046	0.000	2.858

For each constant life, the amplitude increases from zero to a maximum value at R = -1 when mean increases from UCS to zero. The amplitude then decreases from maximum value to zero when mean increases from zero to UTS. Table 10 show that high accuracy was achieved when predicting fatigue data under R = -0.5 and R = -2. This is also demonstrated in Figure 27 where it can be seen that constant life lines under these R-ratios connect to all data points for this ratios. The table again shows the model to have enough accuracy for R = 10; however, constant life lines do not connect to all data points for this ratio, as the diagram shows. Table 10 and Figure 27 show that the model is inaccurate in predicting fatigue data under R = 0.5, R = 0.1 and R = 2. The model also shows symmetry around R = -1.

5.4. Third-order modeling

The model is also based on the existence of fatigue data under R = -1. Any constant life line in Figure 28 can be calculated by:

$$\sigma_a = \alpha{\sigma_m}^3 + \beta{\sigma_m}^2 + \gamma\sigma_m + \sigma_{R=-1} \quad 27$$

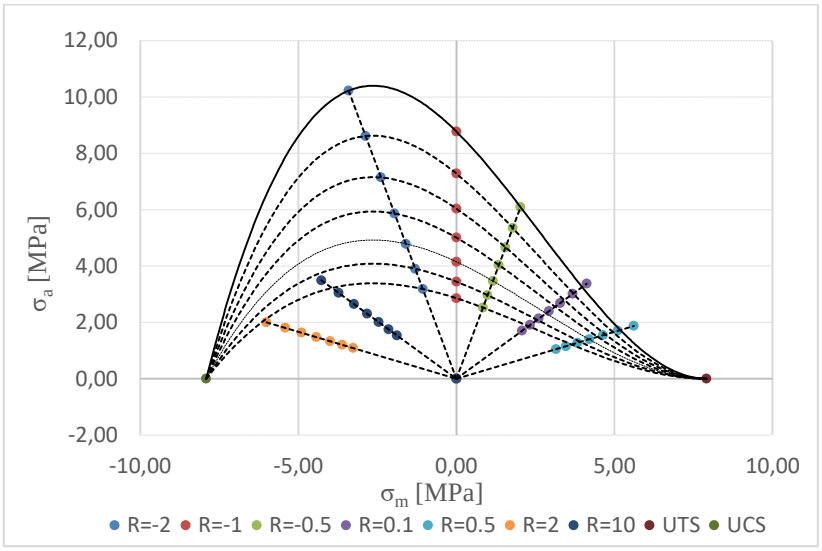

Figure 28: Third-order

Mean and amplitude stress values under other R-ratios were calculated simultaneously using Equation 4 and Equation 27. Model parameters, α, β and γ are calculated by the solution of three systems of simultaneous equations applied at UCS and UTS. The first two equations are found by applying UCS and UTS in the equation, and the last one by differentiating the equation and applying UTS. Table 13 below shows these parameters for all number of cycles.

Table 13: Third-order model coefficients

Cycles	α	β	γ	$\sigma_{R=-1}$
0	0	0	0	0
1.E+01	0.018	-0.140	-1.109	8.773
1.E+02	0.015	-0.116	-0.920	7.277
1.E+03	0.012	-0.096	-0.763	6.036
1.E+04	0.010	-0.080	-0.633	5.007
1.E+05	0.008	-0.066	-0.525	4.153
1.E+06	0.007	-0.055	-0.435	3.445
1.E+07	0.006	-0.046	-0.361	2.858

For each constant life curve, the amplitude increases from zero to a maximum value when mean increases from UCS to –2.64 MPa. The amplitude then decreases from maximum to zero when mean increases from -2.64 MPa to UTS. The amplitude has different maximum values for different

lives and the CLD tends to shift toward compression and compression dominated region. The model therefore shows that the change from static compression loading to compression-tension fatigue loading increases both mean and amplitude stresses, while changing from static tension loading to tension-compression fatigue loading decreases the mean and increases amplitude. Comparison of this model with others shows that it has one of the highest prediction accuracy levels amongst all models considered. As Table 10 and Figure 28 show, the model is also accurate when predicting data under R = -0.5 and R = -2 and performs very poorly at R = 0.1 and R = 2. Figure 28 also show the model to be performing poorly at R = 10, contradicting the high r^2-value in Table 10.

5.5. Fourth-order modeling

The model is also employed using fatigue data of joints tested under R = -1. Each constant life in Figure 29 can be determined by:

$$\sigma_a = \alpha{\sigma_m}^4 + \beta{\sigma_m}^3 + \gamma{\sigma_m}^2 + \delta\sigma_m + \sigma_{R=-1} \qquad 28$$

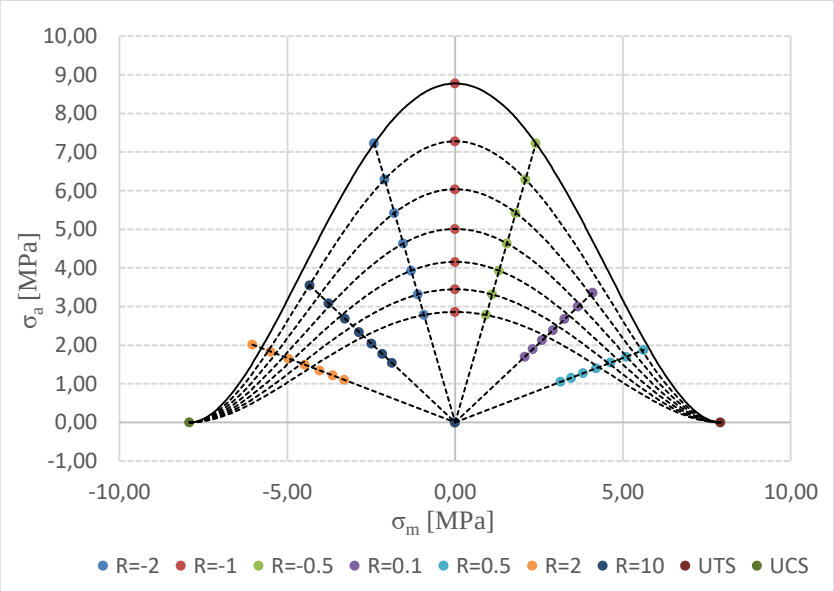

Figure 29: Fourth-order

Model parameters, α, β, γ and δ are calculated by the solution of four systems of simultaneous equations applied at UCS and UTS. The first two equations are found by applying UCS and UTS in the equation, and the last two by differentiating the equation and applying UCS and UTS data points. The parameters are shown for all cycles below in Table 14.

Table 14: Fourth-order model coefficients

Cycles	α	β	γ	δ	$\sigma_{R=-1}$
0	0	0	0	0	0
1.E+01	0.002	0.000	-0.280	0.000	8.773
1.E+02	0.002	0.000	-0.233	0.000	7.277
1.E+03	0.002	0.000	-0.193	0.000	6.036
1.E+04	0.001	0.000	-0.160	0.000	5.007
1.E+05	0.001	0.000	-0.133	0.000	4.153
1.E+06	0.001	0.000	-0.110	0.000	3.445
1.E+07	0.001	0.000	-0.091	0.000	2.858

For each constant life curve, the amplitude increases from zero to a maximum value at R = -1 when mean stress increases from UCS to zero. The amplitude then decreases from maximum to zero when the mean increases from zero MPa to UTS. The model therefore shows that when using only the data under R = -1, the change from static compression loading to compression-tension fatigue loading increases both mean and amplitude stresses, while changing from static tension loading to tension-compression fatigue loading decreases the mean and increases amplitude. The model performs poorly when predicting fatigue data under R = 0.1 and R = 2, as shown by the low r^2-values in Table 10. The highest accuracy was achieved for fatigue data under R = 0.5, R = 10, R = -0.5 and R = -2. However, Figure 29 shows that constant life lines connect to all data points only for R = -0.5 and R = -2.

5.6. Other composite materials modeling

The model parameters for all models above are functions of fatigue life, and the CLD formulation is only applicable for a range of mean stress values defined between UCS and UTS. To compare with the above formulas, existing models normally used in composite materials and composite laminates are also applied in this work. As summarized in Table 15, the accuracy of each model was again evaluated in terms of statistical distance between model and experimental data for all R-ratios predicted.

Table 15: Comparison of r^2-values for other models

R-ratio	Triangular	Piecewise	Harris	Kawai
-2	0.809	**0.818**	0.661	0.691
-0.5	**0.823**	0.819	0.661	0.691
0.1	0.201	-	-	**0.362**
0.5	0.393	0.587	0.582	**0.899**
2	0.469	**0.512**	0.107	0.291
10	0.634	-	-	**1.00**

Table 15 also compares the r^2-value between amplitude values predicted by each model and the experimental values of amplitude at randomly selected number of cycles. This is once again done to assess the closeness of the two data sets for each R-ratio examined. The following sections use r^2-values in Table 15 to evaluate each of the models developed. High r^2-values under each R-ratio are shown in bold. All amplitude and mean stress values calculated under each of these models are given in Appendix C.

5.6.1. Triangular modeling

The triangular model does not depend on specification of UCS and UTS. The model was applied in this work using experimental data under R = -1 as basis. Each constant life in Figure 30 is given by Equation 5, with k and σ_0 as parameters of the power law equation which describes the S-N curve under R = -1 fatigue loading.

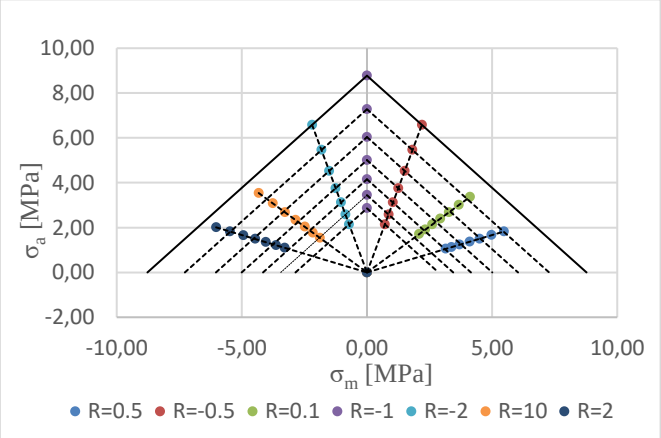

Figure 30: Triangular

The model parameters, k and σ_0 are given in Table 16 below.

Table 16: Triangular model coefficients

Cycles	*k*	σ_0
0	0	0
1.E+01	-0.081	10.577
1.E+02	-0.081	10.577
1.E+03	-0.081	10.577
1.E+04	-0.081	10.577
1.E+05	-0.081	10.577
1.E+06	-0.081	10.577
1.E+07	-0.081	10.577

The amplitude is calculated for all values of mean stress between minimum and maximum stresses under R = -1 fatigue loading. The model exhibits symmetry around R = -1 as observed in Figure 30. The model shows that the mean increases with an increasing amplitude from compression-compression loading to compression-tension loading. The amplitude also increases with a decreasing mean from tension-compression to tension-tension fatigue loading. Table 15 shows that the model has better accuracy for joints tested at R = -0.5, R = -2 and R =10 as compared to other R-ratios. The lowest accuracy was obtained when predicting fatigue data under R = 0.1, R = 0.5 and R = 2. The diagram in Figure 30 therefore disapproves with r^2-values contained in Table 15.

5.6.2. Piecewise linear modeling

Fatigue loading data under R= 0.1, R -1 and R =10 was used for this model. The mean and amplitude are related by Equation 6, 7 and 8 for different regions of constant life diagram, as explained in section 2.8.2

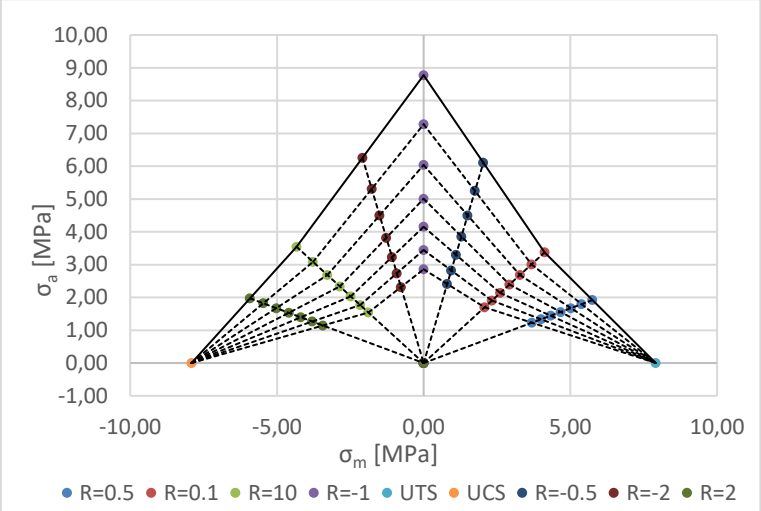

Figure 31: Piecewise linear

Table 17 below shows the values of parameters, as described in section 2.8.2, for all number of cycles used.

Table 17: Piecewise model coefficients

Cycles	$r'_{(0.5)}$	r_{1TT}	$\sigma_{a,1TT}$	$r_{i+1\,(-1)}$	$\sigma_{a,i+1\,(-1)}$	$r'_{(-0.5)}$	$r'_{(-2)}$	$r_{i+1\,(10)}$	$\sigma_{a,i+1\,(10)}$	$r'_{(2)}$
0	3.000	1.222	0	0	0	0.333	-0.333	-1.222	0	-3.000
1.E+01	3.000	1.222	3.372	0	8.773	0.333	-0.333	-1.222	3.543	-3.000
1.E+02	3.000	1.222	3.008	0	7.277	0.333	-0.333	-1.222	3.083	-3.000
1.E+03	3.000	1.222	2.684	0	6.036	0.333	-0.333	-1.222	2.683	-3.000
1.E+04	3.000	1.222	2.394	0	5.007	0.333	-0.333	-1.222	2.335	-3.000
1.E+05	3.000	1.222	2.136	0	4.153	0.333	-0.333	-1.222	2.033	-3.000
1.E+06	3.000	1.222	1.905	0	3.445	0.333	-0.333	-1.222	1.769	-3.000
1.E+07	3.000	1.222	1.700	0	2.858	0.333	-0.333	-1.222	1.540	-3.000

As Figure 31 shows, for any constant life, the amplitude increases with an increasing mean between UCS and zero. The mean then increases with decreasing amplitude between zero and UTS. The model shows symmetry around R = -1; maximum amplitude value is also at this R-ratio. A change from static tension loading to tension-compression fatigue loading increases amplitude stress and decreases the mean stress. Changing from static compression loading to compression-tension fatigue loading increases both mean and amplitude-stress values. The model exhibited high accuracy for most of the predicted R-ratios, with the lowest r^2-value being under R = 0.5 and R = 2. All constant life lines connect to fatigue data points for all R-ratios examined, showing therefore consistency between the diagram and r^2-values in Table 15. This makes piecewise modeling to be the most accurate method of constructing a constant life diagram thus far.

5.6.3. Harris modeling

The Harris model was applied by using Equation 9 to fatigue data under R = 0.1, R = -1 and R = 10. Simultaneous solution Equation 9 at these three values of R-ratios provides values for *f*, *u*, and *v* for all cycles. These parameters are shown below in Table 18.

Table 18: Harris model coefficients

	f	u	v	A_i	B_i
0	0	0	0		
1.E+01	1.110	2.924	2.810	-0.081	1.337
1.E+02	0.921	3.524	3.437	0.081	2.426
1.E+03	0.764	4.247	4.205	0.088	2.296
1.E+04	0.634	5.119	5.144	i = 1 to 3	
1.E+05	0.526	6.170	6.293		
1.E+06	0.437	7.436	7.698		
1.E+07	0.362	8.962	9.417		

The polynomial curves almost similar to the ones given by second-order and fourth-order model can be seen in the diagram (see Figure 32). The mean is ranged between UCS and UTS.

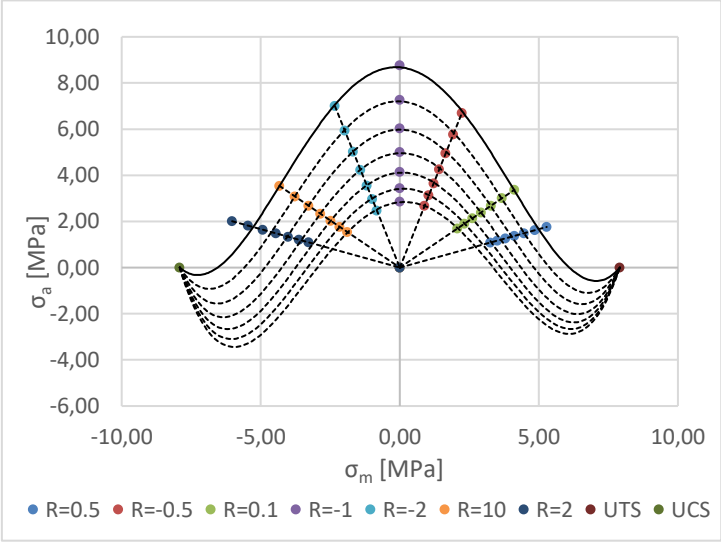

Figure 32: Harris

This model also shows symmetry around R = -1, as shown in Figure 32. The model shows that the change from static compression loading to compression-tension fatigue loading increases both mean and amplitude loads, while changing from static tension loading to tension-compression fatigue loading decreases mean and increases amplitude. The lowest accuracy was observed for joints tested under R = 2, as both Table 15 and Figure 32 illustrate. The table and diagram show

that the model exhibited high accuracy when predicting fatigue data under both R = -2 and R = -0.5.

5.6.4. Kawai modeling

The model by Kawai is given by Equation 10 and 11 for any constant life curve, as shown in Figure 33. The data under R = -1 was used as critical R-ratio for the application of this model. The model was applied for the entire spectrum of mean stress, ranging from UCS to UTS. The parameters calculated for this model, as explained in section 2.8.4, are shown in Table 19 below.

Table 19: Kawai model coefficients

Cycles	σ_{max}^{γ}	ψ_{γ}	σ_B
0	0	0	7.91
1.E+01	8.773	1.109	
1.E+02	7.277	0.920	
1.E+03	6.036	0.763	
1.E+04	5.007	0.633	
1.E+05	4.153	0.525	
1.E+06	3.445	0.435	
1.E+07	2.858	0.361	

Figure 33 below illustrates the constant curves established; polynomial curves of sixth-order were used for various regions of the CLD:

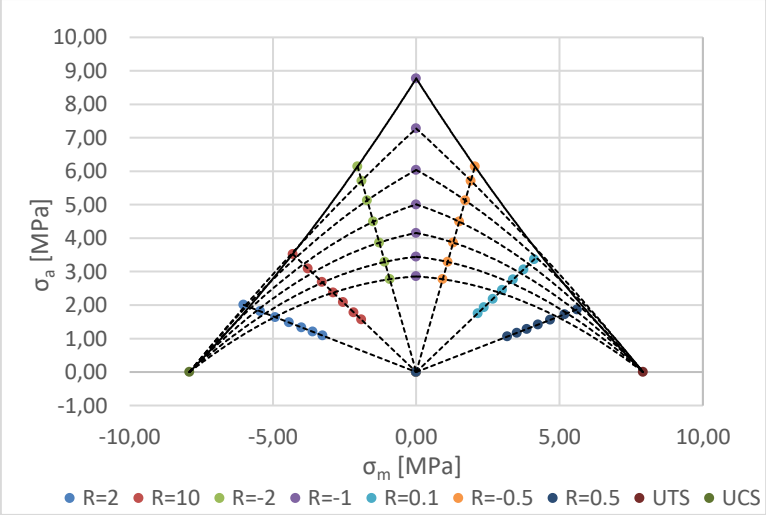

Figure 33: Kawai

The diagram in Figure 33 shows that constant curves of Kawai's model become second-order polynomials as number of cycles is increased. The diagram is also symmetrical around R = -1. For any constant life curve, the amplitude stress increases with an increasing mean stress between UCS

and zero, while it decreases with an increasing mean stress between zero and UTS. The change from static compression loading to compression-tension fatigue loading causes an increase in both mean and amplitude stresses for any number of cycles. Changing from static tension loading to tension-compression loading decreases mean and increases amplitude. The stress ratios of 0.1 and 2 exhibited the lowest accuracy, as Table 15 and Figure 33 show. The highest accuracy achieved was at R = -0.5, R = 0.5, R = -2 and R =10. The curves do not connect to all data points at both R = 0.5 and R = 10.

5.7. Model comparisons

The comparison process of each of the above discussed formulas was carried out for each R-ratio tested**.** The statistical distance between experimental amplitude values and amplitude values predicted by each model was again used as a comparison tool, as given in Appendix D. Table 10 and Table 15 give a summary of r^2-values for all models investigated. The two tables show that linear, third-order, piecewise linear and Kawai models have highest r^2-values for most R-ratios tested. This section compares and discusses these four models using S-N curves established from the experiments and the S-N curves predicted by each of these models under each R-ratio. The curves are plotted at selected number of cycles from the experiments and are shown below in Figure 34. A power regression line is fitted for experimental values under each R-ratio, in order to be able to visually observe the distance between values predicted by each model and the experimental values.

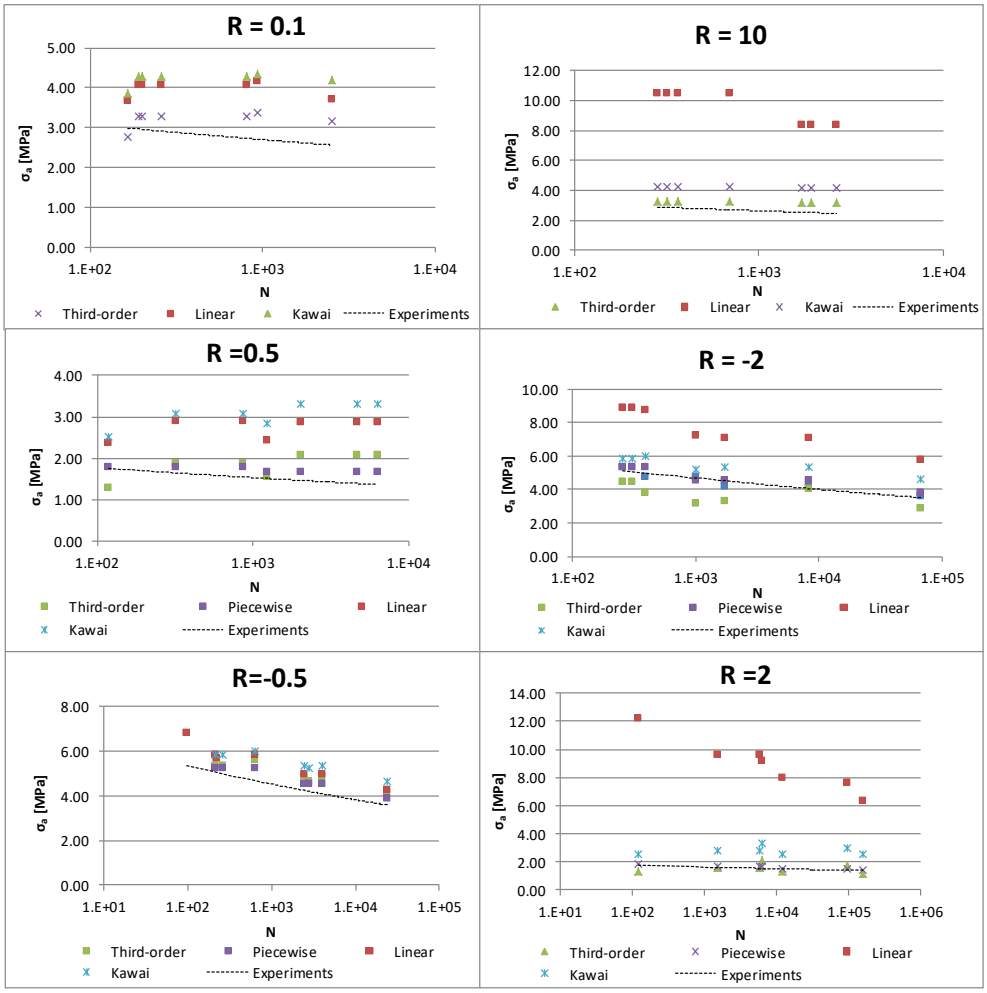

Figure 34: Models and experimental data comparison

For samples tested at R = 0.1, Figure 34 shows that the third-order model closely approximates the experimental points for the chosen number of cycles. The data points of the two curves are close together, as can be observed. Values predicted by linear modeling are the second closest to the experimental values, while values predicted by Kawai are the farthest. Under R =10, the third-order polynomial model again closely approximates experimental values as compared to other models, the two S-N curves have almost the same slopes. The second-closest values to the experimental values are given by the Kawai model, while values predicted by the linear modeling are the farthest in this case. Piecewise and third-order models closely approximate experimental values for the joints tested under R = 0.5. Values given by both linear and Kawai models are the farthest from the experimental values for this R-ratio. For samples tested under R = -2, piecewise, third-order and Kawai models closely approximate the established experimental values. Linear modeling values are the farthest away from the experimental values for these joints. The S-N values predicted again by piecewise and third-order are the closest to the experimental values for

samples tested at R = -0.5. There is minimal difference between the slopes of these values and the experimental values. The farthest values away from the experimental values are given by the Kawai model. Under R = 2, the points by piecewise, third-order and Kawai closely approximate the experimental points. The points by linear modeling are once again the farthest from the experimental values.

5.8. Conclusion

The benefit of modeling is that the experimental work required studying fatigue behavior of various materials, and failure of parts or components can be reduced by accurate application of these models. A tool for the accurate prediction of various S-N curves for different loading conditions can therefore be established. Linear, third-order, piecewise and Kawai models proved to be acceptable tools for constructing constant life diagrams. This was based on the statistical distance observed between experiment data and the data predicted by each of these models. However, further analysis revealed that the piecewise linear model was the only model with high r^2-values in which all constant life lines on the diagram connect to mean-amplitude data points under all R-ratios examined. The piecewise linear model can thus be effectively used to predict mean and amplitude stress values under R = 0.5, R = -0.5, R = -2 and R = 2, using values of mean and amplitude stress at R = 0.1, R = -1 and R = 10.

CHAPTER 6: CONCLUSIONS AND RECOMMENDATIONS

6.1. Overview

An experimental investigation into fatigue behavior of adhesively-bonded double strap lap glass fiber joints was performed. The joints were tested under fatigue loading at different stress ratios; namely R = 0.1, R = -1, R = 10, R = 0.5, R = -0.5, R = -2 and R = 2. In Chapter 2, a review of literature discussing adhesive bonding, failure modes expected for bonded joints, general fatigue and failure of materials, fatigue life of materials, fatigue loading, testing methods and standards and precision of data for fatigue was carried out. The chapter also discussed the mean and amplitude stress effect on fatigue life. Modeling and its necessity for predicting fatigue behavior of the tested joints was also discussed in this chapter. An experimental methodology was developed for the purpose of deriving fatigue data for the examined joints in Chapter 3. The material, specimen geometry and fabrication, experimental set-up and testing were some of the factors explained in this Chapter 3. In Chapter 4, the experimental results were then discussed and analyzed in terms of both static and fatigue testing. Curve-fitting through load-cycles data and repeatability of measured cycles were discussed. Stress-life comparison, curve-fitting through stress-cycles data, and various combinations of the constant life diagrams were also discussed in Chapter 4. In Chapter 5, different mathematical combinations were then considered for modeling the relationship between mean and amplitude stress at a randomly chosen number of cycles from the experiments. These models were evaluated for each R-ratio by comparing the established data with the experimental derived data.

6.2. Conclusions

The S-N curves showed that both mean and amplitude strength of double strap lap joints decreases with increasing number of applied cycles for all fatigue loading conditions. As expected, mean strength is zero for joints tested under R = -1. Using the tested R-ratios, the S-N curves show that amplitude strength of the joints is low under tension-tension and compression-compression fatigue loading. Amplitude strength is high under both compression-tension and tension-compression fatigue loading. Inversely, the mean strength of joints is high under both tension-tension and compression-compression fatigue loading. Mean strength is low under compression-tension and tension-compression loading. The amplitude strength therefore decreases when the load changes from both mixture of tension and compression to either pure compression or tension loading. The mean decreases when the load is changed from pure tension to tension-compression fatigue loading, and also when the load changes from pure compression loading to compression-tension

loading. The same observations made on the S-N curves can be made on the mean-amplitude constant life diagram. The behavior and failure of double lap strap glass fiber joints under fatigue loading conditions examined can thus be described using mean and amplitude strengths. The mean and amplitude strengths can also be used to simulate the behavior of other joints and also of aircraft joint components (double-strap lap joint components) subjected to fatigue loading conditions under which no experimental data exist. This comprehensive knowledge can therefore be used in practice to design against fatigue failure, instead of only designing static failure. The following conclusions can further be made about fatigue behavior of double lap strap glass fiber joints under the loading conditions tested:

- The mean-amplitude diagram for the loading conditions shows no symmetry around zero R = -1. However, the symmetry exists around R = -1 for loading conditions defined by R = 0.5, R = 0.1 and R =10, R = 2. As seen in the diagram, the symmetry demonstrate proportion and balance between tension-tension and compression-compression fatigue loading for these R-ratios.
- As shown by the mean-amplitude stress constant life diagram, a general conservative design rule will be: For fatigue life of 1×10^7 cycles, an average applied stress (peel plus shear stress) on the overlap area of double strap lap joint should be less than 2.86 MPa.
- The fatigue life of joints increases when the mean is increased from static compression strength to zero at constant amplitude loading.
- The life also increases at constant amplitude loading when the mean increases from zero to static tensile strength.
- Different formulas can be considered for modeling the fatigue behavior of the examined joints.
- Piecewise-linear will be a preferable method for the modelling of mean and amplitude stress.

6.3. Contributions and limitations

The study can be used as part of ongoing investigations into the behavior of composite materials and bonded joints under the action of both static and dynamic loading. Such further studies may include some of the following:

- A methodology for testing complex bonded parts or structures can be developed
- The behavior of the joint configuration for these complex parts under different loading conditions can be predicted
- Predictive tools for fatigue behavior of these parts can be modeled
- New and more design-allowable values can be developed, and
- Heavy structures that consume a lot of material can therefore be avoided in order to preserve natural resources.

Some of the limitations experienced during the course of this work were that, as a result of time constraints and limited resources, additional fatigue loading conditions and a higher number of applied cycles could not be investigated. Testing at a higher number of cycles would provide more accurate values for the parameters of the power law used to simulate fatigue behavior. Testing more R-ratios means more observations about mean and amplitude stress could be made from the constant life diagrams.

6.4. Recommendations

Fatigue behavior of composite bonded joints is therefore not typical and not like that of other materials such as metals. Various factors have an influence on fatigue of composite joints, meaning there is always a need for further testing to build on the existing experimental data. The following recommendations can be made for further investigations:

- Different adhesive system can be used
- Different bond thickness can be investigated
- Different matrix and environmental impacts can be studied
- Different fabric orientation of fibers can also be investigated
- The manufacturing process of laminates can be varied
- The effect of different materials across the adhesive layer can be studied
- Different specimen geometries can be tested

- The effect of laboratory conditions (temperature and humidity) can be examined
- More stress ratios can be tested
- Testing at higher number of cycles can also be considered
- Mechanically fastened joints can be studied
- A mixture of adhesively-bonded and mechanically fastened joints can also be evaluated
- Modelling mean and amplitude in terms of using more than one R-ratio can also be investigated

BIBLIOGRAPHY

AMTS, 2010. *AMTS STANDARD WORKSHOP PRACTICE,* s.l.: Technology innovation agency.

AMTS, 2011. *AMTS STANDARD WORKSHOP PRACTICE,* s.l.: Technology innovation agency.

ASTM, 1996. Standard Test Method for Strength of Double lap Shear Adhesive Joints by Tension Loading. pp. 1-4.

ASTM, 2002. *Standard Test Method for Tension-Tension Fatigue of Polymer Matrix Composite Materials,* West Conshohocken: ASTM International.

ASTM, 2006. Standard Practice for Conducting an Interlaboratory Study to Determine the Precision of a Test Method. *ASTM International,* 4 8, E691(05), pp. 1-23.

Bendouba, M., Aid, A. & Benguediab, M., 2014. Fatigue Life Prediction of Composite Under Two Fatigue Life Prediction of Composite Under Two. *Engineering, Technology & Applied Science Research,* 4(1), pp. 587-590.

Boerstra, G. K., 2006. *Wind turbines and constructions.* [Online]
Available at: www.wmc.eu
[Accessed 10 February 2006].

Cerny, I. & Mayer, R. M., 2011. Fatigue of selected GRP composite components and joints with damage evaluation. *Elsevier,* 7 September, Issue 94, pp. 664-670.

Chowdhury, N., Chiu, W. k. & Wang, J., 2014. Review on thee fatigue of composite hybrid joints used in aircraft structures. *Advanced Materials Research,* Volume 891-892, pp. 1591-1596.

Devorce, J. & Farnum, N., 2005. Other Confidence Levels and a General Formula. In: C. Crockett , A. Day & R. Letts, eds. *Applied Statistics for Engineers and Scientists.* 2nd ed. Belmont, CA 94002: Brooks/Cole, pp. 298-299.

Duthinh, D., 2000. Connections of fiber-reinforced polymer (FRP) structural members: A review of the state of the art. In: D. Duthinh, ed. *Connections of fiber-reinforced polymer (FRP) structural members: A review of the state of the art.* Gaithersburg, Maryland: National institute of standards and technology, pp. 1-67.

Harris, B., 2003 b. A parametric constant-life model for prediction of the fatigue lives of fibre reinforced plastics. pp. 546-68.

Harris, B., 2003. *Fatigue in composites.* Cambridge: Woodhead publishing limited.

Hexion, C. S., 2006. *Laminating resin MGS L285,* Stuttgart: Hexion Speciality Chemicals.

Hoke, M. J., 2005. *Cozy builders.* [Online]
Available at: www.cozybuilders.org
[Accessed 05 July 2014].

ISO, 1994. Accuracy (trueness and prceison) of measurement methods and results-Part 6: Use in practice of accuracy values. *ISO,* 5725(6), pp. 1-33.

ISO, 2003. Fibre-reinforced plastics — Determination of fatigue properties under cyclic loading conditions. 15 12.pp. 1-6.

ISO, 2005. Fibre-reinforced plastic-Methods of producing test plates: Part 4. *International Standard Organization,* 15 03.pp. 1-6.

Kassapoglou, C., 2007. Fatigue Life Prediction of Composite Structures Under Constant Amplitude Loading. *Journal of Composite Materials,* 41(22), pp. 2737-2754.

Kawai, M. & Koizumi, M., 2007. Nonlinear constant fatigue life diagrams for carbon/epoxy laminates at room temeperature. *ScienceDirect,* Part A(38), pp. 2342-2353.

Kensche, C. W., 1996. *Fatigue of materials and components for wind turbine rotor blades.* Brussels: European commission.

Mischke, C. R., Shigley, J. E. & Budynas, R. G., 2004. Introduction to fatigue in metals. In: J. P. Holman & J. R. Lloyd, eds. *Mechanical engineering design.* 7th ed. New York: McGraw-Hill, pp. 306-307.

Passipoularidis, V. A. & Philippidis, T. P., 2008. A study of factors affecting life prediction of composite under spectrum loading. *International Journal of Fatigue,* 24 July, Issue 31, pp. 408-417.

Philippidis, T. P. & Vassilopoulos, A. P., 2004. Life prediction metholodgy for GFRP laminates under spectrum loading. *Elsevier,* 19 February, Part A(35), pp. 657-666.

Sarfaraz, R., Vassilopoulos, A. P. & Keller, T., 2011. Experimental investigation of the fatigue behaviour of adhesivley-bonded pultruded GFRP joints under different load ratios. *International Journal of Fatigue,* Issue 33, pp. 1451-1460.

Sarfaraz, R., Vassilopoulos, A. P. & Keller, T., 2012. Experimental investigation and modeling of mean load effect on fatigue behavior of adhesively-bonded pultruded GFRP joints. *International Journal of fatigue,* Issue 44, pp. 245-252.

Sarfaraz, R., Vassilopoulos, A. P. & Keller, T., 2013. Variable amplitude fatigue of adhesively-bonded pultruded GFRP joints. *International journal of fatigue,* Issue 55, pp. 22-32.

Shahverdi, M., Vassilopoulos, A. P. & Kellar, T., 2012. Experimental investigation of R-ratio effects on fatigue crack growth of adhesively-bonded pultruded GFRP DCB joints under CA loading. *Composites: Part A,* 24 October, Issue 43, p. 1689–1697.

Shahverdi, M., Vassilopoulos, A. P. & Keller, T., 2012. A total fatigue life model for the prediction of the R-ratio effects on fatigue crack growth of adhesively-bonded pultruded GFRP DCB joints. *Elsevier,* May, Composite: Part A(43), pp. 1783-1790.

Solana, A. G., Crocombe, A. D. & Ashcroft, I. A., 2010. Fatigue life and backface strain predictions in adhesively bonded joints. *International journal of adhesion and adhesives,* Issue 30, pp. 36-42.

Taylor, B. N. & Kuyatt, C. E., 1994. *Guidelines for Evaluating and Expressing the Uncertainty of NIST Measurement Results,* s.l.: NIST.

Vassilopoulos, A. P., Manshadi, B. D. & Keller, T., 2010. Influence of the constant life diagram formulation on the fatigue life prediction of composite materials. *International Journal of fataigue,* Issue 32, pp. 659-669.

Vassilopoulos, A. P., Manshadi, B. D. & Keller, T., 2010. Piecewise non-linear constant life diagram formulation for FRP composite materials. *International Journal of Fatigue,* Issue 32, pp. 1731-1738.

Zhang, Y., Vassilopoulos, A. P. & Keller, T., 2008. Stiffness degradation and fatigue life prediction of adhesively-bonded joints for fiber-reinforced polymer composites. *International journal of fatigue,* 28 February, Issue 30, p. 1813–1820.

APPENDIX A: EXPERIMENTAL RESULTS AND ANALYSIS

Table 20: Effect of adhesive thickness

Thickness [mm]	Specimen number	Peak load [kN]	Tensile stress [MPa]
1	1	3.50	7.78
	2	4.25	9.44
	3	3.50	7.78
	4	4.39	9.76
	5	3.55	7.89
2	1	3.65	8.11
	2	3.19	7.09
	3	2.85	6.33
	4	3.15	7.00
	5	3.13	6.96
3	1	2.94	6.53
	2	2.82	6.27
	3	3.56	7.91
	4	4.00	8.89
	5	2.57	5.71
4	1	3.16	7.02
	2	2.63	5.84
	3	2.69	5.98
	4	2.66	5.91
	5	2.14	4.76
5	1	1.93	4.29
	2	3.23	7.18
	3	2.82	6.27
	4	2.15	4.78
	5	1.83	4.07

Table 21: Static tension

Specimen ID	Bond area [mm2]	Peak load [kN]	Nominal stress [MPa]
TC1	450	3.40	7.56
TC2	450	3.40	7.56
TC3	450	3.64	8.09
TC4	450	3.80	8.44
Average	450	3.56	7.91

Table 22: Static compression

Specimen ID	Bond area [mm2]	Peak load [kN]	Average stress [MPa]
C1	450	-3.15	-7.00
C2	450	-3.65	-8.11
C3	450	-3.19	-7.09
C4	450	-2.85	-6.33
Average		-3.21	-7.13

Table 23: Measured and calculated fatigue data (Load-cycles)

R ratio	Specimen ID	Percent level [%]	Applied load [kN]	Cycles to failure	Maximum cyclic load [kN]	Minimum cyclic load [kN]	Amplitude load [kN]	Mean Load [kN]
0.1	T019001	90	3.20	5.00E+00	3.204	0.320	1.442	1.762
	T019002	90	3.20	1.00E+01	3.204	0.320	1.442	1.762
	T019003	90	3.20	8.00E+01	3.204	0.320	1.442	1.762
	T019004	90	3.20	1.23E+02	3.204	0.320	1.442	1.762
	T019005	90	3.20	1.66E+02	3.204	0.320	1.442	1.762
	T018001	80	2.85	1.92E+02	2.848	0.285	1.282	1.566
	T018002	80	2.85	1.99E+02	2.848	0.285	1.282	1.566
	T018003	80	2.85	2.58E+02	2.848	0.285	1.282	1.566
	T018004	80	2.85	8.10E+02	2.848	0.285	1.282	1.566
	T017801	78	2.78	9.41E+02	2.777	0.278	1.250	1.527
	T017001	70	2.49	2.54E+03	2.492	0.249	1.121	1.371
	T017002	70	2.49	3.33E+03	2.492	0.249	1.121	1.371
	T017003	70	2.49	7.26E+03	2.492	0.249	1.121	1.371
	T017004	70	2.49	9.71E+03	2.492	0.249	1.121	1.371
	T016901	69	2.46	3.58E+03	2.456	0.246	1.105	1.351
	T016101	61	2.17	1.20E+04	2.172	0.217	0.977	1.194
	T016001	60	2.14	2.98E+05	2.136	0.214	0.961	1.175
	T015001	50	1.78	1.02E+06	1.780	0.178	0.801	0.979
-1	TC-19201	92	3.28	1.84E+02	3.275	-3.275	3.275	0.000
	TC-19102	91	3.24	4.90E+01	3.240	-3.240	3.240	0.000
	TC-19003	90	3.20	1.61E+02	3.204	-3.204	3.204	0.000
	TC-18904	90	3.20	2.47E+02	3.204	-3.204	3.204	0.000
	TC-18805	90	3.20	2.51E+02	3.204	-3.204	3.204	0.000
	TC-18001	80	2.85	2.50E+02	2.848	-2.848	2.848	0.000
	TC-18002	80	2.85	3.69E+02	2.848	-2.848	2.848	0.000
	TC-18003	80	2.85	5.56E+02	2.848	-2.848	2.848	0.000
	TC-18004	80	2.85	6.84E+02	2.848	-2.848	2.848	0.000
	TC-18005	80	2.85	1.06E+03	2.848	-2.848	2.848	0.000

	TC-17001	70	2.49	2.23E+03	2.492	-2.492	2.492	0.000
	TC-17002	70	2.49	1.78E+03	2.492	-2.492	2.492	0.000
	TC-17003	70	2.49	1.78E+03	2.492	-2.492	2.492	0.000
	TC-16001	60	2.14	1.65E+04	2.136	-2.136	2.136	0.000
	TC-16002	60	2.14	2.60E+04	2.136	-2.136	2.136	0.000
	TC-16003	60	2.14	2.82E+04	2.136	-2.136	2.136	0.000
	TC-15001	50	1.78	4.36E+05	1.780	-1.780	1.780	0.000
	TC-14001	40	1.42	1.01E+06	1.424	-1.424	1.424	0.000
10	C109101	91	3.24	8.60E+01	3.240	0.324	1.458	1.782
	C109001	90	3.20	1.71E+02	3.204	0.320	1.442	1.762
	C108901	89	3.17	5.90E+01	3.168	0.317	1.426	1.743
	C108001	80	2.85	3.16E+02	2.848	0.285	1.282	1.566
	C108002	80	2.85	3.63E+02	2.848	0.285	1.282	1.566
	C108003	80	2.85	2.81E+02	2.848	0.285	1.282	1.566
	C108004	80	2.85	6.91E+02	2.848	0.285	1.282	1.566
	C107001	70	2.49	1.71E+03	2.492	0.249	1.121	1.371
	C107002	70	2.49	2.63E+03	2.492	0.249	1.121	1.371
	C107003	70	2.49	1.92E+03	2.492	0.249	1.121	1.371
	C107004	70	2.49	1.98E+03	2.492	0.249	1.121	1.371
	C106001	60	2.14	1.58E+04	2.136	0.214	0.961	1.175
	C106002	60	2.14	2.81E+04	2.136	0.214	0.961	1.175
	C106003	60	2.14	1.98E+05	2.136	0.214	0.961	1.175
	C105001	50	1.78	1.02E+06	1.780	0.178	0.801	0.979
0.5	T059001	90	3.20	3.20E+01	3.204	1.602	0.801	2.403
	T059002	90	3.20	5.70E+01	3.204	1.602	0.801	2.403
	T059003	90	3.20	1.18E+02	3.204	1.602	0.801	2.403
	T058001	80	2.85	3.20E+02	2.848	1.424	0.712	2.136
	T058002	80	2.85	8.72E+02	2.848	1.424	0.712	2.136
	T058003	80	2.85	1.23E+03	2.848	1.424	0.712	2.136
	T057001	70	2.49	2.04E+03	2.492	1.246	0.623	1.869
	T057002	70	2.49	4.66E+03	2.492	1.246	0.623	1.869
	T057003	70	2.49	6.31E+03	2.492	1.246	0.623	1.869
	T056001	60	2.14	1.88E+06	2.136	1.068	0.534	1.602
	T056002	60	2.14	1.98E+06	2.136	1.068	0.534	1.602
	T055001	50	1.78	1.03E+07	1.780	0.890	0.445	1.335
2	C29001	90	3.20	3.15E+02	3.204	1.602	0.801	2.403
	C29002	90	3.20	6.25E+01	3.204	1.602	0.801	2.403
	C29003	90	3.20	1.23E+02	3.204	1.602	0.801	2.403
	C28001	80	2.85	1.53E+03	2.848	1.424	0.712	2.136
	C28002	80	2.85	5.81E+03	2.848	1.424	0.712	2.136
	C28003	80	2.85	1.21E+04	2.848	1.424	0.712	2.136
	C27001	70	2.49	6.37E+03	2.492	1.246	0.623	1.869

	C27002	70	2.49	9.81E+04	2.492	1.246	0.623	1.869
	C27003	70	2.49	1.58E+05	2.492	1.246	0.623	1.869
	C26001	60	2.14	5.22E+05	2.136	1.068	0.534	1.602
	C26002	60	2.14	5.89E+06	2.136	1.068	0.534	1.602
-2	CT-29001	90	3.20	2.54E+02	3.204	-1.602	2.403	0.801
	CT-29002	90	3.20	3.04E+02	3.204	-1.602	2.403	0.801
	CT-28001	80	2.85	3.89E+02	2.848	-1.424	2.136	0.712
	CT-28002	80	2.85	1.00E+03	2.848	-1.424	2.136	0.712
	CT-27001	70	2.49	8.27E+03	2.492	-1.246	1.869	0.623
	CT-27002	70	2.49	1.74E+03	2.492	-1.246	1.869	0.623
	CT-26002	60	2.14	6.71E+04	2.136	-1.068	1.602	0.534
	CT-25001	50	1.78	1.90E+05	1.780	-0.890	1.335	0.445
-0.5	TC-059001	90	3.20	2.24E+02	3.204	-1.602	2.403	0.801
	TC-059002	90	3.20	9.80E+01	3.204	-1.602	2.403	0.801
	TC-058001	80	2.85	2.17E+02	2.848	-1.424	2.136	0.712
	TC-058002	80	2.85	6.39E+02	2.848	-1.424	2.136	0.712
	TC-057001	70	2.49	2.49E+03	2.492	-1.246	1.869	0.623
	TC-057002	70	2.49	4.07E+03	2.492	-1.246	1.869	0.623
	TC-056001	60	2.14	2.38E+04	2.136	-1.068	1.602	0.534

Table 24: Sarfaraz experiments parameters

Parameter	-2	-1	-0.5	0.1	0.5	2	10
k1	0.088	0.104	0.095	0.083	0.075	0.032	0.043
σ_1	36.740	39.770	28.150	17.320	10.780	7.590	14.600

Table 25: Curve-fitting through Load-cycles data

Amplitude load [kN]									
R	**Cycles to failure**	**Current fit**	**Sarfaraz fit**	**%Error[1]**	**%Error per R-ratio[1]**	**%Error[2]**	**%Error per R-ratio[2]**	**r^2-value[1]**	**r^2-value[2]**
0.1	5.00E+00	1.571	2.729	8.93	4.57	47.16	30.72	0.875	0.851
	1.00E+01	1.518	2.576	5.25		44.04			
	8.00E+01	1.369	2.169	5.06		33.52			
	1.23E+02	1.340	2.093	7.07		31.11			
	1.66E+02	1.320	2.042	8.44		29.38			
	1.92E+02	1.311	2.017	2.27		36.47			
	1.99E+02	1.308	2.011	2.09		36.28			
	2.58E+02	1.292	1.969	0.78		34.90			
	8.10E+02	1.220	1.791	4.78		28.43			
	9.41E+02	1.211	1.769	3.06		29.34			

	2.54E+03	1.153	1.629	2.83		31.16			
	3.33E+03	1.138	1.593	1.46		29.60			
	7.26E+03	1.095	1.493	2.39		24.91			
	9.71E+03	1.079	1.458	3.79		23.08			
	3.58E+03	1.134	1.583	2.55		30.18			
	1.20E+04	1.068	1.432	9.24		31.77			
	2.98E+05	0.910	1.098	5.28		12.46			
	1.02E+06	0.856	0.992	6.93		19.21			
-1	1.84E+02	3.117	4.166	4.84	4.07	21.39	20.89	0.947	0.943
	4.90E+01	3.470	4.780	7.11		32.22			
	1.61E+02	3.151	4.224	1.67		24.15			
	2.47E+02	3.043	4.041	5.02		20.71			
	2.51E+02	3.039	4.034	5.15		20.58			
	2.50E+02	3.040	4.036	6.74		29.43			
	3.69E+02	2.945	3.876	3.42		26.52			
	5.56E+02	2.849	3.714	0.04		23.33			
	6.84E+02	2.801	3.635	1.63		21.66			
	1.06E+03	2.703	3.473	5.09		17.99			
	2.23E+03	2.545	3.216	2.14		22.52			
	1.78E+03	2.593	3.293	4.04		24.32			
	1.78E+03	2.592	3.292	4.03		24.31			
	1.65E+04	2.163	2.613	1.29		18.24			
	2.60E+04	2.085	2.492	2.38		14.29			
	2.82E+04	2.071	2.471	3.02		13.57			
	4.36E+05	1.658	1.860	6.84		4.28			
	1.01E+06	1.549	1.704	8.77		16.44			
10	8.60E+01	1.400	2.174	3.95	3.27	32.94	38.95	0.941	0.934
	1.71E+02	1.343	2.111	6.83		31.70			
	5.90E+01	1.432	2.209	0.46		35.45			
	3.16E+02	1.294	2.057	1.00		37.68			
	3.63E+02	1.284	2.044	0.16		37.31			
	2.81E+02	1.304	2.067	1.72		37.99			
	6.91E+02	1.235	1.989	3.65		35.57			
	1.71E+03	1.169	1.914	4.24		41.40			
	2.63E+03	1.139	1.879	1.59		40.33			
	1.92E+03	1.161	1.905	3.54		41.12			
	1.98E+03	1.159	1.902	3.33		41.04			
	1.58E+04	1.022	1.741	6.34		44.78			
	2.81E+04	0.987	1.699	2.73		43.41			
	1.98E+05	0.878	1.563	8.69		38.50			
	1.02E+06	0.795	1.458	0.74		45.05			
0.5	3.20E+01	0.803	1.495	0.25		46.43			
	5.70E+01	0.784	1.432	2.15		44.05			
	1.18E+02	0.760	1.355	5.10	3.96	40.91	35.90	0.939	0.945

	3.20E+02	0.729	1.257	2.37		43.38			
	8.72E+02	0.699	1.166	1.86		38.95			
	1.23E+03	0.689	1.136	3.27		37.35			
	2.04E+03	0.674	1.094	8.22		43.06			
	4.66E+03	0.651	1.028	4.52		39.41			
	6.31E+03	0.643	1.005	3.19		38.00			
	1.88E+06	0.506	0.655	5.28		18.43			
	1.98E+06	0.505	0.652	5.50		18.11			
	1.03E+07	0.471	0.576	5.81		22.76			
2	3.15E+02	0.770	1.136	3.85	3.83	29.52	33.83	0.898	0.898
	6.25E+01	0.821	1.197	2.46		33.08			
	1.23E+02	0.799	1.171	0.22		31.62			
	1.53E+03	0.724	1.080	1.65		34.10			
	5.81E+03	0.687	1.035	3.54		31.23			
	1.21E+04	0.667	1.011	6.29		29.59			
	6.37E+03	0.684	1.032	9.83		39.65			
	9.81E+04	0.615	0.946	1.36		34.13			
	1.58E+05	0.603	0.932	3.18		33.12			
	5.22E+05	0.575	0.896	7.76		40.43			
	5.89E+06	0.523	0.830	2.04		35.63			
-2	2.54E+02	2.340	4.056	2.61	4.56	40.76	40.68	0.929	0.929
	3.04E+02	2.308	3.992	3.96		39.81			
	3.89E+02	2.264	3.906	5.99		45.32			
	1.00E+03	2.104	3.594	1.50		40.56			
	8.27E+03	1.786	2.982	4.45		37.32			
	1.74E+03	2.015	3.422	7.83		45.38			
	6.71E+04	1.518	2.479	5.23		35.36			
	1.90E+05	1.400	2.261	4.90		40.95			
-0.5	2.24E+02	2.270	3.032	5.54	2.61	20.74	22.64	0.923	0.922
	9.80E+01	2.411	3.279	0.35		26.72			
	2.17E+02	2.275	3.041	6.51		29.76			
	6.39E+02	2.102	2.745	1.59		22.18			
	2.49E+03	1.903	2.412	1.81		22.53			
	4.07E+03	1.835	2.302	1.80		18.82			
	2.38E+04	1.613	1.947	0.67		17.73			

Note:

[1]: Between current experiments and current model fit

[2]: Between current experiments and Sarfaraz model fit

Table 26: Calculated fatigue data (Stress-cycles)

R ratios	Specimen ID	Percent level [%]	Applied load [kN]	Cycles to failure	Maximum stress [MPa]	Minimum Stress [MPa]	Mean stress [MPa]	Amplitude stress [MPa]
0.1	T019001	90	3.20	5.00E+00	7.120	0.712	3.916	3.204
	T019002	90	3.20	1.00E+01	7.120	0.712	3.916	3.204
	T019003	90	3.20	8.00E+01	7.120	0.712	3.916	3.204
	T019004	90	3.20	1.23E+02	7.120	0.712	3.916	3.204
	T019005	90	3.20	1.66E+02	7.120	0.712	3.916	3.204
	T018001	80	2.85	1.92E+02	6.329	0.633	3.481	2.848
	T018002	80	2.85	1.99E+02	6.329	0.633	3.481	2.848
	T018003	80	2.85	2.58E+02	6.329	0.633	3.481	2.848
	T018004	80	2.85	8.10E+02	6.329	0.633	3.481	2.848
	T017801	78	2.78	9.41E+02	6.171	0.617	3.394	2.777
	T017001	70	2.49	2.54E+03	5.538	0.554	3.046	2.492
	T017002	70	2.49	3.33E+03	5.538	0.554	3.046	2.492
	T017003	70	2.49	7.26E+03	5.538	0.554	3.046	2.492
	T017004	70	2.49	9.71E+03	5.538	0.554	3.046	2.492
	T016901	69	2.46	3.58E+03	5.459	0.546	3.002	2.456
	T016101	61	2.17	1.20E+04	4.826	0.483	2.654	2.172
	T016001	60	2.14	2.98E+05	4.747	0.475	2.611	2.136
	T015001	50	1.78	1.02E+06	3.956	0.396	2.176	1.780
-1	TC-19201	92	3.28	1.84E+02	7.278	-7.278	0.000	7.278
	TC-19102	91	3.24	4.90E+01	7.199	-7.199	0.000	7.199
	TC-19003	90	3.20	1.61E+02	7.120	-7.120	0.000	7.120
	TC-18904	90	3.20	2.47E+02	7.120	-7.120	0.000	7.120
	TC-18805	90	3.20	2.51E+02	7.120	-7.120	0.000	7.120
	TC-18001	80	2.85	2.50E+02	6.329	-6.329	0.000	6.329
	TC-18002	80	2.85	3.69E+02	6.329	-6.329	0.000	6.329
	TC-18003	80	2.85	5.56E+02	6.329	-6.329	0.000	6.329
	TC-18004	80	2.85	6.84E+02	6.329	-6.329	0.000	6.329
	TC-18005	80	2.85	1.06E+03	6.329	-6.329	0.000	6.329
	TC-17001	70	2.49	2.23E+03	5.538	-5.538	0.000	5.538
	TC-17002	70	2.49	1.78E+03	5.538	-5.538	0.000	5.538
	TC-17003	70	2.49	1.78E+03	5.538	-5.538	0.000	5.538
	TC-16001	60	2.14	1.65E+04	4.747	-4.747	0.000	4.747
	TC-16002	60	2.14	2.60E+04	4.747	-4.747	0.000	4.747
	TC-16003	60	2.14	2.82E+04	4.747	-4.747	0.000	4.747
	TC-15001	50	1.78	4.36E+05	3.956	-3.956	0.000	3.956
	TC-14001	40	1.42	1.01E+06	3.164	-3.164	0.000	3.164
10	C109101	91	3.24	8.60E+01	7.199	0.720	3.960	3.240
	C109001	90	3.20	1.71E+02	7.120	0.712	3.916	3.204
	C108901	89	3.17	5.90E+01	7.041	0.704	3.872	3.168

	C108001	80	2.85	3.16E+02	6.329	0.633	3.481	2.848
	C108002	80	2.85	3.63E+02	6.329	0.633	3.481	2.848
	C108003	80	2.85	2.81E+02	6.329	0.633	3.481	2.848
	C108004	80	2.85	6.91E+02	6.329	0.633	3.481	2.848
	C107001	70	2.49	1.71E+03	5.538	0.554	3.046	2.492
	C107002	70	2.49	2.63E+03	5.538	0.554	3.046	2.492
	C107003	70	2.49	1.92E+03	5.538	0.554	3.046	2.492
	C107004	70	2.49	1.98E+03	5.538	0.554	3.046	2.492
	C106001	60	2.14	1.58E+04	4.747	0.475	2.611	2.136
	C106002	60	2.14	2.81E+04	4.747	0.475	2.611	2.136
	C106003	60	2.14	1.98E+05	4.747	0.475	2.611	2.136
	C105001	50	1.78	1.02E+06	3.956	0.396	2.176	1.780
0.5	T059001	90	3.20	3.20E+01	7.120	3.560	5.340	1.780
	T059002	90	3.20	5.70E+01	7.120	3.560	5.340	1.780
	T059003	90	3.20	1.18E+02	7.120	3.560	5.340	1.780
	T058001	80	2.85	3.20E+02	6.329	3.164	4.747	1.582
	T058002	80	2.85	8.72E+02	6.329	3.164	4.747	1.582
	T058003	80	2.85	1.23E+03	6.329	3.164	4.747	1.582
	T057001	70	2.49	2.04E+03	5.538	2.769	4.153	1.384
	T057002	70	2.49	4.66E+03	5.538	2.769	4.153	1.384
	T057003	70	2.49	6.31E+03	5.538	2.769	4.153	1.384
	T056001	60	2.14	1.88E+06	4.747	2.373	3.560	1.187
	T056002	60	2.14	1.98E+06	4.747	2.373	3.560	1.187
	T055001	50	1.78	1.03E+07	3.956	1.978	2.967	0.989
2	C29001	90	3.20	3.15E+02	7.120	3.560	5.340	1.780
	C29002	90	3.20	6.25E+01	7.120	3.560	5.340	1.780
	C29003	90	3.20	1.23E+02	7.120	3.560	5.340	1.780
	C28001	80	2.85	1.53E+03	6.329	3.164	4.747	1.582
	C28002	80	2.85	5.81E+03	6.329	3.164	4.747	1.582
	C28003	80	2.85	1.21E+04	6.329	3.164	4.747	1.582
	C27001	70	2.49	6.37E+03	5.538	2.769	4.153	1.384
	C27002	70	2.49	9.81E+04	5.538	2.769	4.153	1.384
	C27003	70	2.49	1.58E+05	5.538	2.769	4.153	1.384
	C26001	60	2.14	5.22E+05	4.747	2.373	3.560	1.187
	C26002	60	2.14	5.89E+06	4.747	2.373	3.560	1.187
-2	CT-29001	90	3.20	2.54E+02	7.120	-3.560	1.780	5.340
	CT-29002	90	3.20	3.04E+02	7.120	-3.560	1.780	5.340
	CT-28001	80	2.85	3.89E+02	6.329	-3.164	1.582	4.747
	CT-28002	80	2.85	1.00E+03	6.329	-3.164	1.582	4.747
	CT-27001	70	2.49	8.27E+03	5.538	-2.769	1.384	4.153
	CT-27002	70	2.49	1.74E+03	5.538	-2.769	1.384	4.153
	CT-26002	60	2.14	6.71E+04	4.747	-2.373	1.187	3.560
	CT-25001	50	1.78	1.90E+05	3.956	-1.978	0.989	2.967
-0.5	TC-059001	90	3.20	2.24E+02	7.120	-3.560	1.780	5.340

	TC-059002	90	3.20	9.80E+01	7.120	-3.560	1.780	5.340
	TC-058001	80	2.85	2.17E+02	6.329	-3.164	1.582	4.747
	TC-058002	80	2.85	6.39E+02	6.329	-3.164	1.582	4.747
	TC-057001	70	2.49	2.49E+03	5.538	-2.769	1.384	4.153
	TC-057002	70	2.49	4.07E+03	5.538	-2.769	1.384	4.153
	TC-056001	60	2.14	2.38E+04	4.747	-2.373	1.187	3.560

Table 27: Curve-fitting through stress-cycles data

Amplitude stress [MPa]										
R ratio	Cycles to failure	Experiments [MPa]	Current fit [MPa]	Sarfaraz fit [MPa]	%Error [1]	%Error per R ratio [1]	%Error [2]	%Error per R ratio [2]	r^2- value per R ratio [1]	r^2-value per R ratio [2]
0.1	1.66E+02	3.204	2.934	4.537	8.44		29.38			
	1.92E+02	2.848	2.913	4.483	2.27		36.47			
	1.99E+02	2.848	2.907	4.470	2.09		36.28			
	2.58E+02	2.848	2.870	4.374	0.78	3.46	34.90	32.28	0.616	0.614
	8.10E+02	2.848	2.712	3.979	4.78		28.43			
	9.41E+02	2.777	2.692	3.930	3.06		29.34			
	2.54E+03	2.492	2.563	3.620	2.83		31.16			
-1	1.84E+02	7.278	6.926	9.258	4.84		21.39			
	4.90E+01	7.199	7.711	10.621	7.11		32.22			
	1.61E+02	7.120	7.001	9.387	1.67		24.15			
	2.47E+02	7.120	6.762	8.980	5.02	4.85	20.71	25.00	0.278	0.274
	2.51E+02	7.120	6.753	8.965	5.15		20.58			
	2.50E+02	6.329	6.756	8.968	6.74		29.43			
	3.69E+02	6.329	6.545	8.613	3.42		26.52			
10	3.16E+02	2.848	2.877	4.570	1.00		37.68			
	3.63E+02	2.848	2.853	4.543	0.16		37.31			
	2.81E+02	2.848	2.897	4.593	1.72		37.99			
	6.91E+02	2.848	2.744	4.420	3.65	2.27	35.57	38.77	0.887	0.888
	1.71E+03	2.492	2.598	4.252	4.24		41.40			
	2.63E+03	2.492	2.532	4.176	1.59		40.33			
	1.92E+03	2.492	2.580	4.232	3.54		41.12			
0.5	1.18E+02	1.780	1.689	3.012	5.10		40.91			
	3.20E+02	1.582	1.620	2.794	2.37		43.38			
	8.72E+02	1.582	1.553	2.592	1.86	4.08	38.95	40.15	0.865	0.866
	1.23E+03	1.582	1.530	2.525	3.27		37.35			
	2.04E+03	1.384	1.498	2.431	8.22		43.06			

	4.66E+03	1.384	1.447	2.285	4.52		39.41			
	6.31E+03	1.384	1.429	2.233	3.19		38.00			
2	1.23E+02	1.780	1.689	2.603	0.22		31.62			
	1.53E+03	1.582	1.620	2.401	1.65		34.10			
	5.81E+03	1.582	1.553	2.301	3.54		31.23			
	1.21E+04	1.582	1.530	2.247	6.29	3.73	29.59	33.35	0.760	0.758
	6.37E+03	1.384	1.498	2.294	9.83		39.65			
	9.81E+04	1.384	1.447	2.102	1.36		34.13			
	1.58E+05	1.384	1.429	2.070	3.18		33.12			
-2	2.54E+02	5.340	5.200	9.014	2.61		40.76			
	3.04E+02	5.340	5.128	8.872	3.96		39.81			
	3.89E+02	4.747	5.031	8.681	5.99		45.32			
	1.00E+03	4.747	4.675	7.986	1.50	4.51	40.56	40.64	0.884	0.887
	8.27E+03	4.153	3.969	6.626	4.45		37.32			
	1.74E+03	4.153	4.478	7.604	7.83		45.38			
	6.71E+04	3.560	3.374	5.508	5.23		35.36			
-0.5	2.24E+02	5.340	5.044	6.738	5.54		20.74			
	9.80E+01	5.340	5.359	7.287	0.35		26.72			
	2.17E+02	4.747	5.056	6.758	6.51		29.76			
	6.39E+02	4.747	4.671	6.100	1.59	2.61	22.18	22.64	0.923	0.922
	2.49E+03	4.153	4.228	5.361	1.81		22.53			
	4.07E+03	4.153	4.079	5.116	1.80		18.82			
	2.38E+04	3.560	3.584	4.327	0.67		17.73			

Note: [1]: Between amplitude stress values in Table 25 and current model fit

[2]: Between amplitude stress values in Table 25 and Sarfaraz model fit

Table 28: Calculated mean and amplitude stress values

	Amplitude Stress [MPa]							Mean Stress [MPa]						
Ratio/Cycles	-2	-1	-0.5	0.1	0.5	2	10	-2	-1	-0.5	0.1	0.5	2	10
0	0	0	0	0	0	0	0	0	0	0	0	0	0	0
1.E+01	6.68	8.77	6.33	3.37	1.87	1.96	3.54	-2.23	0.00	2.11	4.12	5.62	-5.88	-4.33
1.E+02	5.59	7.28	5.35	3.01	1.70	1.79	3.08	-1.86	0.00	1.78	3.68	5.10	-5.37	-3.77
1.E+03	4.68	6.04	4.52	2.68	1.54	1.64	2.68	-1.56	0.00	1.51	3.28	4.63	-4.91	-3.28
1.E+04	3.91	5.01	3.82	2.39	1.40	1.49	2.34	-1.30	0.00	1.27	2.93	4.20	-4.48	-2.85
1.E+05	3.27	4.15	3.23	2.14	1.27	1.36	2.03	-1.09	0.00	1.08	2.61	3.82	-4.09	-2.48
1.E+06	2.74	3.45	2.73	1.91	1.15	1.25	1.77	-0.91	0.00	0.91	2.33	3.46	-3.74	-2.16
1.E+07	2.29	2.86	2.30	1.70	1.05	1.14	1.54	-0.76	0.00	0.77	2.08	3.14	-3.42	-1.88

APPENDIX B: MEAN-AMPLITUDE STRESS MODEL COEFFICIENTS

Derivation of parameters for linear, second-order, third-order and fourth-order polynomial models is discussed. The coefficients are calculated for any constant life between 10^1 and 10^7.

B.1. Linear modeling

From Equation 21a:

$\sigma_a = 0 \quad when \quad \sigma_m = UCS$

$\therefore k_1 = -\frac{\sigma_{R=-1}}{UCS}$

From Equation 21b:

$\sigma_a = 0 \quad when \quad \sigma_m = UTS$

$\therefore k_2 = -\frac{\sigma_{R=-1}}{UTS}$

B.2. Second-order modeling

From Equation 22:

$\sigma_a = 0 \quad when \quad \sigma_m = UCS$

$\therefore aUCS^2 + bUCS + \sigma_{R=-1} = 0$

$\sigma_a = 0 \quad when \quad \sigma_m = UTS$---

$\therefore aUTS^2 + bUTS + \sigma_{R=-1} = 0$

Simultaneous solution of the above two equations gives:

$$a = \frac{(\sigma_{R=-1})\left(\frac{UTS}{UC} - 1\right)}{UTS^2 - (UCS)(UTS)}$$

$$b = \left(-\frac{\sigma_{R=-1}}{UCS}\right) - \frac{(\sigma_{R=-1})(UTS - UCS)}{UTS^2 - (UCS)(UTS)}$$

B.3. Third-order modeling

From Equation 23:

$\sigma_a = 0 \;\; when \;\; \sigma_m = UCS$

$\therefore \alpha UCS^3 + \beta UCS^2 + \gamma UCS + \sigma_{R=-1} = 0$

$\sigma_a = 0 \quad when \quad \sigma_m = UTS$

$\therefore \alpha UTS^3 + \beta UTS^2 + \gamma UTS + \sigma_{R=-1} = 0$

$\sigma_a' = 0 \quad when \;\; \sigma_m = \; UTS$ (Derivative of equation 23)

$\therefore 3\alpha UTS^2 + 2\beta UTS + \gamma = 0$

Simultaneous solution of the above three equations gives:

$$\alpha = \frac{(-\sigma_{R=-1})\left(\frac{UCS}{UTS} - 1\right)^2}{UCS^3 - 2(UTS)(UCS^2) + (UTS^2)(UCS)}$$

$$\beta = \frac{\sigma_{R=-1}}{UTS^2} + \frac{2(\sigma_{R=-1})\left(\frac{UCS}{UTS} - 1\right)^2 UTS}{UCS^3 - 2(UTS)(UCS^2) + (UTS^2)(UCS)}$$

$$\gamma = \frac{(-\sigma_{R=-1})\left(\frac{UCS}{UTS} - 1\right)^2 UTS^2}{UCS^3 - 2(UTS)(UCS^2) + (UTS^2)(UCS)} - \frac{2\sigma_{R=-1}}{UTS}$$

B.4. Fourth-order modeling

From Equation 24:

$\sigma_a = 0 \;\; when \;\; \sigma_m = UCS$

$\therefore \alpha UCS^4 + \beta UCS^3 + \gamma UCS^2 + \delta UCS + \sigma_{R=-1} = 0$

$\sigma_a = 0 \quad when \quad \sigma_m = UTS$

$\therefore \alpha UTS^4 + \beta UTS^3 + \gamma UTS^2 + \delta UTS + \sigma_{R=-1} = 0$

$\sigma_a' = 0 \quad when \;\; \sigma_m = \; UCS$ (Derivative of equation 24)

$\therefore 4\alpha UCS^3 + 3\beta UCS^2 + 2\gamma UCS + \delta = 0$

$\sigma_a' = 0 \quad when \;\; \sigma_m = \; UTS$ (Derivative of equation 24)

$\therefore 4\alpha UTS^3 + 3\beta UTS^2 + 2\gamma UTS + \delta = 0$

Simultaneous solution of the above four equations gives:

$$\alpha = \frac{\sigma_{R=-1}}{\big((UTS)(UCS)\big)^2}$$

$$\beta = \frac{-2(UTS + UCS)\sigma_{R=-1}}{\big((UTS)(UCS)\big)^2}$$

$$\gamma = \frac{[(UTS + UCS)^2 + 2UTSUCS]\sigma_{R=-1}}{(UTS(UCS)^2}$$

$$\delta = \frac{-2(UTS + UCS)\sigma_{R=-1}}{(UTS)UCS)}$$

APPENDIX C: MEAN-AMPLITUDE STRESS TABLES

The mean and amplitude stress under each R-ratio tested, as calculated by each of the models in Chapter 5, are given in the following tables.

Table 29: Linear CLD

	Amplitude Stress [MPa]							Mean Stress [MPa]						
Ratio/Cycles	-2	-1	-0.5	0.1	0.5	2	10	-2	-1	-0.5	0.1	0.5	2	10
0	0	0	0	0	0	0	0	0	0	0	0	0	0	0
1.E+01	6.41	8.77	6.41	1.76	1.82	1.88	1.63	-2.14	0.00	2.14	2.15	5.47	-5.64	-1.99
1.E+02	5.57	7.28	5.57	2.08	1.69	1.73	1.97	-1.86	0.00	1.86	2.55	5.07	-5.20	-2.41
1.E+03	4.81	6.04	4.81	2.37	1.57	1.60	2.27	-1.60	0.00	1.60	2.90	4.71	-4.79	-2.78
1.E+04	4.13	5.01	4.13	2.63	1.46	1.48	2.53	-1.38	0.00	1.38	3.21	4.37	-4.43	-3.09
1.E+05	3.53	4.15	3.53	2.86	1.36	1.37	2.76	-1.18	0.00	1.18	3.49	4.07	-4.10	-3.37
1.E+06	3.01	3.45	3.01	3.06	1.27	1.27	2.95	-1.00	0.00	1.00	3.74	3.80	-3.80	-3.61
1.E+07	2.55	2.86	2.55	3.24	1.18	1.18	3.13	-0.85	0.00	0.85	3.96	3.55	-3.54	-3.82

Table 30: Second-order CLD

	Amplitude Stress [MPa]							Mean Stress [MPa]						
Ratio/Cycles	-2	-1	-0.5	0.1	0.5	2	10	-2	-1	-0.5	0.1	0.5	2	10
0	0	0	0	0	0	0	0	0	0	0	0	0	0	0
1.E+01	7.82	8.77	7.82	3.37	1.85	1.98	3.44	-2.61	0.00	2.61	4.12	5.55	-5.95	-4.20
1.E+02	6.70	7.28	6.70	3.01	1.68	1.79	2.99	-2.23	0.00	2.23	3.68	5.03	-5.37	-3.66
1.E+03	5.69	6.04	5.69	2.69	1.52	1.62	2.61	-1.90	0.00	1.90	3.28	4.57	-4.85	-3.18
1.E+04	4.80	5.01	4.80	2.40	1.38	1.46	2.27	-1.60	0.00	1.60	2.93	4.14	-4.38	-2.78
1.E+05	4.03	4.15	4.03	2.14	1.25	1.32	1.98	-1.34	0.00	1.34	2.61	3.75	-3.95	-2.42
1.E+06	3.38	3.45	3.38	1.91	1.14	1.19	1.73	-1.13	0.00	1.13	2.33	3.42	-3.56	-2.11
1.E+07	2.82	2.86	2.82	1.70	1.05	1.09	1.54	-0.94	0.00	0.94	2.08	3.14	-3.27	-1.88

Table 31: Third-order CLD

	Amplitude Stress [MPa]							Mean Stress [MPa]						
Ratio/Cycles	-2	-1	-0.5	0.1	0.5	2	10	-2	-1	-0.5	0.1	0.5	2	10
0	0	0	0	0	0	0	0	0	0	0	0	0	0	0
1.E+01	10.22	8.77	6.09	3.37	1.87	2.00	3.49	-3.41	0.00	2.03	4.12	5.62	-6.01	-4.27
1.E+02	8.61	7.28	5.35	3.01	1.70	1.80	3.04	-2.87	0.00	1.78	3.68	5.11	-5.41	-3.72
1.E+03	7.14	6.04	4.66	2.68	1.55	1.63	2.65	-2.38	0.00	1.55	3.28	4.64	-4.90	-3.24
1.E+04	5.86	5.01	4.04	2.39	1.40	1.48	2.31	-1.95	0.00	1.35	2.93	4.21	-4.43	-2.82
1.E+05	4.79	4.15	3.47	2.14	1.28	1.33	2.01	-1.60	0.00	1.16	2.61	3.83	-3.99	-2.46
1.E+06	3.90	3.45	2.97	1.91	1.15	1.20	1.75	-1.30	0.00	0.99	2.33	3.46	-3.60	-2.14
1.E+07	3.18	2.86	2.52	1.70	1.05	1.09	1.54	-1.06	0.00	0.84	2.08	3.15	-3.27	-1.88

Table 32: Fourth-order CLD

	Amplitude Stress [MPa]							Mean Stress [MPa]						
Ratio/Cycles	-2	-1	-0.5	0.1	0.5	2	10	-2	-1	-0.5	0.1	0.5	2	10
0	0	0	0	0	0	0	0	0	0	0	0	0	0	0
1.E+01	7.22	8.77	7.22	3.36	1.87	2.01	3.54	-2.41	0.00	2.41	4.10	5.62	-6.04	-4.33
1.E+02	6.29	7.28	6.29	3.00	1.70	1.83	3.09	-2.10	0.00	2.10	3.66	5.10	-5.49	-3.77
1.E+03	5.42	6.04	5.42	2.67	1.55	1.65	2.69	-1.81	0.00	1.81	3.27	4.64	-4.96	-3.28
1.E+04	4.63	5.01	4.63	2.38	1.40	1.49	2.34	-1.54	0.00	1.54	2.91	4.20	-4.47	-2.86
1.E+05	3.93	4.15	3.93	2.13	1.27	1.34	2.03	-1.31	0.00	1.31	2.60	3.82	-4.03	-2.49
1.E+06	3.31	3.45	3.31	1.90	1.15	1.21	1.77	-1.10	0.00	1.10	2.32	3.46	-3.64	-2.16
1.E+07	2.78	2.86	2.78	1.70	1.05	1.10	1.54	-0.93	0.00	0.93	2.08	3.14	-3.30	-1.88

Table 33: Triangular CLD

	Amplitude Stress [MPa]							Mean Stress [MPa]						
Ratio/Cycles	2	10	-2	-1	0.1	-0.5	0.5	2	10	-2	-1	0.1	-0.5	0.5
0	0	0	0	0	0	0	0	0	0	0	0	0	0	0
1.E+01	2.01	3.54	6.58	8.77	3.37	6.58	1.82	-6.03	-4.33	-2.19	0.00	4.12	2.19	5.47
1.E+02	1.83	3.08	5.46	7.28	3.01	5.46	1.66	-5.48	-3.77	-1.82	0.00	3.67	1.82	4.98
1.E+03	1.65	2.68	4.53	6.04	2.68	4.53	1.50	-4.94	-3.28	-1.51	0.00	3.28	1.51	4.50
1.E+04	1.49	2.34	3.76	5.01	2.39	3.76	1.37	-4.47	-2.85	-1.25	0.00	2.93	1.25	4.10
1.E+05	1.35	2.03	3.12	4.15	2.14	3.12	1.23	-4.05	-2.49	-1.04	0.00	2.61	1.04	3.70
1.E+06	1.21	1.77	2.58	3.45	1.90	2.58	1.12	-3.64	-2.16	-0.86	0.00	2.33	0.86	3.37
1.E+07	1.10	1.54	2.14	2.86	1.70	2.14	1.05	-3.29	-1.88	-0.71	0.00	2.08	0.71	3.15

Table 34: Piecewise Linear CLD

	Amplitude Stress [MPa]							Mean Stress [MPa						
Ratio/Cycles	2	10	-2	-1	0.1	-0.5	0.5	2	10	-2	-1	0.1	-0.5	0.5
0	0	0	0	0	0	0	0	0	0	0	0	0	0	0
1.E+01	1.97	3.54	6.25	8.77	3.37	6.11	1.92	-5.92	-4.33	-2.08	0.00	4.12	2.04	5.76
1.E+02	1.82	3.08	5.31	7.28	3.01	5.25	1.79	-5.46	-3.77	-1.77	0.00	3.68	1.75	5.38
1.E+03	1.67	2.68	4.50	6.04	2.68	4.50	1.67	-5.02	-3.28	-1.50	0.00	3.28	1.50	5.02
1.E+04	1.53	2.34	3.82	5.01	2.39	3.86	1.56	-4.59	-2.85	-1.27	0.00	2.93	1.29	4.67
1.E+05	1.40	2.03	3.23	4.15	2.14	3.30	1.44	-4.19	-2.48	-1.08	0.00	2.61	1.10	4.33
1.E+06	1.27	1.77	2.74	3.45	1.91	2.82	1.33	-3.80	-2.16	-0.91	0.00	2.33	0.94	4.00
1.E+07	1.14	1.54	2.32	2.86	1.70	2.41	1.23	-3.43	-1.88	-0.77	0.00	2.08	0.80	3.69

Table 35: Harris CLD

	Amplitude Stress [MPa]							Mean Stress [MPa						
Ratio/Cycles	2	10	-2	-1	0.1	-0.5	0.5	2	10	-2	-1	0.1	-0.5	0.5
0	0	0	0	0	0	0	0	0	0	0	0	0	0	0
1.E+01	2.01	3.54	7.00	8.77	3.37	6.70	1.76	-6.03	-4.33	-2.33	0.00	4.12	2.23	5.28
1.E+02	1.82	3.08	5.94	7.28	3.01	5.77	1.62	-5.45	-3.77	-1.98	0.00	3.68	1.92	4.86
1.E+03	1.64	2.68	5.03	6.04	2.68	4.96	1.49	-4.92	-3.28	-1.68	0.00	3.28	1.65	4.47
1.E+04	1.48	2.34	4.23	5.01	2.39	4.26	1.37	-4.45	-2.85	-1.41	0.00	2.93	1.42	4.12
1.E+05	1.34	2.03	3.55	4.15	2.14	3.65	1.27	-4.02	-2.48	-1.18	0.00	2.61	1.22	3.81
1.E+06	1.21	1.77	2.97	3.45	1.91	3.13	1.17	-3.63	-2.16	-0.99	0.00	2.33	1.04	3.52
1.E+07	1.09	1.54	2.47	2.86	1.70	2.68	1.09	-3.27	-1.88	-0.82	0.00	2.08	0.89	3.26

Table 36: Kawai CLD

	Amplitude Stress [MPa]							Mean Stress [MPa]						
Ratio/Cycles	2	10	-2	-1	0.1	-0.5	0.5	2	10	-2	-1	0.1	-0.5	0.5
0	0	0	0	0	0	0	0	0	0	0	0	0	0	0
1.E+01	2.01	3.52	6.14	8.77	3.37	6.14	1.87	-6.02	-4.30	-2.05	0.00	4.12	2.05	5.61
1.E+02	1.82	3.09	5.71	7.28	3.06	5.71	1.72	-5.45	-3.77	-1.90	0.00	3.74	1.90	5.17
1.E+03	1.64	2.69	5.13	6.04	2.76	5.13	1.56	-4.92	-3.29	-1.71	0.00	3.38	1.71	4.67
1.E+04	1.48	2.37	4.49	5.01	2.45	4.49	1.42	-4.44	-2.90	-1.50	0.00	3.00	1.50	4.25
1.E+05	1.34	2.09	3.87	4.15	2.19	3.87	1.29	-4.01	-2.55	-1.29	0.00	2.67	1.29	3.86
1.E+06	1.20	1.78	3.29	3.45	1.94	3.29	1.17	-3.61	-2.18	-1.10	0.00	2.37	1.10	3.51
1.E+07	1.09	1.57	2.77	2.86	1.76	2.77	1.06	-3.27	-1.92	-0.92	0.00	2.15	0.92	3.18

APPENDIX D: MEAN-AMPLITUDE STRESS MODEL EVALUATIONS

All constant life diagrams models discussed in chapter 5 are evaluated through the following tables.

Table 37: Linear model evaluation

0.1	N	1.66E+02	1.92E+02	1.99E+02	2.58E+02	8.10E+02	9.41E+02	2.54E+03	r^2 value
	Exp. Mean [MPa]	3.92	3.48	3.48	3.48	3.48	3.39	3.05	0.011
	Exp. Amplitude [MPa]	3.20	2.85	2.85	2.85	2.85	2.78	2.49	
	Model Amplitude [MPa]	3.68	4.08	4.08	4.08	4.08	4.16	3.71	
10	N	3.16E+02	3.63E+02	2.81E+02	6.91E+02	1.71E+03	2.63E+03	1.92E+03	1.000
	Exp. Mean [MPa]	3.48	3.48	3.48	3.48	3.05	3.05	3.05	
	Exp. Amplitude [MPa]	2.85	2.85	2.85	2.85	2.49	2.49	2.49	
	Model Amplitude [MPa]	10.48	10.48	10.48	10.48	8.36	8.36	8.36	
0.5	N	1.18E+02	3.20E+02	8.72E+02	1.23E+03	2.04E+03	4.66E+03	6.31E+03	0.464
	Exp. Mean [MPa]	5.34	4.75	4.75	4.75	4.15	4.15	4.15	
	Exp. Amplitude [MPa]	1.78	1.58	1.58	1.58	1.38	1.38	1.38	
	Model Amplitude [MPa]	2.37	2.91	2.91	2.41	2.87	2.87	2.87	
-2	N	3.E+02	3.E+02	4.E+02	1.E+03	8.E+03	2.E+03	7.E+04	0.864
	Exp. Mean [MPa]	1.78	1.78	1.58	1.58	1.38	1.38	1.19	
	Exp. Amplitude [MPa]	5.34	5.34	4.75	4.75	4.15	4.15	3.56	
	Model Amplitude [MPa]	8.91	8.91	8.73	7.24	7.09	7.09	5.76	
-0.5	N	2.24E+02	9.80E+01	2.17E+02	6.39E+02	2.49E+03	4.07E+03	2.38E+04	0.812
	Exp. Mean [MPa]	1.78	1.78	1.58	1.58	1.38	1.38	1.19	
	Exp. Amplitude [MPa]	5.34	5.34	4.75	4.75	4.15	4.15	3.56	
	Model Amplitude [MPa]	5.64	6.80	5.82	5.82	4.98	4.98	4.26	
2	N	1.23E+02	1.53E+03	5.81E+03	1.21E+04	6.37E+03	9.81E+04	1.58E+05	0.666
	Exp. Mean [MPa]	5.34	4.75	4.75	4.75	4.15	4.15	4.15	
	Exp. Amplitude [MPa]	1.78	1.58	1.58	1.58	1.38	1.38	1.38	
	Model Amplitude [MPa]	12.19	9.66	9.66	8.01	9.21	7.64	6.33	

Table 38: Second-order model evaluation

0.1	N	1.66E+02	1.92E+02	1.99E+02	2.58E+02	8.10E+02	9.41E+02	2.54E+03	r^2 value
	Exp. Mean [MPa]	3.92	3.48	3.48	3.48	3.48	3.39	3.05	0.090
	Exp. Amplitude [MPa]	3.20	2.85	2.85	2.85	2.85	2.78	2.49	
	Model Amplitude [MPa]	5.49	5.87	5.87	5.87	5.87	5.94	5.14	
10	N	3.16E+02	3.63E+02	2.81E+02	6.91E+02	1.71E+03	2.63E+03	1.92E+03	1.000
	Exp. Mean [MPa]	3.48	3.48	3.48	3.48	3.05	3.05	3.05	
	Exp. Amplitude [MPa]	2.85	2.85	2.85	2.85	2.49	2.49	2.49	
	Model Amplitude [MPa]	5.87	5.87	5.87	5.87	5.14	5.14	5.14	

0.5	N	1.18E+02	3.20E+02	8.72E+02	1.23E+03	2.04E+03	4.66E+03	6.31E+03	0.133
	Exp. Mean [MPa]	5.34	4.75	4.75	4.75	4.15	4.15	4.15	
	Exp. Amplitude [MPa]	1.78	1.58	1.58	1.58	1.38	1.38	1.38	
	Model Amplitude [MPa]	3.96	4.66	4.66	3.86	4.37	4.37	4.37	
-2	N	3.E+02	3.E+02	4.E+02	1.E+03	8.E+03	2.E+03	7.E+04	0.787
	Exp. Mean [MPa]	1.78	1.78	1.58	1.58	1.38	1.38	1.19	
	Exp. Amplitude [MPa]	5.34	5.34	4.75	4.75	4.15	4.15	3.56	
	Model Amplitude [MPa]	6.91	6.91	6.99	5.80	5.85	5.85	4.89	
-0.5	N	2.24E+02	9.80E+01	2.17E+02	6.39E+02	2.49E+03	4.07E+03	2.38E+04	0.851
	Exp. Mean [MPa]	1.78	1.78	1.58	1.58	1.38	1.38	1.19	
	Exp. Amplitude [MPa]	5.34	5.34	4.75	4.75	4.15	4.15	3.56	
	Model Amplitude [MPa]	6.91	8.33	6.99	6.99	5.85	5.85	4.89	
2	N	1.23E+02	1.53E+03	5.81E+03	1.21E+04	6.37E+03	9.81E+04	1.58E+05	0.028
	Exp. Mean [MPa]	5.34	4.75	4.75	4.75	4.15	4.15	4.15	
	Exp. Amplitude [MPa]	1.78	1.58	1.58	1.58	1.38	1.38	1.38	
	Model Amplitude [MPa]	3.96	3.86	3.86	3.20	4.37	3.63	3.01	

Table 39: Third-order model evaluation

0.1	N	1.66E+02	1.92E+02	1.99E+02	2.58E+02	8.10E+02	9.41E+02	2.54E+03	r^2 value
	Exp. Mean [MPa]	3.92	3.48	3.48	3.48	3.48	3.39	3.05	
	Exp. Amplitude [MPa]	3.20	2.85	2.85	2.85	2.85	2.78	2.49	0.356
	Model Amplitude [MPa]	2.77	3.29	3.29	3.29	3.29	3.39	3.16	
10	N	3.16E+02	3.63E+02	2.81E+02	6.91E+02	1.71E+03	2.63E+03	1.92E+03	
	Exp. Mean [MPa]	3.48	3.48	3.48	3.48	3.05	3.05	3.05	
	Exp. Amplitude [MPa]	2.85	2.85	2.85	2.85	2.49	2.49	2.49	1.000
	Model Amplitude [MPa]	3.29	3.29	3.29	3.29	3.16	3.16	3.16	
0.5	N	1.18E+02	3.20E+02	8.72E+02	1.23E+03	2.04E+03	4.66E+03	6.31E+03	
	Exp. Mean [MPa]	5.34	4.75	4.75	4.75	4.15	4.15	4.15	
	Exp. Amplitude [MPa]	1.78	1.58	1.58	1.58	1.38	1.38	1.38	0.865
	Model Amplitude [MPa]	1.29	1.86	1.86	1.55	2.08	2.08	2.08	
-2	N	3.E+02	3.E+02	4.E+02	1.E+03	8.E+03	2.E+03	7.E+04	
	Exp. Mean [MPa]	1.78	1.78	1.58	1.58	1.38	1.38	1.19	
	Exp. Amplitude [MPa]	5.34	5.34	4.75	4.75	4.15	4.15	3.56	0.631
	Model Amplitude [MPa]	4.44	4.44	3.85	3.19	4.00	3.32	2.86	
-0.5	N	2.59E+02	2.17E+02	6.39E+02	2.78E+03	2.49E+03	4.07E+03	2.38E+04	
	Exp. Mean [MPa]	1.78	1.78	1.58	1.58	1.38	1.38	1.19	
	Exp. Amplitude [MPa]	5.34	5.34	4.75	4.75	4.15	4.15	3.56	0.642
	Model Amplitude [MPa]	5.35	5.35	5.59	4.64	4.83	4.83	4.16	
2	N	1.23E+02	1.53E+03	5.81E+03	1.21E+04	6.37E+03	9.81E+04	1.58E+05	
	Exp. Mean [MPa]	5.34	4.75	4.75	4.75	4.15	4.15	4.15	
	Exp. Amplitude [MPa]	1.78	1.58	1.58	1.58	1.38	1.38	1.38	0.218
	Model Amplitude [MPa]	1.29	1.55	1.55	1.28	2.08	1.72	1.19	

Table 40: Fourth-order model evaluation

0.1	N	1.66E+02	1.92E+02	1.99E+02	2.58E+02	8.10E+02	9.41E+02	2.54E+03	r^2 value
	Exp. Mean [MPa]	3.92	3.48	3.48	3.48	3.48	3.39	3.05	0.099
	Exp. Amplitude [MPa]	3.20	2.85	2.85	2.85	2.85	2.78	2.49	
	Model Amplitude [MPa]	4.15	4.73	4.73	4.73	4.73	4.85	4.38	
10	N	3.16E+02	3.63E+02	2.81E+02	6.91E+02	1.71E+03	2.63E+03	1.92E+03	1.000
	Exp. Mean [MPa]	3.48	3.48	3.48	3.48	3.05	3.05	3.05	
	Exp. Amplitude [MPa]	2.85	2.85	2.85	2.85	2.49	2.49	2.49	
	Model Amplitude [MPa]	4.73	4.73	4.73	4.73	4.38	4.38	4.38	
0.5	N	1.18E+02	3.20E+02	8.72E+02	1.23E+03	2.04E+03	4.66E+03	6.31E+03	0.785
	Exp. Mean [MPa]	5.34	4.75	4.75	4.75	4.15	4.15	4.15	
	Exp. Amplitude [MPa]	1.78	1.58	1.58	1.58	1.38	1.38	1.38	
	Model Amplitude [MPa]	2.16	2.98	2.98	2.47	3.17	3.17	3.17	
-2	N	3.E+02	3.E+02	4.E+02	1.E+03	8.E+03	2.E+03	7.E+04	0.701
	Exp. Mean [MPa]	1.78	1.78	1.58	1.58	1.38	1.38	1.19	
	Exp. Amplitude [MPa]	5.34	5.34	4.75	4.75	4.15	4.15	3.56	
	Model Amplitude [MPa]	5.44	5.44	4.61	3.83	4.71	3.90	3.29	
-0.5	N	2.59E+02	2.17E+02	6.39E+02	2.78E+03	2.49E+03	4.07E+03	2.38E+04	0.748
	Exp. Mean [MPa]	1.78	1.78	1.58	1.58	1.38	1.38	1.19	
	Exp. Amplitude [MPa]	5.34	5.34	4.75	4.75	4.15	4.15	3.56	
	Model Amplitude [MPa]	6.56	6.56	6.71	5.56	5.67	5.67	4.78	
2	N	1.23E+02	1.53E+03	5.81E+03	1.21E+04	6.37E+03	9.81E+04	1.58E+05	0.288
	Exp. Mean [MPa]	5.34	4.75	4.75	4.75	4.15	4.15	4.15	
	Exp. Amplitude [MPa]	1.78	1.58	1.58	1.58	1.38	1.38	1.38	
	Model Amplitude [MPa]	2.16	2.47	2.47	2.05	3.17	2.63	2.18	

Other composite models

Table 41: Triangular model evaluation

0.1	N	1.66E+02	1.92E+02	1.99E+02	2.58E+02	8.10E+02	9.41E+02	2.54E+03	r^2 value
	Exp. Mean [MPa]	3.92	3.48	3.48	3.48	3.48	3.39	3.05	0.201
	Exp. Amplitude [MPa]	3.20	2.85	2.85	2.85	2.85	2.78	2.49	
	Model Amplitude [MPa]	3.07	3.42	3.40	3.26	2.66	2.67	2.55	
10	N	3.16E+02	3.63E+02	2.81E+02	6.91E+02	1.71E+03	2.63E+03	1.92E+03	0.634
	Exp. Mean [MPa]	3.48	3.48	3.48	3.48	3.05	3.05	3.05	
	Exp. Amplitude [MPa]	2.85	2.85	2.85	2.85	2.49	2.49	2.49	
	Model Amplitude [MPa]	3.15	3.07	3.21	2.74	2.73	2.54	2.68	
0.5	N	1.18E+02	3.20E+02	8.72E+02	1.23E+03	2.04E+03	4.66E+03	6.31E+03	0.393
	Exp. Mean [MPa]	5.34	4.75	4.75	4.75	4.15	4.15	4.15	
	Exp. Amplitude [MPa]	1.78	1.58	1.58	1.58	1.38	1.38	1.38	

	Model Amplitude [MPa]	1.84	1.87	1.36	1.19	1.54	1.17	1.04	
-2	N	3.E+02	3.E+02	4.E+02	1.E+03	8.E+03	2.E+03	7.E+04	0.809
	Exp. Mean [MPa]	1.78	1.78	1.58	1.58	1.38	1.38	1.19	
	Exp. Amplitude [MPa]	5.34	5.34	4.75	4.75	4.15	4.15	3.56	
	Model Amplitude [MPa]	4.97	4.87	4.94	4.45	3.70	4.39	3.10	
-0.5	N	2.59E+02	2.17E+02	6.39E+02	2.78E+03	2.49E+03	4.07E+03	2.38E+04	0.823
	Exp. Mean [MPa]	1.78	1.78	1.58	1.58	1.38	1.38	1.19	
	Exp. Amplitude [MPa]	5.34	5.34	4.75	4.75	4.15	4.15	3.56	
	Model Amplitude [MPa]	4.96	5.05	4.68	3.97	4.22	4.00	3.48	
2	N	1.23E+02	1.53E+03	5.81E+03	1.21E+04	6.37E+03	9.81E+04	1.58E+05	0.469
	Exp. Mean [MPa]	5.34	4.75	4.75	4.75	4.15	4.15	4.15	
	Exp. Amplitude [MPa]	1.78	1.58	1.58	1.58	1.38	1.38	1.38	
	Model Amplitude [MPa]	1.82	1.09	0.49	0.18	1.04	0.01	-0.15	

Table 42: Piecewise model evaluation

0.5	N	1.18E+02	3.20E+02	8.72E+02	1.23E+03	2.04E+03	4.66E+03	6.31E+03	r^2 value
	Exp. Mean [MPa]	5.34	4.75	4.75	4.75	4.15	4.15	4.15	
	Exp. Amplitude [MPa]	1.78	1.58	1.58	1.58	1.38	1.38	1.38	0.587
	Model Amplitude [MPa]	1.79	1.79	1.79	1.67	1.67	1.67	1.67	
-2	N	2.54E+02	3.04E+02	3.89E+02	1.00E+03	8.27E+03	1.74E+03	6.71E+04	
	Exp. Mean [MPa]	1.78	1.78	1.58	1.58	1.38	1.38	1.19	
	Exp. Amplitude [MPa]	5.34	5.34	4.75	4.75	4.15	4.15	3.56	0.818
	Model Amplitude [MPa]	5.31	5.31	5.31	4.50	4.50	4.50	3.82	
-0.5	N	2.59E+02	2.17E+02	6.39E+02	2.78E+03	2.49E+03	4.07E+03	2.38E+04	
	Exp. Mean [MPa]	1.78	1.78	1.58	1.58	1.38	1.38	1.19	
	Exp. Amplitude [MPa]	5.34	5.34	4.75	4.75	4.15	4.15	3.56	0.819
	Model Amplitude [MPa]	5.25	5.25	5.25	4.50	4.50	4.50	3.86	
2	N	1.23E+02	1.53E+03	5.81E+03	1.21E+04	6.37E+03	9.81E+04	1.58E+05	
	Exp. Mean [MPa]	5.34	4.75	4.75	4.75	4.15	4.15	4.15	
	Exp. Amplitude [MPa]	1.78	1.58	1.58	1.58	1.38	1.38	1.38	0.512
	Model Amplitude [MPa]	1.82	1.67	1.67	1.53	1.67	1.53	1.40	

Table 43: Harris model evaluation

0.5	N	1.18E+02	3.20E+02	8.72E+02	1.23E+03	2.04E+03	4.66E+03	6.31E+03	r^2 value
	Exp. Mean [MPa]	5.34	4.75	4.75	4.75	4.15	4.15	4.15	0.582
	Exp. Amplitude [MPa]	1.78	1.58	1.58	1.58	1.38	1.38	1.38	
	Model Amplitude [MPa]	0.82	1.45	1.45	0.87	1.49	1.49	1.49	
-2	N	2.54E+02	3.04E+02	3.89E+02	1.00E+03	8.27E+03	1.74E+03	6.71E+04	0.661
	Exp. Mean [MPa]	1.78	1.78	1.58	1.58	1.38	1.38	1.19	

	Exp. Amplitude [MPa]	5.34	5.34	4.75	4.75	4.15	4.15	3.56	
	Model Amplitude [MPa]	5.96	5.96	6.21	5.05	5.27	5.27	4.49	
-0.5	N	2.59E+02	2.17E+02	6.39E+02	2.78E+03	2.49E+03	4.07E+03	2.38E+04	0.661
	Exp. Mean [MPa]	1.78	1.78	1.58	1.58	1.38	1.38	1.19	
	Exp. Amplitude [MPa]	5.34	5.34	4.75	4.75	4.15	4.15	3.56	
	Model Amplitude [MPa]	5.96	5.96	6.21	5.05	5.27	5.27	4.49	
2	N	1.23E+02	1.53E+03	5.81E+03	1.21E+04	6.37E+03	9.81E+04	1.58E+05	0.107
	Exp. Mean [MPa]	5.34	4.75	4.75	4.75	4.15	4.15	4.15	
	Exp. Amplitude [MPa]	1.78	1.58	1.58	1.58	1.38	1.38	1.38	
	Model Amplitude [MPa]	0.82	0.87	0.87	0.50	1.49	0.95	0.59	

Table 44: Kawai model evaluation

0.1	N	1.66E+02	1.92E+02	1.99E+02	2.58E+02	8.10E+02	9.41E+02	2.54E+03	r^2 value
	Exp. Mean [MPa]	3.92	3.48	3.48	3.48	3.48	3.39	3.05	0.362
	Exp. Amplitude [MPa]	3.20	2.85	2.85	2.85	2.85	2.78	2.49	
	Model Amplitude [MPa]	3.87	4.28	4.28	4.28	4.28	4.36	4.18	
10	N	3.16E+02	3.63E+02	2.81E+02	6.91E+02	1.71E+03	2.63E+03	1.92E+03	1.000
	Exp. Mean [MPa]	3.48	3.48	3.48	3.48	3.05	3.05	3.05	
	Exp. Amplitude [MPa]	2.85	2.85	2.85	2.85	2.49	2.49	2.49	
	Model Amplitude [MPa]	4.28	4.28	4.28	4.28	4.18	4.18	4.18	
0.5	N	1.18E+02	3.20E+02	8.72E+02	1.23E+03	2.04E+03	4.66E+03	6.31E+03	0.899
	Exp. Mean [MPa]	5.34	4.75	4.75	4.75	4.15	4.15	4.15	
	Exp. Amplitude [MPa]	1.78	1.58	1.58	1.58	1.38	1.38	1.38	
	Model Amplitude [MPa]	2.52	3.09	3.09	2.83	3.32	3.32	3.32	
-2	N	3.E+02	3.E+02	4.E+02	1.E+03	8.E+03	2.E+03	7.E+04	0.691
	Exp. Mean [MPa]	1.78	1.78	1.58	1.58	1.38	1.38	1.19	
	Exp. Amplitude [MPa]	5.34	5.34	4.75	4.75	4.15	4.15	3.56	
	Model Amplitude [MPa]	5.82	5.82	6.00	5.21	5.34	5.34	4.63	
-0.5	N	2.59E+02	2.17E+02	6.39E+02	2.78E+03	2.49E+03	4.07E+03	2.38E+04	0.691
	Exp. Mean [MPa]	1.78	1.78	1.58	1.58	1.38	1.38	1.19	
	Exp. Amplitude [MPa]	5.34	5.34	4.75	4.75	4.15	4.15	3.56	
	Model Amplitude [MPa]	5.82	5.82	6.00	5.21	5.34	5.34	4.63	
2	N	1.23E+02	1.53E+03	5.81E+03	1.21E+04	6.37E+03	9.81E+04	1.58E+05	0.291
	Exp. Mean [MPa]	5.34	4.75	4.75	4.75	4.15	4.15	4.15	
	Exp. Amplitude [MPa]	1.78	1.58	1.58	1.58	1.38	1.38	1.38	
	Model Amplitude [MPa]	2.52	2.83	2.83	2.52	3.32	2.93	2.55	

APPENDIX E: MANUFACTURING PROCESS OF JOINTS

- Glass fiber and peel ply fabrics are firstly square cut ($0/90^0$) into sizes, using a pair of scissors:

  12 layers of glass fibers are used for the inner laminates

  6 layers are used for the outer laminates

Figure 35: Composite fibers

- The next step is to mix the epoxy resin and the slow hardener according to the standards available from Jonker Sailplanes factory.

Figure 36: Epoxy-mixing

- The resin-hardener mixture is then spread over the granite block.
- The first layer to be placed on the block is peel-ply. The layer is rolled until it becomes clear.
- The second layer is glass fiber, which is placed using the same process. Other layers of glass fibers then follow, using the same method.

Figure 37: Fabric lay-up

- The last layer to be placed (once all the glass layers are in place) is peel ply. This last sheet is rolled until it becomes clear.

Figure 38: GFRP laminate

- Depending on whether the laminate is inner or outer, a metal spacer of 1.5 or 3 mm is used to ensure the correct thickness of the laminate.

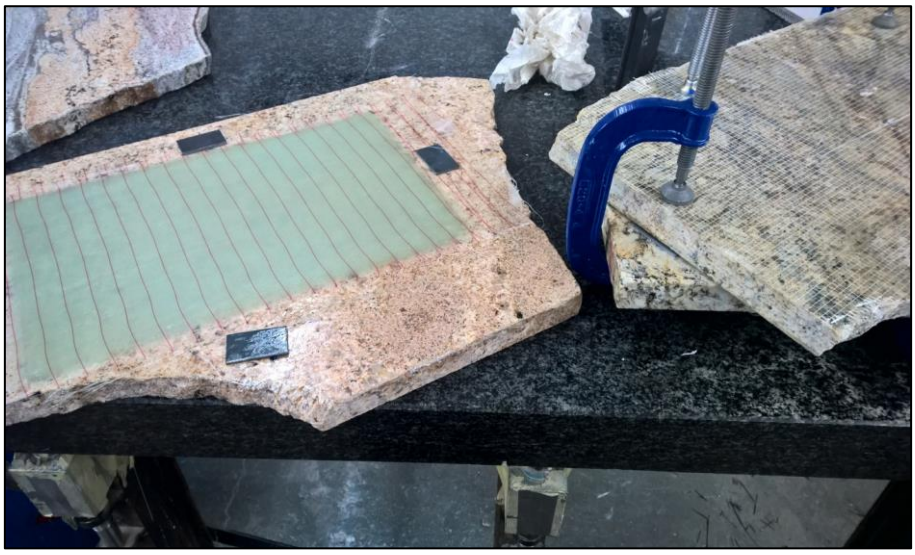

Figure 39: Laminate thickening

- The second granite block is then used to compress the fibers and the epoxy, to give a smooth, flat surface finish.
- The two granite blocks are then clamped together and placed in the curing oven to allow curing for at least 24 hours.
- After curing time has been accomplished, the granite blocks may be removed from the oven and the laminates can be removed from the granite surface smoothly, using a hammer and a chisel.
- The material is now ready to be cut to the correct dimensions, using a band saw or any suitable cutting tool.
- The pieces can now be sanded down using a belt sander to ensure smoothed edges as well as ensuring that all the pieces are identical in size.

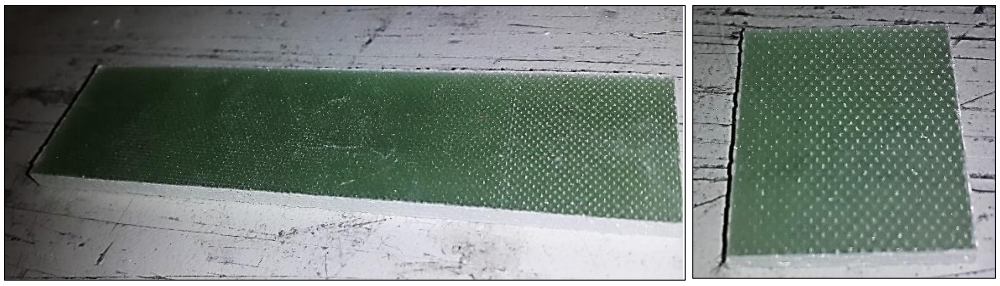

Figure 40: Inner and outer laminates

- The peel-ply can now be removed from both surfaces of the laminate.

- The mixture of matrix, cotton flocks and cab-o-sil additives is then prepared as an adhesive system using the available workshop standards.
- The adhesive is applied on the laminate surfaces, using a syringe to allow for easier application.

Figure 41: Adhesive bonding of laminates

- A bonding jig made from Perspex is surface prepared with wax polish to ensure that the samples can easily be removed from the jig.
- The 2 mm thickness of the adhesive is kept constant by using metal and Perspex spacers of the same size.

Figure 42: Bonding jig

- The samples are then left for 24 hours to allow the adhesive to set and harden.
- The samples are then taken out of the jig and sanded smooth, using a belt sander.

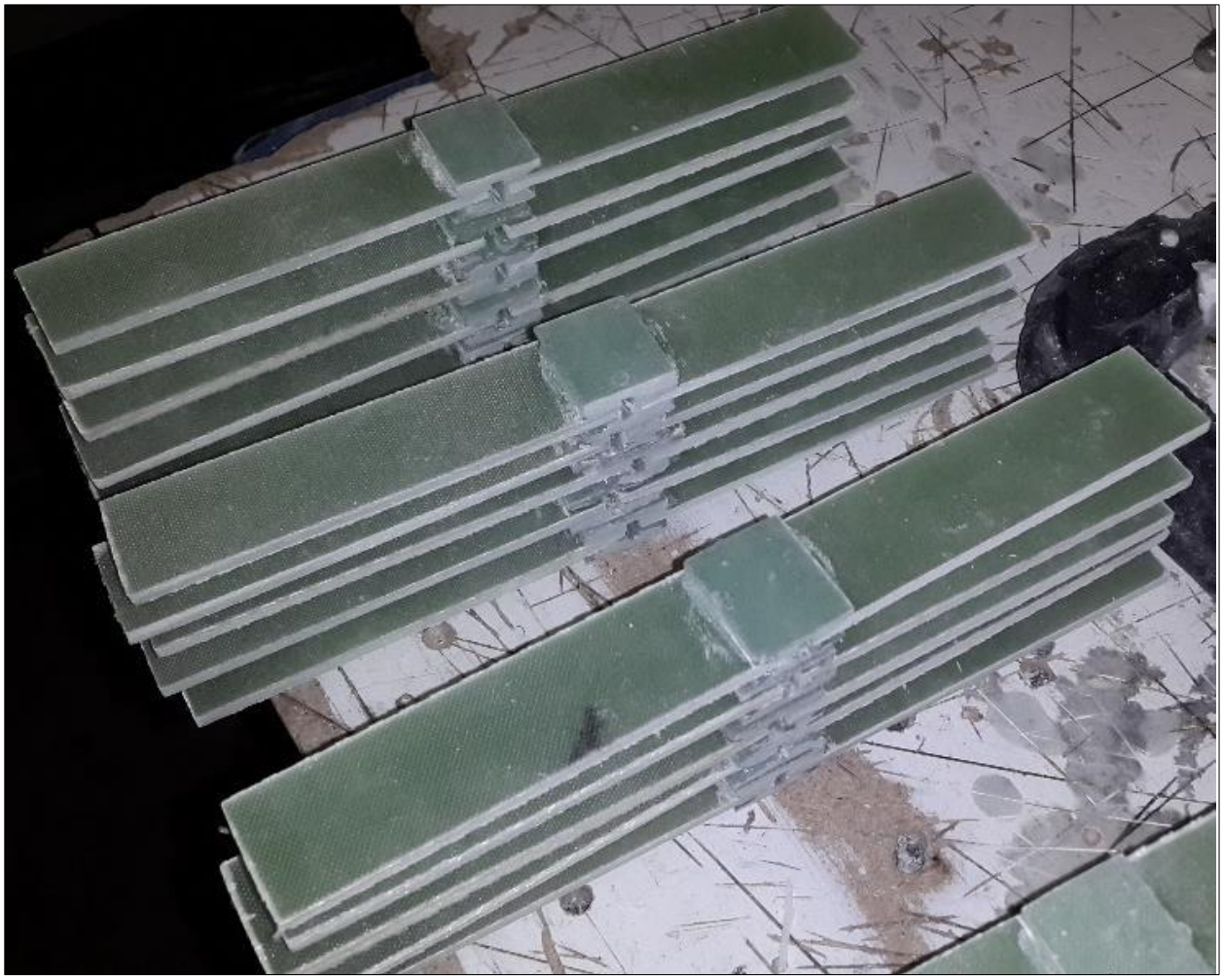

Figure 43: Double-lap strap joints

APPENDIX F: EXPERIMENTAL SET-UP AND TESTING

Machine templates for both static tension and compression tests are used. The ultimate tensile and compression strengths can be determined through these tests. Program templates for fatigue testing of samples under different loading conditions have to be written.

The layout of the fatigue test is illustrated below:

The programming carried out in the Multipurpose Elite software of the MTS as follows:

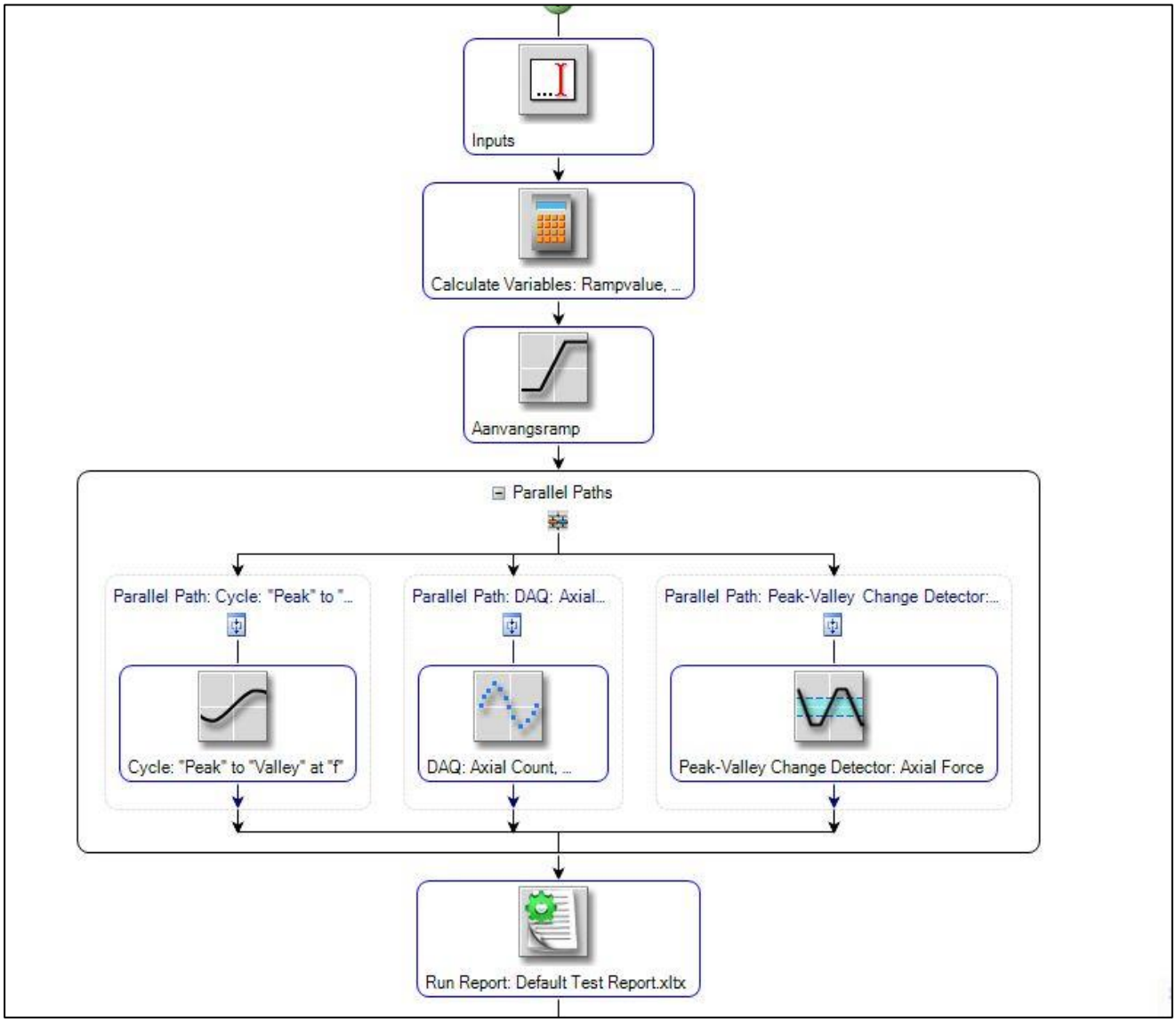

Figure 44: Multipurpose Elite Software

- Inputs:
  This is the first stage of the program, where the input parameters are needed. A pop-up window opens where force, geometry and load percentage must be inserted.
- Calculate variables:
  This function is used to calculate variables such as the peak load, the valley load, the ramp value, etc.
- Ramp function:
  This function is used to apply the defined ramp force to the specimen.
- The cycle function:
  This function predefines the minimum and maximum forces which subject the specimen to fatigue.
- DAQ function:
  This is the data acquisition function which presents the force, number of cycles and the displacement of the specimen.
- Peak-Valley change detector function:
  This function detects the axial force that the specimen experiences and plots the function.
- Run report function:
  This function allows for a report to be generated when the test has finished running.

Starting a new fatigue test

- The first window that opens is the specimen selection window where a new specimen can be described for testing.
- The next window is the setup variables window where the user can insert any comments about the specimen, for example there could be a defect on the specimen.
- Now the input parameters can be inserted. A ramp function is calculated within the program which is basically the mean stress value. This is used so that the specimen is gradually loaded and so that it does not break instantly, as in a static testing.
- Once the specimen is clamped in the machine, the program will show a small force load being felt by the specimen before the test has begun (see below). This is because of the natural frequency of the clamping system, and it is so small that its effects can be neglected.
- Once the test has started, the program monitors the force compared to the time in seconds that it takes for the test to run. A compensator function is included to correlate the response parameter with the input parameter. The two graphs at first look different, but

they then become the same as a result of the compensator, and the results become more accurate.

Experimental parameters

The following parameters must be kept constant throughout testing:

- The dimensions:
  - Total length = 192 [mm]
  - Width = 25 [mm]
  - Inner laminate = 3 [mm]
  - Outer laminate = 1.5 [mm]
  - Outer laminate length = 20 [mm]
  - Bond thickness = 2 [mm]
- UTS and UCS
- Load R-ratio
- The material, resin and adhesive

The following may be varied:

- Percentage load
- Frequency
- Sample rate

Experimental set-up

The following must be done before testing of samples:

- The testing station must always be started up correctly.
- All power must be switched on and the PC must be started up.
- The station manager program must be started on the PC desktop and the exclusive control must be activated.

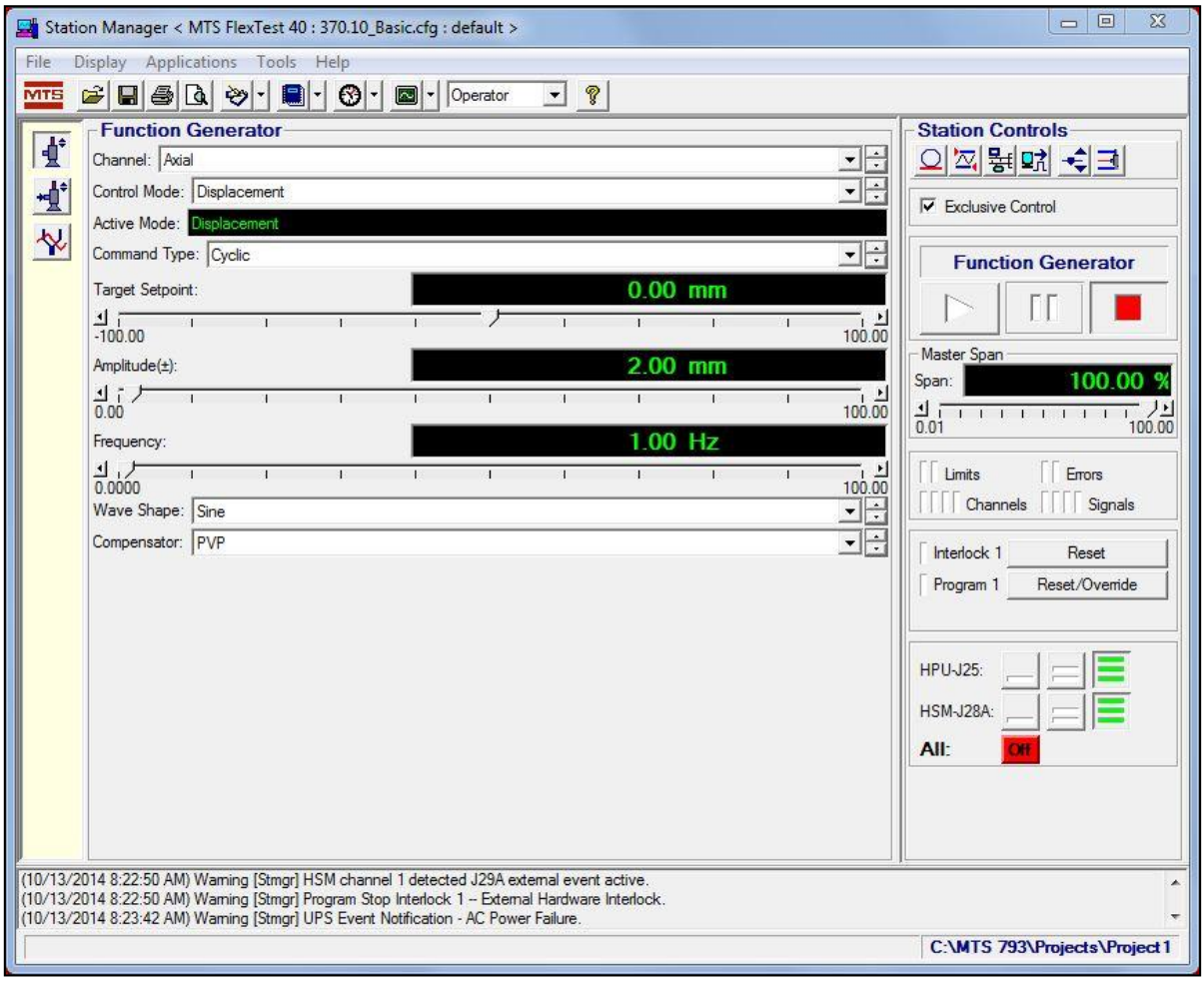

Figure 45: MTS station manager

- The pump settings must be set so that it can be remotely operated.
- Using the station manager, the pump can be started using a left to right sequence from top to bottom.
- The chiller can now be switched on and set to the correct temperature values.
- The hydraulic oil is now able to circulate properly throughout the entire system.
- Once the machine is warmed up, the tests may begin.

Static Testing

- The TW Elite program is then started from the desktop and the correct template is then opened for the static testing.
- Once the specimen is clamped in the machine, the test can begin.
- The results can then be recorded in an Excel spreadsheet.

Frequency testing

- Measure and record the initial temperature of the specimen, using laser temperature meter.
- Start fatigue testing at a higher selected frequency while monitoring the sample temperature.
- Stop the test when the temperature of the specimen increases by 10 ^{0}C compared to the initially recorded temperature.
- Insert a new specimen and test at lower selected frequency while monitoring the 10 ^{0}C temperature increase.
- Repeat the above steps until a stable frequency is reached at a temperature difference less than 10 ^{0}C

Fatigue Testing

- The Multipurpose Elite program can be started from the desktop and the programmed template can then be loaded.
- The specimen must then be clamped in the hydraulic clamps at a stress of 500 [kPa]. It must be properly aligned in the clamps, otherwise extra loads and forces could be implemented onto the specimen.
- Then the procedure discussed under “Starting a new fatigue test” can be followed.
- Once the test run is completed, the program can be stopped and the specimen can be removed.